INSIGHTS INTO THE MECHANISM OF HUMAN

ERYTHROCYTE HEXOSE TRANSPORT:

A TRANSFERRED NOE STUDY OF GLUCOSE BINDING TO *GLUT1*

Thesis by

Scott Alan Ross

In Partial Fulfillment of the Requirements

for the Degree of

Doctor of Philosophy

California Institute of Technology

Pasadena, California

1994

(Submitted October 15, 1993)

The work of thought is one of the most

ancient and useful activities of humankind.

To generate thought is to create life, liveliness, community.

Consensus isn't important. What's important is

how the generative power of our thought makes life vivid

and burns out the dead brush,

dead habits, dead institutions.

-- Michael Ventura

ACKNOWLEDGEMENTS

My long tenure as a graduate student gave me time to involve a great many people in the experience. First, I wish to thank the people who have contributed directly to my training and research. Foremost among these, I am grateful to my research advisor Sunney Chan for lending me the keys and letting me stay out late. Sunney always encouraged me in my natural inclination to work and think independently, while frequently stepping in to point out significant results where I saw none, or to place them in a broader context. I am indebted to James Yesinowski and Helmut Eckert for their unstinting sharing of their time and NMR expertise. My enthusiasm for NMR largely has its origin in James' example. Paula Watnick, Kathy Kanes and Nancy Vogelaar also contributed in many ways to my training in NMR and membrane protein chemistry, as well as to the quality of life in the lab. Bog Kuszta, Tim Kelly from Bruker, and especially Tom Dunn taught me much about instrumentation as we struggled to keep the AM 500 running. Dr. Yu-Teh Li provided me with an interesting and instructive excursion into aspects of NMR of sugars unrelated to my thesis work. Many thanks also to Silvia Cavagnero for interesting and pertinent discussions and for the pep talks in the latter days, and to Doug Early, who performed a statistical analysis of my data at a moment's notice. Many people in the Division offices helped me more times and in more ways than I could remember; I particularly want to single out Priscilla Boon here. I also wish to acknowledge the NSF, which provided a fellowship in my first three years, and the NIH, whose grants (to Sunney) made the research described in this thesis possible. Finally, the folks at the Los Angeles chapter of the American Red Cross, particularly Jim Popko and Tony Raven, kept me in blood.

Aside from my research project, my experience at Caltech has been richer for having known the following people: Elise Gabriel, Paul Smith, Robert Copeland and Rich Blaylock, for discussions of science and life, and Mark Li and particularly Joel Morgan for the same and for movies and Chinese food. In Joel I found a kindred spirit,

as I did in Alan Van Asselt, Tom Brown, Bob Sweeney, Erica Harvey, Ann Heil and Claudia Barner. Claudia has been in this with me for six years now, patient and loving and inspiring and funny; it is unclear whether I could've completed this project without her support.

My circle of family and friends outside of Caltech is very important to me. Much love and many thanks to my parents Richard and Karen, my sister Susann, my grandmother Olive and mother-in-law DeEtte for their support. My stepson Remus Lightning Thorsen encouraged me and believed in me all the way. Suzanna deBaca, Bruce Kahl, Ed Steinbrecher, Jeanine Burton, Harley Swiftdeer, Diana Hurlbut, Janneke Koole and all the A. P. P., men's group and L. A. lodge folks were there for me at critical junctures, each with their particular magic, as were Sophie, Red, Bump and Boo, and as are Micky, Pook and Willy. A final, special tip of the coffee cup to Micky, who never left my side as I wrote this thesis, and indeed tried to write sections of it himself.

v

ABSTRACT

This study examines binding of α- and β-D-glucose in their equilibrium mixture
to the glucose transporter (GLUT1) in human erythrocyte membrane preparations by an
^{1}H NMR method, the transferred NOE (TRNOE). This method is shown theoretically
and experimentally to be a sensitive probe of weak ligand-macromolecule interactions.
The TRNOEs observed are shown to arise solely from glucose binding to GLUT1. Sites
at both membrane faces contribute to the TRNOEs. Binding curves obtained are
consistent with a homogeneous class of sugar sites, with an apparent K_D which varies
(from ~30 mM to ~70 mM for both anomers) depending on the membrane preparation
examined. Preparations with a higher proportion of the cytoplasmic membrane face
exposed to bulk solution yield higher apparent K_Ds. The glucose transport inhibitor
cytochalasin B essentially eliminates the TRNOE. Nonlinearity was found in the
dependence on sugar concentration of the apparent inhibition constant for cytochalasin B
reversal of the TRNOE observed in the α anomer (and probably the β anomer); such
nonlinearity implies the existence of ternary complexes of sugar, inhibitor and
transporter. The inhibition results furthermore imply the presence of a class of relatively
high-affinity ($K_D < 2$mM) sugar sites specific for the α anomer which do not contribute
to NMR-observable binding. The presence of two classes of sugar-sensitive cytochalasin
B sites is also indicated. These results are compared with predictions of the alternating
conformer model of glucose transport. Variation of apparent K_D in the NMR-observable
sites, the formation of ternary complexes and the presence of an anomer-specific site are
shown to be inconsistent with this model. An alternate model is developed which
reconciles these results with the known transport behavior of GLUT1. In this model, the
transporter possesses (at minimum) three classes of sugar sites: (i) transport sites, which
are alternately exposed to the cytoplasmic or the extracellular compartment, but never to
both simultaneously, (ii) a class of sites (probably relatively low-affinity) which are

confined to one compartment, and (iii) the high-affinity α anomer-specific sites, which are confined to the cytoplasmic compartment.

TABLE OF CONTENTS

LIST OF FIGURES AND TABLES

CHAPTER 1

INTRODUCTION TO *GLUT1*

Transport of sugars across membranes is a fundamental process in biological systems. Sugar transport proteins have been found in every cell type examined. Animal tissues possess sugar transporters specific for pyranose monosaccharides, most notably glucose. These proteins play a vital role in hexose metabolism, mediating the absorption of sugars from the gastrointestinal tract and their distribution to storage tissues, as well as providing fuel for the metabolic needs of all cells. As yet, despite the ubiquity and importance of these proteins, the molecular basis of the transport process has not been characterized. The objective of the present work is to contribute to the understanding of the molecular mechanism of transmembrane transport of glucose by GLUT1, a relatively well-characterized sugar transport protein. The binding of glucose to GLUT1 has been monitored by ^{1}H NMR in order to determine the number of binding sites on the protein and the relationships of these sites to one another and to the transport mechanism.

THE *GLUT* FAMILY OF MAMMALIAN HEXOSE TRANSPORTERS

Except at the brush border membranes of the small intestine and the renal proximal tubules, where sugar transport is coupled to the transmembrane Na^+ gradient, the transport of hexoses across mammalian cell membranes occurs by an energy-independent process. Recent DNA cloning studies have revealed a family of homologous integral membrane proteins which mediate this "facilitated diffusion," designated GLUT1 through GLUT5. There is 39-65% sequence identity and 50-76% sequence similarity between isoforms. Most of the sequence divergences are in the amino- and carboxy-terminal segments and in a hydrophilic exofacial loop; the putative membrane-spanning segments are more highly conserved.[1] Indeed, the GLUT proteins may be members of a larger superfamily of transport proteins: significant sequence homology has been noted with several yeast hexose transporters[2], *E. coli* H^+/sugar symporters (but not *lac* permease)[3], and the H^+/Mg^{2+}-tetracycline antiporter of gram-negative bacteria[4]. The

mammalian Na^+/glucose symporter shares little sequence homology with these proteins and is believed to belong to another transporter superfamily.[5]

The GLUT isoforms differ in their tissue distributions, their affinities for sugars and their response to insulin. GLUT1, the first to be sequenced[6] and the object of this study, is found in all cell types, but is abundant only in adult primate erythrocytes, fetal erythrocytes of all mammals, placenta and in the capillary walls of the blood-brain barrier.[1] GLUT1 has also been found to be expressed in every transformed cell line tested. GLUT2 is found in liver, the basolateral membranes of the intestinal and renal epithelia, and pancreatic islet β cells. This isoform is notable for its high K_m for glucose exchange (66 mM in intact hepatocytes[7], compared to 20 mM for erythrocyte GLUT1[8]): sugar flux through GLUT2 should be essentially linear in sugar concentration under physiological conditions. In pancreatic β cells, this linear transport may be part of the mechanism by which postprandial insulin release is scaled. GLUT3, an isoform with somewhat higher affinity for sugars than GLUT1, is expressed exclusively in neural tissues.[9] The isoform expressed only in muscle and adipose tissue, GLUT4, has attracted much attention. Under basal conditions, GLUT4 is predominantly localized to an intracellular vesicle fraction, with very little present in the plasma membrane. Application of insulin causes recruitment of this fraction to the plasma membrane, with a concommitant 20- to 30-fold increase in glucose transport activity due primarily to GLUT4.[10] A defect in the signalling pathway by which insulin recruits GLUT4 is considered a likely factor in Type II non-insulin-dependent diabetes mellitus.[11] The least-characterized member of the GLUT family, GLUT5, is expressed at the apical membrane of the jejunum.[12]

GLUT1: THE HUMAN ERYTHROCYTE GLUCOSE TRANSPORTER

The presence, at low levels, of the GLUT1 transporter in all tissues thus far examined suggests that this isoform mediates basal glucose transport in all cell types. As

noted, *GLUT1 is* particularly abundant in erythrocytes and at the blood-brain barrier. The presence of a high-capacity glucose transport system in erythrocytes provides a larger glucose space in the blood, likely enhancing transfer of glucose to regions of high metabolic activity. Similarly, the GLUT1 system at the blood-brain barrier mediates efficient uptake of glucose into the brain.[13] Recently it was shown that a defect in GLUT1 in these tissues is associated with a syndrome of seizures and developmental delay in human infants.[14]

The human erythrocyte protein is the most thoroughly-investigated sugar transporter, indeed the most thoroughly-investigated transporter of any nonionic substrate. Many of the principles of protein-mediated transport were originally elucidated in studies of this system.[8] Several factors led to the choice of this transporter in early work; the same factors governed the choice of the erythrocyte system for the present study. The ready availability and ease of handling of erythrocytes and the high transporter concentration in the membranes are the paramount factors. The relatively simple composition of the erythrocyte membrane, the absence of organellar membranes, the ease with which cytoplasmic proteins may be removed and the existence of methods of controlling membrane orientation in purified preparations all contribute to making erythrocytes an excellent system in which to study transport.

In work done over the past fifteen years, the erythrocyte transporter has been identified as the primary component of band 4.5 in electrophoretic gels of erythrocyte membrane proteins (nomenclature of Steck[15]). This protein has been purified and functionally reconstituted into liposomes by a variety of protocols.[16, 17, 18] More recently, GLUT1 has been expressed in *E. coli*[19], *Xenopus laevis* oocytes[20], and Chinese hamster ovary cells[21]: molecular biological studies are just now beginning to contribute to our understanding of the structure and function of this transporter (*vide infra*).

THE STRUCTURE OF *GLUT1*

GLUT1 is a Glycoprotein. GLUT1 is a single 492 amino acid polypeptide chain. On electrophoretic gels, the native protein migrates as a broad band at 55 kDa apparent molecular weight due to a single, heterogeneous N-linked oligosaccharide of the erythroglycan type.[22] The protein contains ~15% carbohydrate by weight; deglycosylation prior to electrophoresis results in a sharp band migrating at 46 kDa.[23] A portion of the oligosaccharide appears to be essential to protein function. N-glycanase treatment of purified GLUT1 reconstituted into proteoliposomes reduced glucose transport activity by 50%.[24] The residual activity was shown to be due to transporter molecules which had reconstituted with non-native orientation in the liposome membranes, such that the carbohydrate moiety faced the liposome interior and was inaccessible to N-glycanase. Thus completely deglycosylated transporters are inactive. In contrast, partial deglycosylation by sialidase and/or endo-β-galactosidase treatment does not significantly affect transport activity.[25] The precise role of the oligosaccharide in transporter structure and the transport process remains to be elucidated.

The Monomer is the Minimal Sugar Transport Competent Unit. GLUT1 has been reconstituted into homogenous unilamellar vesicles in which there is, on average, less than one binding site per vesicle for the transport inhibitor cytochalasin B.[26] As the stoichiometry of cytochalasin B: GLUT1 binding is 1:1 under the experimental conditions used[27, 28], this implies that the vesicles contain, on average, < 1 polypeptide. The reconstituted transporters show stereospecific D-glucose transport activity, albeit at about 5% of the *in vivo* rate. More recently, it was shown that inclusion of erythrocyte lipids in the reconstitution of octyl glucoside-solubilized transporters raised the specific activity of GLUT1 monomers in proteoliposomes to 35-55% of that predicted based on glucose transport in intact erythrocytes.[29] These results demonstrate that the glucose transporter is capable of functioning as a monomer; all of the structural elements necessary for the complete transport cycle must be present in the sequence and folding of

the monomer. However, oligomerization may be responsible for the increased efficiency of transport observed in intact cells.

GLUT1 is a Tetramer in Erythrocyte Membranes. Results from a variety of studies indicate that the native form of the erythrocyte glucose transporter is an oligomer of GLUT1. Radiation inactivation target size analyses suggest that the cytochalasin B binding and sugar transport competent components of erythrocyte ghost membranes exist as 124 or 220 kDa structures.[30, 31] When chimeric glucose transporters in which the cytoplasmic C-terminal domain of GLUT1 was replaced by that of GLUT4 were expressed in Chinese hamster ovary cells, endogenous GLUT1 was quantitatively co-immunoprecipitated with the chimeric protein by an anti-GLUT4 C-terminal peptide antibody, suggesting oligomerization of GLUT1 in these cells.[32]

Hydrodynamic studies indicate that octyl glucoside-solubilized GLUT1 is a monomer[29], while solubilization in cholic acid yields a mixture of dimers and tetramers[33]. Inclusion of dithiothreitol (DTT) in the solubilization medium favors the dimer; omission of reductant favors the tetramer. Purified tetrameric GLUT1 is quantitatively converted to the dimer by treatment with DTT. The cholate-solubilized oligomers differ in stoichiometry of cytochalasin B binding (1 mole CB/mole GLUT1 for the dimer; 0.5 mole CB/mole GLUT1 for the tetramer) and in D-glucose binding (the dimer displays a single class of sites, while the tetramer displays two classes of sites). Several lines of evidence argue that the cholate-solubilized tetramer corresponds to the physiological state of GLUT1 in erythrocyte membranes. Rabbit antisera against purified tetrameric GLUT1 were shown to react with epitopes of both the purified tetramer and erythrocyte-resident GLUT1, but not with the purified dimer.[28] In contrast, anti-GLUT1 C-terminal peptide antibodies show similar titers for both purified oligomers. The number of cell surface, anti-GLUT1 tetramer antibody-reactive proteins was found to be 3×10^5 / cell, in close agreement with previous estimates of GLUT1 density.[34] Since erythrocytes contain 1.5×10^5 D-glucose-sensitive cytochalasin B binding sites per cell,[35]

the stoichiometry of cytochalasin B binding by GLUT1 in intact cells and ghosts is similar to that of the purified tetramer rather than the purified dimer. Additionally, treatment of ghosts with DTT at high pH has effects consonant with a transition from tetrameric to dimeric GLUT1: the cytochalasin B binding capacity doubles, while the anti-GLUT1 tetramer antibody binding capacity is sharply reduced. These effects are reversed by physiological concentrations of glutathione disulfide. Thus the available evidence favors a tetrameric structure for erythrocyte GLUT1.

GLUT1 Contains 12 Transmembrane Segments. Amino acid sequences deduced for GLUT1 from rat brain and human HepG2 hepatoma cells exhibit 98% homology, with mostly conservative substitutions in the residues which differ, bespeaking a strong dependence of function on primary structure.[36] A model of the transmembrane disposition of GLUT1 has been presented based on hydropathy analysis of the deduced HepG2 protein sequence.[6] In this model (Figure 1), GLUT1 is arranged in three major domains: (1) 12 membrane-spanning α-helices, (2) a large, highly charged cytoplasmic domain (residues 207-271), and (3) a smaller extracellular domain (residues 34-66) bearing the carbohydrate moiety.

Proteolytic digestion and antibody binding studies of the erythrocyte protein support this model. Extensive papain digestion of purified erythrocyte GLUT1 reconstituted in erythrocyte lipids yields a mixture of 3-4 kDa fragments, of appropriate size to be transmembrane segments.[37] Trypsin cleaves only at the cytoplasmic surface of GLUT1, in accord with the model which predicts no trypsin-susceptible sites exposed on the exofacial surface. Trypsin digestion yields two large membrane-bound fragments: a fragment of 23 kDa apparent molecular weight (after deglycosylation) derived from the N-terminal half of the protein, and an 18 kDa fragment which retains cytochalasin B binding activity derived from the C-terminal half. Trypsin digestion additionally releases soluble fragments whose sequences match those of the predicted cytoplasmic loop and C-terminus. The cytoplasmic location of the C-terminus was corroborated by the

Figure 1.1

Model of the Transmembrane Disposition of GLUT1. This model is based on that of Ref. 6. The twelve rectangles represent membrane-spanning α-helices, connected by extra-membranous domains. The carbohydrate moiety at Asn45 is represented by a "tree." Trypsin cleavage sites which release the large cytoplasmic domain between helices 6 and 7 and the C-terminal domain are indicated by arrows. The specific residues identified are those referred to in the text.

OUTSIDE
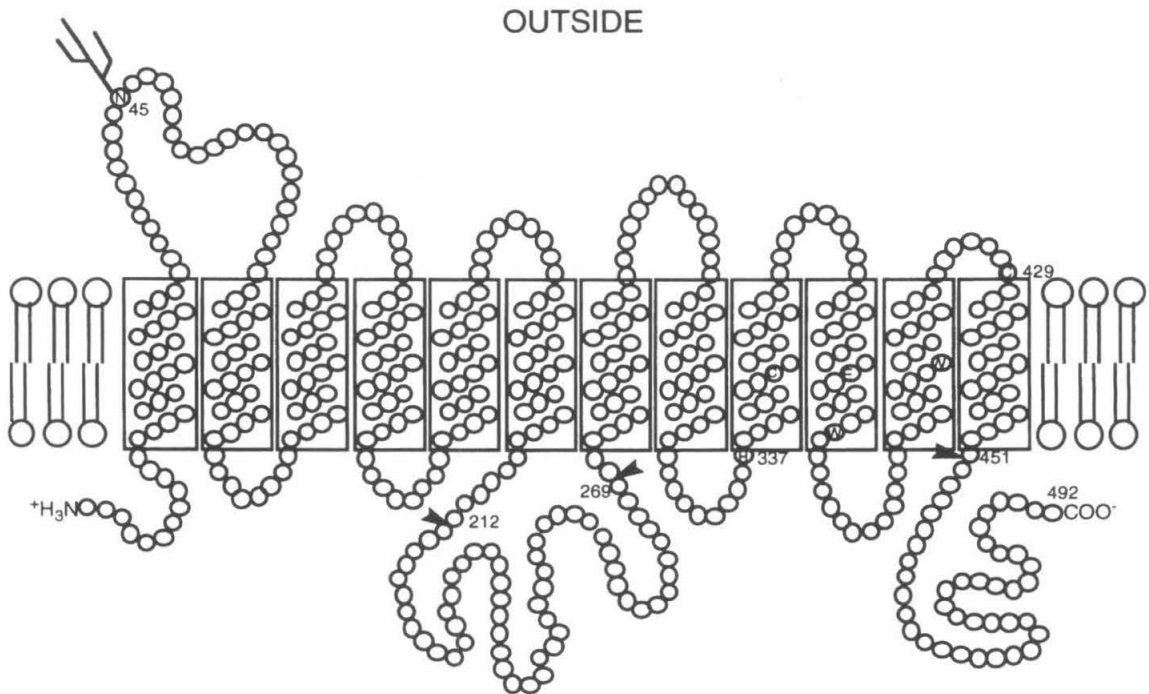
side-specific reactivity of antibodies raised against a synthetic peptide corresponding to residues 477-492.[38]

A recent chemical labeling study also lends credence to the model of Figure 1, which predicts that Cys 429 lies in the exofacial loop between helices 11 and 12. Of the six cysteine residues in GLUT1, only one is reactive toward membrane-impermeant thiol reagents in intact cells and resealed ghosts. This reactive residue was identified as Cys 429 by radiolabeling, chemical cleavage of the protein and immunoblotting with sequence-specific antibodies.[39] Finally, spectroscopic studies have shed some light on GLUT1 secondary structure and transmembrane disposition. Fourier transform infrared (FT-IR)[40] and circular dichroism (CD)[41] measurements of purified erythrocyte GLUT1 are consistent with roughly 70% α-helical structure; β-turn and random coil structure are present as well. Conflicting results have been presented on the presence of β-sheet structure. FT-IR of the soluble trypsin cleavage fragments of GLUT1 show α-helical structure in the extramembranous domains.[37] Polarized FT-IR and ultraviolet CD of oriented lipid films containing GLUT1 indicate that the α-helical portions of the protein are oriented, on average, roughly perpendicular to the plane of the membrane, with a tilt angle of < 38° relative to the bilayer normal.[42]

The Location and Structure of the Sugar Binding Site or Sites is Unknown. GLUT1 displays at least one sugar binding site and two conformations (*vide infra*). The binding site must include hydrogen bond donors and/or acceptors spatially arranged to accommodate D-glucose, but none of the residues involved have been identified in the primary structure. Helices 3, 5, 7, 8 and 11 are amphipathic and may be arranged in native GLUT1 as a bundle with sugar binding site(s) in its hydrophilic core. A hydrogen exchange study indicates that a high proportion of the polypeptide backbone is accessible to solvent, consistent with a water-filled channel-like structure.[43]

Studies of the intrinsic fluorescence of GLUT1 yield some information on structural elements affected by ligand binding and transport. One report of pH effects on

intrinsic *tryptophan* fluorescence suggests that in the absence of ligands, Trp388 interacts with His337 and Trp412 interacts with Cys347, reflecting associations of helix 9 with helices 10 and 11.[44] Binding of D-glucose or inhibitors produces changes in the quenching pH profile consistent with a rotation of helix 10 to break the contact between Trp388 and His337 and to bring Glu380 close to Trp412. A recent site-directed mutagenesis study corroborates the involvement of Trp412 and Trp388 either as sugar or cytochalasin B binding site components, respectively, or in maintaining local tertiary structure in functionally important regions of the protein.[45] Each of the six Trp residues in GLUT1 was changed to either Gly or Ile. The mutants were expressed in *Xenopus laevis* oocytes and assayed for transport activity and cytochalasin B binding. Only the Trp388 and Trp412 mutants showed diminished sugar transport: the Trp388 mutant due to decreased targeting to the plasma membrane and a small decrease in intrinsic affinity, the Trp412 mutant due to a drastic decrease in intrinsic affinity. Affinity of the Trp388 mutant for cytochalasin B was an order of magnitude smaller than that of wild-type GLUT1, while that of the Trp412 mutant was unaltered. More site-directed mutagenesis studies will likely add to these encouraging results in the near future. Ultimately, however, it is to be hoped that efforts underway to crystallize GLUT1 are successful; only a crystal structure holds the promise of revealing the precise roles of specific residues in ligand binding.

The structural determinants which make a sugar a suitable ligand for GLUT1 have been explored using epimers, deoxy and fluorodeoxy derivatives of D-glucose as inhibitors of L-sorbose transport.[46, 47] It was shown that 1) sugars locked in a pyranose ring (1-deoxyglucose and glucosides) bind to the transporter, and 2) epimerization or substitution of a hydroxyl group by hydrogen or fluorine at C-1, C-3 and C-6 of D-glucose significantly diminishes apparent affinity. These observations suggest that the physiological substrate is D-glucopyranose, which interacts with GLUT1 through hydrogen bonds at C-1, C-3 and C-6. D-glucal was also found to be an effective inhibitor

of *L*-sorbose transport, indicating that a chair conformation of the sugar is not critical. Finally, bulky nonpolar substituents at C-1 and C-4 or C-6 yield impermeant ligands with high apparent affinities when applied to the cytoplasmic and extracellular faces of the transporter, respectively, suggesting two conformations of the transport site: an inward-facing conformation in which a hydrophobic domain is exposed near C-1 and an outward-facing conformation in which a hydrophobic domain is exposed near C-4 and C-6.

MODELS OF THE SUGAR TRANSPORT CYCLE

Human erythrocyte sugar transport has been studied for over four decades. The transport shows the classical characteristics of facilitated diffusion: saturation, competitive and noncompetitive inhibition, and trans-acceleration (which eliminates a simple pore or channel).[8] The majority of results of steady-state[48, 49a,b, 50] and transient[51] kinetic studies, particularly recent ones, yield kinetic parameters consistent with an alternating conformer model of transport, in which a single sugar binding site is alternately exposed to one side of the membrane or the other, but never to both sides simultaneously. Evidence from inhibition and fluorescence studies are consistent with the existence of (at least) one inside-facing and one outside-facing conformation of the transporter. The nontransported inhibitors phloretin and maltose are competitive with external glucose and noncompetitive with internal glucose, suggesting that they interact with an outward-facing conformer; conversely, cytochalasin B appears to interact with an inward-facing conformer.[8] Two spectroscopically distinct states of purified GLUT1 bound to such side-specific ligands have been detected[52] and a fluorescence transient corresponding to a single half-turnover has been observed[53].

The alternating conformer model is the simplest model of transport consistent with kinetic data; the actual transport mechanism may be more complex. The effects of sugars on cytochalasin B binding[54] and patterns of inhibition of glucose transport by combinations of cytochalasin B and maltose[55] have been interpreted to indicate the

presence of 2 distinguishable binding sites per carrier unit. It has also been argued that the transport mechanism depends on the oligomeric state of GLUT1 in the membrane.[28] Two models have been proposed which incorporate these observations yet retain kinetics indistinguishable under most experimental conditions from those of the alternating conformer model.[56] These models feature binding sites simultaneously exposed at both membrane faces.

THE PRESENT STRATEGY

Studies of transport kinetics offer but a crude level of description of mechanism: experimental parameters (half-saturation concentrations and maximal velocities) obtained in steady-state experiments are complicated composites of microscopic rate and equilibrium constants. The alternating conformer model is merely the simplest of an infinite family of models consistent with observed transport kinetics.

The comparison of ligand binding behavior of GLUT1 with transport behavior permits at least partial deconvolution of the elementary components of the transport cycle and thus provides a complementary test of mechanism. Prior to work in this laboratory, no direct assay of sugar binding to glucose transporters in erythrocyte membranes had been employed. Transport competition studies yield inhibition constants for sugars which again are related to microscopic dissociation constants in a model-dependent fashion. Interpretation of sugar inhibition of cytochalasin B binding likewise depends on the assumed model of transport and inhibition thereof. Although fluorescence assays have been used to measure sugar binding to the purified protein, thus far attempts in this laboratory to replicate reported measurement of intrinsic fluorescence in erythrocyte ghosts and intact cells[35, 57] have been unsuccessful.[58] The affinity of GLUT1 for sugars is sufficiently low that classical measurements of binding such as equilibrium dialysis are inapplicable. However, methods which detect an exchange-averaged signal *may* be used

to monitor binding. The nuclear Overhauser effect between two ^{1}H nuclei on a sugar molecule provides such a signal.

The approach employed here to study the molecular events involved in glucose transport was to directly observe sugar binding to GLUT1 using ^{1}H NMR. In the next chapter, the physical basis of the transferred NOE binding assay is described. In Chapter 3, the study begins with identification of the NMR-observable binding of D-glucose in erythrocyte membrane suspensions as binding to GLUT1. The binding assay is then applied (Chapter 4) to preparations of erythrocyte membranes differing in exposure of the extracellular and cytoplasmic membrane faces to test the adequacy of the alternating conformer model as a description of GLUT1 mechanism. In Chapter 5, the effect of the transport inhibitor cytochalasin B on NMR-observable binding is investigated. The results presented here demonstrate for the first time that both α- and β-D-glucose bind to GLUT1, indicate that the transporter bears at least two sugar binding sites in addition to the transport site(s) of the one- and two-site models previously elaborated, one of which is specific for the α anomer, and provide further evidence for the existence of ternary complexes of GLUT1, sugar and cytochalasin B. In the concluding chapter of this thesis, a model is presented which reconciles the presence of additional sites with the observed kinetics of glucose transport.

REFERENCES

1. Pessin, J. E., and Bell, G. I., Ann. Rev. Physiol., **54** (1992) 911-930.

2. Celenza, J. L., Marshall-Carlson, L., and Carlson, M., Proc. Natl. Acad. Sci. (USA), **85** (1988) 2130-2134.

3. Henderson, P. J. F., Res. Microbiol., **141** (1990) 316-328.

4. Henderson, P. J. F., Curr. Opin. Struct. Biol., **1** (1991) 590-601.

5. Burant, C. F., Sivitz, W. I., Fukumoto, H., Kayano, T., Nagamatsu, S., Seino, S., Pessin, J. E., and Bell, G. I., Rec. Prog. Horm. Res., **47** (1991) 349-388.

6. Mueckler, M., Caruso, C., Baldwin, S. A., Panico, M., Blench, I., Morris, H. R., Allard, W. J., Lienhard, G. E., and Lodish, H. F., Science **229** (1985) 942-945.

7. Elliot, K. R. F., and Craik, J. D., Biochem. Soc. Trans., **10** (1983) 12-13.

8. Stein, W. D., Transport and Diffusion Across Cell Membranes, pp. 231-337, Academic Press, Orlando, 1986.

9. Gould, G. W., Brant, A. M., Shepherd, P. R.., Khan, B. B., McCoid, S., and Gibbs, E.M., Diabetologia, **35** (1992) 304-309.

10. Silverman, M., Ann. Rev. Biochem., **94** (1991) 757-794.

11. Mueckler, M., Diabetes, **39** (1990) 6-11.

12. Kayano, T., Burant, C. F., Fukumoto, H., Gould, G. W., Fan, Y.-S., Eddy, R. L., Byers, M. G., Shows, T. B., Seino, S., and Bell, G. I., J. Biol. Chem., **265** (1990) 13276-13282.

13. Jacquez, J. A., Am. J. Physiol., **246** (1984) R289-R298.

14. De Vivo, D. C., Trifiletti, R. R., Jacobson, R. I., Rosen, G. M., Behmand, R. A., and Harik, S. I., New Engl. J. Med., **325** (1991) 703-709.

15. Steck, T. L., J. Cell. Biol., **62** (1974) 1-19.

16. Kasahara, M., and Hinkle, P. C., J. Biol. Chem., **252** (1977) 7384-7390.

17. Carruthers, A., and Melchior, D. L., Biochemistry, **23** (1984) 2712-2718.

18. Wheeler, T. J., Biochim. Biophys. Acta, **859** (1986) 180-188.

19. Sarkar, H. K., Thorens, B., Lodish, H. F., and Kaback, H. R., Proc. Natl. Acad. USA, **85** (1988) 5463-5467.

20. Keller, K., Strube, M., and Mueckler, M., J. Biol. Chem., **264** (1989) 18884-18889.

21. Oka, Y., Asano, T., Shibasaki, Y., Lin, J.-L., Tsukuda, K., Katagiri, H., Akanuma, Y., and Takaku, F., Nature, **345** (1990) 550-553.

22. Gorga, F. R., Baldwin, S. A., and Lienhard, G. E., Biochem. Biophys. Res. Commun., **91** (1979) 955-958.

23. Sogin, D. C., and Hinkle, P. C., J. Supramol. Struct., **8** (1978) 447-451.

24. Feugeas, J.-P., Néel, D., Pavia, A. A., Laham, A., Goussault, Y., and Derappe, C., Biochim. Biophys. Acta, **1030** (1990) 60-64.

25. Feugeas, J.-P., Néel, D., Goussault, Y., and Derappe, C., Biochim. Biophys. Acta, **1066** (1991) 59-62.

26. Baldwin, J. M., Gorga, J. C., and Lienhard, G. E., J. Biol. Chem., **256** (1981) 3685-3689.

27. Baldwin, S. A., Baldwin, J. M., and Lienhard, G. E., Biochemistry, **21** (1982) 3836-3842.

28. Hebert, D. N., and Carruthers, A., J. Biol. Chem., **267** (1992) 23829-23838.

29. Mascher, E., and Lundahl, P., Biochim. Biophys. Acta, **945** (1988) 350-359.

30. Jung, C. Y., Hsu, T. L., Hah, J. S., Cha, C., and Haas, M. N., J. Biol. Chem., **255** (1980) 361-364.

31. Jarvis, S. M., Ellory, J. C., and Young, J. D., Biochim. Biophys. Acta, **855** (1986) 312-315.

32. Pessino, A., Hebert, D. N., Woon, C. W., Harrison, S. A., Clancy, B. M., Buxton, J. M., Carruthers, A., and Czech, M. P., J. Biol. Chem., **266** (1991) 20213-20217.

33. Hebert, D. N., and Carruthers, A., Biochemistry, **30** (1991) 4654-4658.

34. Jones, M. N., and Nickson, J. K., FEBS Letts., **115** (1980) 1-8.

35. Carruthers, A., Biochemistry, **25** (1986) 3592-3602.

36. Birnbaum, M. J., Haspel, H. C., and Rosen, O. M., Proc. Natl. Acad. Sci (USA), **83** (1986) 5784-5789.

37. Cairns, M. T., Alvarez, J., Panico, M., Gibbs, A. F., Morris, H. R., Chapman, D., and Baldwin, S. A., Biochim. Biophys. Acta, **905** (1987) 295-310.

38. Davies, A., Meeran, K., Cairns, M. T., and Baldwin, S. A., J. Biol. Chem., **262** (1987) 9347-9352.

39 May, J. M., Buchs, A., and Carter-Su, C., Biochemistry, **29** (1990) 10393-10398.

40. Alvarez, J., Lee, D. C., Baldwin, S. A., and Chapman, D., J. Biol Chem., **262** (1987) 3502-3509.

41. Chin, J. J., Jung, E. K. Y., Chen, V., and Jung, C. Y., Proc. Natl. Acad. Sci. (USA), **84** (1987) 4113-4116.

42. Chin, J. J., Jung, E. K. Y., and Jung, C. Y., J. Biol. Chem., **261** (1986) 7101-7105.

43. Jung, E. K. Y., Chin, J. J., and Jung, C. Y., J. Biol. Chem., **261** (1986) 9155-9160.

44. Chin, J. J., Jhun, B. H., and Jung, C. Y., Biochemistry, **31** (1992) 1945-1951.

45. Garcia, J. C., Strube, M., Leingang, K., Keller, K., and Mueckler, M. M., J. Biol. Chem., **267** (1992) 7770-7776.

46. Barnett, J. E. G, Holman, G. D., and Munday, K. A., Biochem. J., **131** (1973) 211-221.

47. Barnett, J. E. G., Holman, G. D., Chalkey, R. A., and Munday, K. A., Biochem. J., **135** (1975) 417-429.

48. Lowe, A. G., and Walmsley, A. R., Biochim. Biophys. Acta, **857** (1986) 146-154.

49. a) Wheeler, T. J., Biochim. Biophys. Acta, **862** (1986) 387-398.

    b) Wheeler T. J., and Whelan, J. D., Biochemistry, **27** (1988) 1441-1450.

50. Gasbjerg, P. K., and Brahm, J., Biochim. Biophys. Acta, **1062** (1991) 83-93.

51. Lowe, A. G., and Walmsley, A. R., <u>Biochim. Biophys. Acta</u>, **903** (1987) 547-550.

52. Appleman, J. R., and Lienhard, G. E., <u>Biochemistry</u>, **29** (1989) 8221-8227.

53. Appleman, J. R., and Lienhard, G. E., <u>J. Biol. Chem.</u>, **260** (1985) 4575-4578.

54   Helgerson, A. L., and Carruthers, A., <u>J. Biol. Chem.</u>, **262** (1987) 5464-5475.

55. Carruthers, A., and Helgerson, A. L., <u>Biochemistry</u>, **30** (1991) 3907-3915.

56. Carruthers, A., <u>Biochemistry</u>, **30** (1991) 3898-3906.

57. Janoshazi, A., Kifor, G., and Solomon, A. K., <u>J. Membrane Biol.</u>, **123** (1991) 191-207.

58. Cavagnero, S., personal communication.

CHAPTER 2

^{1}H NMR: THE TRANSFERRED NUCLEAR OVERHAUSER EFFECT AS A

BINDING ASSAY

INTRODUCTION

Nuclear magnetic resonance (NMR) spectroscopy has found wide application in the study of chemical exchange, both conformational changes and chemical reactions. Any interaction of nuclear spins with the magnetic field or with each other may be exploited to yield information on exchange. The timescales accessible range from that of rotations about a single bond to chemical processes as slow as one has patience to examine. If the chemical exchange is slow relative to the nuclear interaction, the different chemical populations give rise to distinct values of the NMR-observable parameter that reflects the interaction, while a chemical process fast relative to the interaction timescale yields a single exchange-averaged NMR-observable parameter. Of particular interest here is the dipole-dipole interaction between ^1H nuclei and its dependence on the correlation time for molecular tumbling. This interaction, through its experimental manifestations spin-lattice and spin-spin relaxation and nuclear Overhauser enhancements, serves as an excellent spectroscopic probe of ligand-macromolecule binding equilibria.

It was noted in 1972 that irradiation of protein proton resonances in mixtures of bovine neurophysin II and Lys-vasopressin resulted in diminution of peptide proton signal intensities.[1] The authors deduced that the effect arose from enhanced cross-relaxation in the (slowly tumbling) bound complex. The effect was dubbed the transferred nuclear Overhauser effect (TRNOE). An analysis of intramolecular TRNOEs for a small ligand binding to a macromolecule by Clore and Gronenborn ten years later[2a, b] demonstrated the extraordinary ability of the TRNOE to transfer information on bound ligand conformation to the readily observed free or exchange-averaged ligand signals, and pointed out that, in contrast to most NMR techniques, sensitivity of the TRNOE increases with increasing molecular weight of the bound complex. Since then, the TRNOE has been applied to evaluation of the bound conformations of a wide variety of ligands, from small molecules such as 5'-adenosine monophosphate[2a] and acetylcholine[3]

up to *20-residue peptides*[4]. The target proteins examined range from 10 to >150 kDa molecular weight, including enzymes[2a, b], monoclonal antibodies[5], lectins[6] and the reconstituted acetylcholine receptor[3].

In studies of bound ligand conformation, independent estimates of equilibrium constants are required in order to extract internuclear distances. Work in this laboratory, including the present study, has made novel use of the TRNOE to directly determine equilibrium constants for binding of sugars to sites on transport proteins in their native membranes. In the discussion below, dipolar coupling and the NOE in a system of two spin-$\frac{1}{2}$ nuclei are briefly reviewed and the limiting cases of fast and slow molecular motion are examined. Next, the effect of chemical exchange on relaxation is considered, culminating in an expression for the TRNOE under conditions of fast exchange on the timescale of free ligand spin-lattice relaxation. In the final section of this chapter, it is shown that for ligands binding to very large proteins, modification of the two-spin TRNOE expression to include the observed relaxation properties of spins in such proteins results in a very simple expression, linear in binding site concentration, from which dissociation constants may be readily calculated and which is the analytical form used throughout the remainder of this thesis.

DIPOLAR INTERACTION AND THE NOE IN A SYSTEM OF TWO HOMONUCLEAR SPINS-$\frac{1}{2}$

^{1}H is a spin-$\frac{1}{2}$ nuclide; it is extensively documented that the interaction of an ^{1}H nucleus with other magnetic dipoles is the dominant mechanism of proton spin relaxation (although spin-rotation coupling is significant for methyl group protons).[7] To reveal the physical basis of the negative signals observed in TRNOE experiments, the theory of the dipolar interaction in a system of two homonuclear spins-$\frac{1}{2}$ is recapitulated below.

Figure 2.1 depicts an energy level diagram for such a system of two spins I and S. In this discussion, scalar coupling is assumed weak, so the states of the system are given

Figure 2.1

Energy Level Diagram for Two Dipolar-Coupled Homonuclear Spins-$\frac{1}{2}$ (I, S). Scalar coupling, if present, is assumed weak. The W_{i-j} represent zero, single and double quantum transition probabilities as indicated.
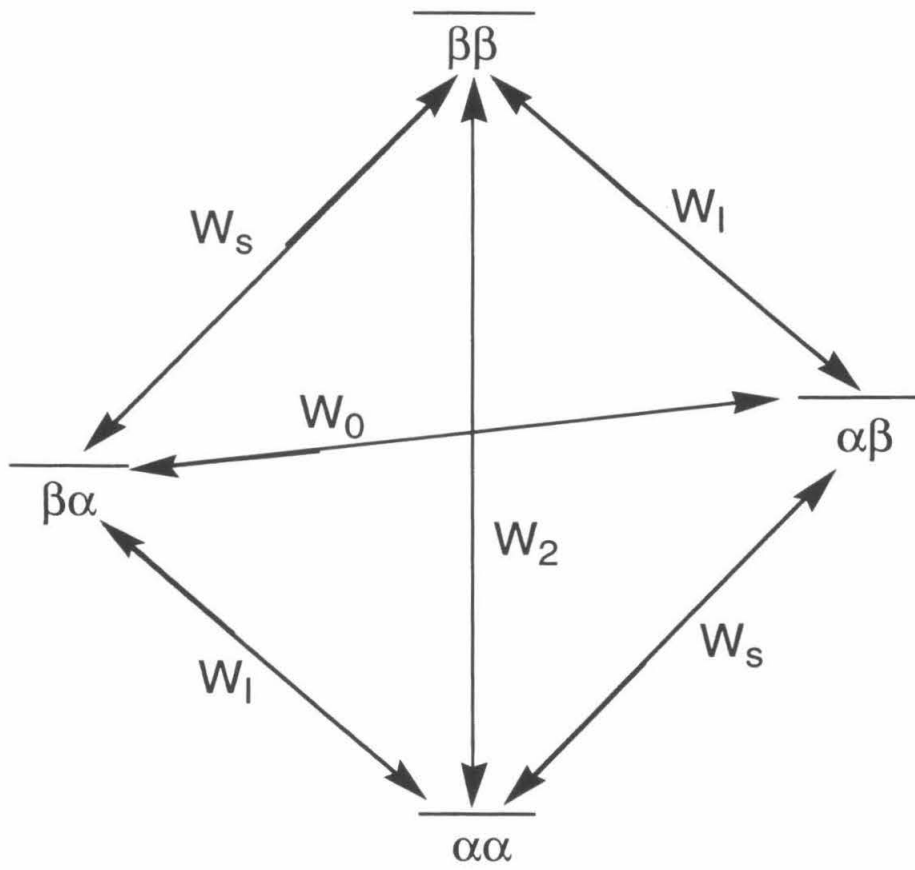
by the product functions. The probabilities per unit time W_{i-j} for zero (W_0), single (W_1, W_S) and double quantum transitions (W_2) are also indicated. For the dipole-dipole interaction subject to perturbations which are a random function of time, perturbation theory yields for the W_{ij}:

$$W_0 = \frac{1}{10} R^2 \frac{\tau_c}{1+(\omega_I - \omega_S)^2 \tau_c^2} \quad , \tag{2.1}$$

$$W_I = \frac{3}{20} R^2 \frac{\tau_c}{1+\omega_I^2 \tau_c^2} \quad , \tag{2.2}$$

$$W_S = \frac{3}{20} R^2 \frac{\tau_c}{1+\omega_S^2 \tau_c^2} \quad , \tag{2.3}$$

$$W_2 = \frac{3}{5} R^2 \frac{\tau_c}{1+(\omega_I + \omega_S)^2 \tau_c^2} \quad , \tag{2.4}$$

where $R = (\mu_o/4\pi) h\gamma_I\gamma_S r_{IS}^{-3}$ is the dipolar interaction constant, ω_I and ω_S are the Larmor frequencies of I and S, and τ_c is the correlation time for rotation of the internuclear vector.[8] For homonuclear I and S, $\omega_I - \omega_S << \omega_I, \omega_S$; also, for any likely value of τ_c, $(\omega_I - \omega_S)^2\tau_c^2 << 1$. Thus W_0 increases essentially linearly with τ_c, while W_I, W_S and W_2 are comparable to W_0 for $\omega\tau_c << 1$, but become negligable for slow molecular tumbling ($\tau_c > 10^{-9}$ s for ^{1}H at 500 MHz).

I and S signal intensities are proportional to the expectation values of the operators I_z and S_z. Relaxation of $\langle I_z \rangle$ and $\langle S_z \rangle$ following a perturbation is described by the well-known Solomon equations[9]:

$$\frac{d}{dt}\langle I_z \rangle = -\rho_I(\langle I_z \rangle - \langle I_{z0} \rangle) - \sigma_{IS}(\langle S_z \rangle - \langle S_{z0} \rangle) \quad , \tag{2.5}$$

$$\frac{d}{dt}\langle S_z \rangle = -\rho_S(\langle S_z \rangle - \langle S_{z0} \rangle) - \sigma_{IS}(\langle I_z \rangle - \langle I_{z0} \rangle) \quad . \tag{2.6}$$

Here $\langle I_{z0} \rangle$ and $\langle S_{z0} \rangle$ are equilibrium values, ρ_I and ρ_S are the "direct" dipolar relaxation rate constants for I and S, and σ_{IS} is the rate constant for cross-relaxation between I and S. In terms of the W_{ij}, the rate constants are

$$\rho_I = W_0 + 2W_I + W_2 \ , \tag{2.7}$$

$$\rho_S = W_0 + 2W_S + W_2 \ , \tag{2.8}$$

$$\sigma_{IS} = W_2 - W_0 \ . \tag{2.9}$$

Under steady-state saturation of S transitions, $\frac{d}{dt}\langle I_z \rangle = 0$ and $\langle S_z \rangle = 0$;

rearrangement of equation (2.5) yields

$$\langle I_z \rangle = \langle I_{z0} \rangle + \frac{\sigma_{IS}}{\rho_I}\langle S_{z0} \rangle \ . \tag{2.10}$$

Since $\langle I_{z0} \rangle = \langle S_{z0} \rangle$ for homonuclear I and S, the fractional enhancement in I signal

intensity upon saturation of S, $f_I\{S\}$, is then

$$f_I\{S\} = \frac{\langle I_z \rangle - \langle I_{z0} \rangle}{\langle I_{z0} \rangle} = \frac{\sigma_{IS}}{\rho_I} \ . \tag{2.11}$$

This is the standard expression for the steady-state NOE. Expressing σ_{IS} and ρ_I in terms

of equations (2.1) - (2.4) and substituting $\omega \approx \omega_I \approx \omega_S$ (homonuclear case) recasts

equation (2.11) in a form which reveals the dependence of $f_I\{S\}$ on $\omega\tau_c$:

$$f_I\{S\} = \frac{5 + \omega^2 \tau_c^2 - 4\omega^4 \tau_c^4}{10 + 23\omega^2 \tau_c^2 + 4\omega^4 \tau_c^4} \ . \tag{2.12}$$

It can be seen that in the extreme narrowing limit ($\omega\tau_c \ll 1$), *e.g.*, for a small ligand

molecule free in solution, $f_I\{S\} = 0.5$. In the limit of slow molecular tumbling

($\omega\tau_c \gg 1$), such as for a ligand bound to a large protein, W_0 dominates relaxation and

$f_I\{S\} = -1$. It is precisely this dependence of the NOE on molecular motion which is

exploited in the TRNOE experiment; chemical exchange carries the negative NOEs of

bound ligand spins into the free (or exchange-averaged) ligand signal.

THE TRNOE IN AN EXCHANGING TWO-SPIN SYSTEM

Magnetization Transfer Pathways. If the spins I and S are on a small ligand

molecule L which is exchanging between the bulk solution and a binding site on a protein

E according to

$$E + L \overset{f}{\underset{b}{\rightleftharpoons}} EL \ , \tag{2.13}$$

neglecting for the moment intermolecular dipole-dipole interactions, pathways of magnetization transfer among free and bound I and S and to the lattice may be represented as

$$(2.14)$$
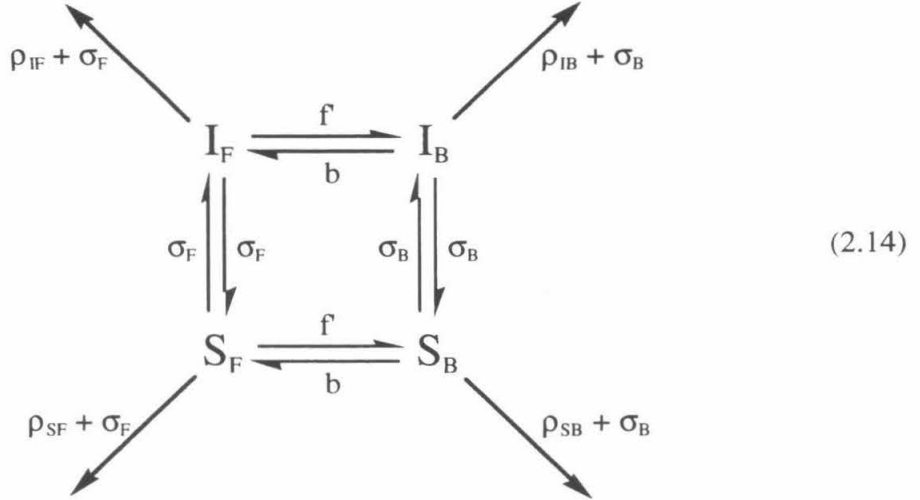
Here I_F, S_F and I_B, S_B are the two nuclei on free and bound ligand, respectively, $f' = f[E]$ is the pseudo-first order rate constant for the association of E and L, σ_F and σ_B are the rate constants for IS cross-relaxation in the free and bound forms, and ρ_{IF}, ρ_{IB}, ρ_{SF}, and ρ_{SB} are the direct dipolar relaxation rate constants for I_F, I_B, S_F, and S_B respectively. Scheme (2.14) portrays pictorially the interplay of chemical exchange and cross-relaxation. Mathematically, the system is described by the coupled equations

$$\frac{d}{dt}\langle I_z \rangle_F = -\rho_{IF}(\langle I_z \rangle_F - \langle I_{z0} \rangle_F) - \sigma_F(\langle S_z \rangle_F - \langle S_{z0} \rangle_F) + b\langle I_z \rangle_B - f'\langle I_z \rangle_F \ , \tag{2.15}$$

$$\frac{d}{dt}\langle I_z \rangle_B = -\rho_{IB}(\langle I_z \rangle_B - \langle I_{z0} \rangle_B) - \sigma_B(\langle S_z \rangle_B - \langle S_{z0} \rangle_B) - b\langle I_z \rangle_B + f'\langle I_z \rangle_F \ , \tag{2.16}$$

$$\frac{d}{dt}\langle S_z \rangle_F = -\rho_{SF}(\langle S_z \rangle_F - \langle S_{z0} \rangle_F) - \sigma_F(\langle I_z \rangle_F - \langle I_{z0} \rangle_F) + b\langle S_z \rangle_B - f'\langle S_z \rangle_F \ , \tag{2.17}$$

$$\frac{d}{dt}\langle S_z \rangle_B = -\rho_{SB}(\langle S_z \rangle_B - \langle S_{z0} \rangle_B) - \sigma_B(\langle I_z \rangle_B - \langle I_{z0} \rangle_B) - b\langle S_z \rangle_B + f'\langle S_z \rangle_F \ . \tag{2.18}$$

The last two terms in each of equations (2.15) - (2.18) account for the effect of chemical exchange.[10] Note that for homonuclear I and S, $\langle I_{z0} \rangle_F = \langle S_{z0} \rangle_F$ and $\langle I_{z0} \rangle_B = \langle S_{z0} \rangle_B$.

In addition to its effect on spin state populations (equations (2.15) - (2.18)), exchange may significantly affect the observed NMR spectrum in two important ways. First, in general I_F and I_B, and S_F and S_B, may experience different shielding and thus have different chemical shifts. Free and bound spins will only give rise to separate resonances in the spectrum if exchange is slow relative to the chemical shift difference. This is germane to the present discussion because the expressions derived for the TRNOE depend in general on which signal or signals are irradiated (S_F, S_B, or $S_F + S_B$) and which observed (I_F, I_B, or $I_F + I_B$). Given the relatively small chemical shift dispersion of proton resonances and the small effect of binding on chemical shifts in diamagnetic systems, exchange in weakly binding systems is very likely to be fast on the chemical shift scale.

More importantly, transverse relaxation, like longitudinal relaxation, is affected by cross-relaxation and exchange: the evolution of transverse components of magnetization such as $\langle I_+ \rangle_F = \langle I_x + iI_y \rangle_F$ is described by a set of coupled equations analogous to equations (2.15) - (2.18). In the limit of slow molecular motions, zero quantum transitions (linear in τ_c) dominate transverse relaxation and T_2^{-1} becomes large. Thus for a large bound complex the bound ligand resonances will be very broad. Then the transverse relaxation timescale places a stringent constraint on steady-state TRNOE measurements: if exchange is slow relative to bound ligand spin T_2^{-1}, the S_B resonance (or the component of S_{obs} due to S_B if exchange is fast on the chemical shift scale) will be too broad to saturate while maintaining the low field strength required for selectivity of irradiation; at best partial saturation may be achieved. Likewise, signal due to I_B will be lost in the baseline. In short, for such systems S_B cannot be saturated nor I_B measured unless exchange is fast on the timescale of bound ligand transverse relaxation. In this fast exchange regime, the observed resonances will be Lorentzian, but broadened relative to free ligand signal to an extent determined by the bound ligand transverse relaxation rate and the relative populations of free and bound forms.

The Steady-State Z-Magnetizations. In order to relate signal enhancements to concentrations of chemical species, we use macroscopic z-magnetizations instead of the expectation values of operators. If N ligand molecules are in the sample, these magnetizations are $M_{IF} = N\langle I_z \rangle_F$, $M_{IB} = N\langle I_z \rangle_B$, $M_{SF} = N\langle S_z \rangle_F$, and $M_{SB} = N\langle S_z \rangle_B$. The total equilibrium z-magnetization of I, M_0, and the equilibrium z-magnetizations of free and bound I, M_{F0} and M_{B0}, are given by $M_0 = M_{F0} + M_{B0} = N\langle I_{z0} \rangle$.

Assuming a sufficiently large bound complex that the linewidth of the S_B resonance is much greater than 50 Hz (the order of magnitude of useful bandwidths for selective irradiation in ^1H spectra), we consider two limiting solutions to equations (2.15) - (2.18): a) saturation of S_F (slow exchange on bound T_2^{-1} timescale) and b) saturation of S_{obs} (fast exchange on this scale).

Case a). Saturation of the S_F resonance gives the initial conditions $M_{SF} = 0$ and $\frac{d}{dt}M_{SF} = 0$. Equations (2.15), (2.16) and (2.18) are then readily solved for M_{IF} and M_{IB} using Laplace transforms.[11] After a time short relative to typical irradiation times, the following steady-state values obtain:

$$M_{IF} = \frac{(\rho_{IF} + \sigma_F)M_{F0} + bM_{IB}}{(\rho_{IF} + f')} \quad , \tag{2.19}$$

$$M_{IB} = \frac{\begin{array}{c}(\rho_{IF} + f')[(\rho_{IB} + \sigma_B)(\rho_{SB} + b) - \sigma_B(\rho_{SB} + \sigma_B)]M_{B0} \\ + f'(\rho_{IF} + \sigma_F)(\rho_{SB} + b)M_{F0}\end{array}}{(\rho_{IF} + f')[(\rho_{IB} + b)(\rho_{SB} + b) - \sigma_B^2] - bf'(\rho_{SB} + b)} \quad . \tag{2.20}$$

Case b). Saturation of S_{obs} yields the initial conditions $M_{SF} = M_{SB} = 0$, $\frac{d}{dt}M_{SF} = \frac{d}{dt}M_{SB} = 0$, and equations (2.15) and (2.16) yield the steady-state values

$$M_{IF} = \frac{(\rho_{IF} + \sigma_F)(\rho_{IB} + b)M_{F0} + b(\rho_{IB} + \sigma_B)M_{B0}}{(\rho_{IF} + f')(\rho_{IB} + b) - bf'} \quad , \tag{2.21}$$

$$M_{IB} = \frac{(\rho_{IB} + \sigma_B)(\rho_{IF} + f')M_{B0} + f'(\rho_{IF} + \sigma_F)M_{F0}}{(\rho_{IF} + f')(\rho_{IB} + b) - bf'} \quad . \tag{2.22}$$

In equations (2.19) - (2.22) there are two contributions to each enhancement; this is particularly evident in the last two expressions. For example, the first term in the

numerator of equation (2.21) reflects direct enhancement of I_F by cross-relaxation with S_F, while the second term reflects the indirect contribution, *via* chemical exchange, of cross-relaxation between I_B and S_B.

The TRNOE: Slow and Fast Exchange Limits. By analogy to equation (2.11), the Overhauser enhancement in I upon irradiation of S is obtained by incorporation of the relevant M_{IF} and M_{IB} expressions into

$$f_I\{S\} = \frac{M_{IF} + M_{IB} - M_0}{M_0} \quad . \tag{2.23}$$

In general, M_{IF} and M_{IB} in equations (2.19) - (2.22) are complicated functions of the exchange rate and the various relaxation rates. However, if exchange is either a) much slower or b) much faster than longitudinal relaxation, far simpler expressions result. Examination of these two cases shows that the TRNOE will only reveal binding to sites on a large macromolecule in the fast exchange regime.

Case a). Exchange slow on the ρ_{IF} timescale (f' << ρ_{IF}) is also slow on the ρ_{IB} timescale. (By construction, $\rho_{IB} > \rho_{IF}$. For excess ligand, b < f'; thence f' << ρ_{IF} implies b << ρ_{IB}.) Furthermore, since for free ligand (in extreme narrowing), longitudinal and transverse relaxation rates are equal, this scenario represents slow exchange on the transverse relaxation timescales as well. Irrespective, then, of the exchange regime on the chemical shift timescale, S_F is irradiated and I_F observed. Equations (2.19) and (2.23) yield in this limit

$$f_I^F\{S_F\} = \frac{M_{IF} - M_{F0}}{M_{F0}} = \frac{\sigma_F}{\rho_{IF}} \quad , \tag{2.24}$$

identical to equation (2.11). Thus in the slow exchange regime, the observed NOE yields no information about the bound ligand.

Case b). If ligand is in fast exchange on both the ρ_{IF} and ρ_{IB} timescales (f' >> ρ_{IF} and b >> ρ_{IB}), it is also likely to be in fast exchange on each of the corresponding transverse relaxation timescales. It is not necessary to make this assumption, however;

the expressions obtained for the TRNOE in this case using either equations (2.19) and (2.20) or (2.21) and (2.22) in equation (2.23) are identical:

$$f_I\{S\} = \frac{\sigma_F M_{F0} + \sigma_B M_{B0}}{\rho_{IF} M_{F0} + \rho_{IB} M_{B0}} \quad . \tag{2.25}$$

Here, the cross-relaxation rate is averaged in the numerator and the direct relaxation rate is averaged in the denominator. The condition for a negative TRNOE in this case is

$$\left| \sigma_B M_{B0} \right| > \left| \sigma_F M_{F0} \right| \quad . \tag{2.26}$$

This is a significant result. Since for a large bound complex $|\sigma_B| \gg |\sigma_F|$, fast exchange amplifies the effect of binding sites on the TRNOE, rendering the technique useful for characterizing binding of ligands to very small amounts of protein.

For many systems of interest (including the GLUT1-glucose system examined in the present work), neither exchange rates nor bound ligand relaxation rates are known. For a large excess of ligand over binding sites, if one makes the reasonable assumption that exchange is fast relative to free ligand relaxation but drops assumptions about the relative magnitudes of exchange and bound ligand relaxation rates, an expression is obtained for $f_I\{S\}$ similar in form to equation (2.25):

$$f_I\{S\} = \frac{\sigma_F M_{F0} + \dfrac{b\sigma_B}{b + \rho_{IB}} M_{B0}}{\rho_{IF} M_{F0} + \dfrac{b\rho_{IB}}{b + \rho_{IB}} M_{B0}} \quad . \tag{2.27}$$

In this case, a negative TRNOE will be observed when the condition

$$\left| \frac{b\sigma_B}{b + \rho_{IB}} M_{B0} \right| > \left| \sigma_F M_{F0} \right| \tag{2.28}$$

is met. The assumption of fast exchange on the ρ_{IF} timescale implies $b \gg \sigma_F$; like constraint (2.26), constraint (2.28) will be met for a large excess of free over bound ligand if $|\sigma_B| \gg |\sigma_F|$.

To summarize this section, when exchange is fast relative to free ligand relaxation and cross-relaxation is much faster for bound ligand than for free, the TRNOE proves a sensitive assay of binding in which the effect of a small number of binding sites is propagated into detectable ligand signal. We next examine the effect of additional relaxation pathways on the form of $f_I\{S\}$ and show that, for sufficiently large bound complexes, a further simplification of equation (2.27) results which is not predicted by the two-spin treatment.

THE TRNOE IN A MULTISPIN SYSTEM

The preceding development is simplistic in its assumption of IS dipolar coupling as the sole mechanism of relaxation. In any real system, additional relaxation mechanisms will be present and may be significant. Of particular interest here are intramolecular dipolar interactions of I and S with additional ligand spins and intermolecular interactions with protein spins.

Consider a system which contains, in addition to I and S, ligand spin(s) J and protein spin(s) X. Coupling to J affects relaxation of both I_F and I_B. For free ligand, we have instead of equation (2.11)[12]

$$f_I^F\{S\} = \frac{\sigma_{IS}^F - \sum_J f_J^F\{S\}\sigma_{IJ}^F}{R_I^F} \qquad (2.29)$$

where the symbols in the numerator are modified slightly from the previous discussion to distinguish the various pairwise interactions,

$$R_I^F = \rho_{IS}^F + \sum_J \rho_{IJ}^F \qquad (2.30)$$

is the total dipolar relaxation rate constant of I_F, and cross-correlation has been neglected. The additional numerator terms in equation (2.29) represent three-spin effects, indirect cross-relaxation between I and S *via* spins J.

For bound ligand, in addition to ligand spin(s) J, protein spin(s) X contribute to indirect cross-relaxation between I and S. Thus, again neglecting cross-correlation, the NOE for bound ligand is

$$f_I^B\{S\} = \frac{\sigma_{IS}^B - \sum_J f_J^B\{S\}\sigma_{IJ}^B - \sum_X f_X^B\{S\}\sigma_{IX}^B}{R_I^B} \tag{2.31}$$

with

$$R_I^B = \rho_{IS}^B + \sum_J \rho_{IJ}^B + \sum_X \rho_{IX}^B \quad . \tag{2.32}$$

The inclusion of additional spins doesn't alter the fundamental phenomenon which gives rise to the TRNOE: as in the two spin case, in the spin diffusion limit ($\omega\tau_c \gg 1$), $f_I^B\{S\}$ in equation (2.31) goes to -1.

Although the numerators in equations (2.29) and (2.31) no longer represent the microscopic rate constants for cross-relaxation between I and S, they still represent overall rate constants for the transfer of magnetization between I and S in free and bound ligand, respectively. As such, the numerators may be considered *effective* cross-relaxation rate constants which can be substituted for σ_F and σ_B in two-spin expressions for the TRNOE. For fast exchange on the R_I^F timescale, then, the multispin analog of equation (2.27) is

$$f_I\{S\} = \frac{\sigma_{F,eff}M_{F0} + \dfrac{b\sigma_{B,eff}}{b + R_I^B}M_{B0}}{R_I^F M_{F0} + \dfrac{bR_I^B}{b + R_I^B}M_{B0}} \tag{2.33}$$

where

$$\sigma_{F,eff} = \sigma_{IS}^F - \sum_J f_J^F\{S\}\sigma_{IJ}^F \quad , \tag{2.34}$$

$$\sigma_{B,eff} = \sigma_{IS}^B - \sum_J f_J^B\{S\}\sigma_{IJ}^B - \sum_X f_X^B\{S\}\sigma_{IX}^B \quad . \tag{2.35}$$

Comparing equations (2.27) and (2.33), it will be noted that the presence of additional spins affects the magnitude of the TRNOE through differences between the

two spin and multispin relaxation terms, rendering internuclear distance determination more complicated; indeed, since the enhancements for all bound I, S spin pairs go to -1 when $\omega\tau_c \gg 1$, spatial information disappears entirely for very large bound complexes. While these multispin effects make the steady-state TRNOE essentially useless for conformational analysis, they do not impair its usefulness as a binding assay: information about concentrations of chemical species in solution is contained entirely in M_{F0} and M_{B0}, which are independent of the complexity of the spin system considered. Since the condition for detection of binding is

$$\left| \frac{b\sigma_{B,eff}}{b + R_I^B} M_{B0} \right| > \left| \sigma_{F,eff} M_{F0} \right| \tag{2.36}$$

by analogy to condition (2.28), and since $|\sigma_{B,eff}| > |\sigma_B|$ for a large bound complex, while $|\sigma_{F,eff}| < |\sigma_F|$, the presence of additional spins actually increases the sensitivity of the TRNOE to binding.

A SIMPLER TRNOE EXPRESSION FOR LARGE PROTEINS

Consideration of the actual relaxation behavior observed for nuclei in large proteins leads to a final, important modification of the TRNOE expression. The two-spin treatment predicts for $\omega\tau_c \gg 1$ that $\rho_B = -\sigma_B$; likewise, the multispin treatment predicts $R_I^B = -\sigma_{B,eff}$. In 1976, Kalk and Berendsen presented a model for ^1H magnetic relaxation in large proteins.[13] In this model, cross-relaxation is very fast and increases with τ_c per equation (2.1), but overall longitudinal relaxation is much slower, being governed by the coupling of rotating methyl groups on protein side chains to the lattice. This model is substantively supported by experiment: 1) spin-lattice relaxation rates for most protons in a given protein are generally found to be roughly equal, evidencing significant cross-relaxation[14], 2) cross-relaxation rates determined from initial rates of TRNOE buildup[2b] have been observed to increase with increasing bound complex molecular weight, while

3) spin-lattice relaxation rates for protons in proteins of molecular weight > 20 kDa are about 1 s^{-1}, independent of τ_c.[13, 15]

These observations suggest that for a sufficiently large protein, R_I^B in equation (2.32) will not be the rate constant predicted based on the large τ_c of the bound complex, but will rather reflect the relatively slow relaxation of protons in large proteins. In this case, $\dfrac{b\sigma_{B,eff}}{b + R_I^B} M_{B0}$ remains large relative to $\sigma_{F,eff} M_{F0}$, but $\dfrac{bR_I^B}{b + R_I^B} M_{B0}$ is *not* large relative to $R_I^F M_{F0}$. Assuming then that the denominator in equation (2.33) differs only slightly from $R_I^F M_{F0}$, the TRNOE expression collapses to a simpler form:

$$f_I\{S\} \approx \frac{\sigma_{F,eff}}{R_I^F} + \frac{\sigma_{B,eff}}{R_I^F}\frac{M_{B0}}{M_{F0}} \quad . \tag{2.37}$$

The first term in equation (2.37) is simply the NOE for the free ligand, $f_I^F\{S\}$ of equation (2.29); the effect of binding sites is contained entirely within the second term.

It is now convenient to express M_{B0}/M_{F0} in terms of the concentrations of ligand and protein. The dissociation constant K_D for equilibrium (2.13) is

$$K_D = \frac{b}{f} = \frac{[E][L]}{[EL]} \quad . \tag{2.38}$$

Let $L_t = [L] + [EL]$ and $E_t = [E] + [EL]$ be the total concentrations of ligand and protein in the sample, respectively. Now $M_{B0}/M_{F0} = [EL]/[L]$. We are interested in systems in which ligand is in great excess over binding sites, so we take $[L] \approx L_t$; with this approximation, we find $M_{B0}/M_{F0} \approx [EL]/L_t$, and

$$f_I\{S\} \approx f_I^F\{S\} + \frac{\sigma_{B,eff}}{R_I^F}\frac{[EL]}{L_t} \quad . \tag{2.39}$$

If in addition $E_t << K_D$, then $M_{B0}/M_{F0} \approx E_t/(K_D + L_t) = E_t K_D^{-1}[L_t^{-1}/(L_t^{-1} + K_D^{-1})]$ and we obtain a TRNOE expression suitable for analysis of ligand binding:

$$f_I\{S\} \approx f_I^F\{S\} + \frac{\sigma_{B,eff}}{R_I^F}\frac{E_t}{K_D}\frac{L_t^{-1}}{L_t^{-1} + K_D^{-1}} \quad . \tag{2.40}$$

According to equation (2.41), a plot of $f_I\{S\} - f_I^F\{S\}$ *vs.* L_t^{-1} will be rectangular-hyperbolic; K_D^{-1} may readily be extracted as the value of L_t^{-1} at which $f_I\{S\} - f_I^F\{S\}$ is half-maximal. The maximum amplitude of the TRNOE also contains useful information: if E_t and R_I^F are known, the amplitude yields an estimate of $\sigma_{B,eff}$.

To qualify the validity of equation (2.40), we now review the assumptions under which it was derived. First, it was assumed that chemical exchange is fast relative to R_I^F: observation of a negative TRNOE when $L_t \gg E_t$ is sufficient evidence that this condition is met. Second, to obtain equation (2.37) from equation (2.33), it was assumed that the exchange-averaged spin-lattice relaxation rate (denominator of equation (2.34)) differs little from R_I^F. This may be verified by measuring spin-lattice relaxation of spin I in the absence and presence of binding sites. Finally, equation (2.40) was derived from equation (2.37) under the assumption $L_t \gg E_t$; it predicts that the TRNOE will be a linear function of E_t, providing another test of its applicability.

THE PRESENT APPLICATION OF THE TRNOE BINDING ASSAY

Several further modifications of equation (2.40) are in order before we move on to application of the TRNOE binding assay. First, in the experiments described, E_t is not known precisely. Instead, the total protein P in the sample is measured. If the proportionality constant Z is defined by $E_t = ZP$, the TRNOE can be normalized to the protein concentration in order to facilitate comparison among data sets:

$$\frac{f_I\{S\} - f_I^F\{S\}}{P} = \frac{\sigma_{B,eff}}{R_I^F} ZK_D^{-1} \frac{L_t^{-1}}{L_t^{-1} + K_D^{-1}} \quad . \tag{2.41}$$

Second, in the following chapters, data will frequently be presented for the TRNOEs observed in both anomers in an equilibrium mixture of α- and β-D-glucose in the presence of macromolecular binding sites. Consider two such ligands α and β, present in a constant ratio r (defined by $\alpha_t = r\beta_t$) and competing for a single class of sites. The TRNOEs observed in α and β signals are

$$\frac{f_I^{\alpha}\{S\} - f_I^{F,\alpha}\{S\}}{P} = \frac{\sigma_{B,eff}^{\alpha}}{R_I^{F,\alpha}} \frac{Z}{K_{D\alpha}} \frac{\alpha_t^{-1}}{\alpha_t^{-1} + K_{D\alpha}^{-1} + r^{-1}K_{D\beta}^{-1}} \quad , \tag{2.42}$$

$$\frac{f_I^{\beta}\{S\} - f_I^{F,\beta}\{S\}}{P} = \frac{\sigma_{B,eff}^{\beta}}{R_I^{F,\beta}} \frac{Z}{K_{D\beta}} \frac{\beta_t^{-1}}{\beta_t^{-1} + rK_{D\alpha}^{-1} + K_{D\beta}^{-1}} \quad , \tag{2.43}$$

respectively, where the additional sub- and superscripts serve to distinguish microscopic rate and equilibrium constants for the two ligands. We focus on the apparent dissociation constants measured as a function of either α_t or β_t:

$$K_{D,app}^{-1}(\alpha_t) = K_{D\alpha}^{-1} + r^{-1}K_{D\beta}^{-1} \quad , \tag{2.44}$$

$$K_{D,app}^{-1}(\beta_t) = rK_{D\alpha}^{-1} + K_{D\beta}^{-1} \quad , \tag{2.45}$$

i.e., each apparent K_D reflects binding of both ligands. Equations (2.44) and (2.45) provide an important consistency test: if the binding observed in the two ligands is to the same class of sites, their apparent K_Ds will differ by the factor r.

Finally, equations (2.40) - (2.45) are appropriate for ligand binding to a single class of binding sites, as in scheme (2.13). If there exist j *different* classes of binding sites at which ligand L is in fast exchange, the TRNOE will reflect the contributions of the classes additively:

$$\frac{f_I\{S\} - f_I^F\{S\}}{P} = \sum_j \frac{\sigma_{Bj,eff}}{R_I^F} \frac{Z_j}{K_{Dj}} \frac{L_t^{-1}}{L_t^{-1} + K_{Dj}^{-1}} \tag{2.46}$$

where $\sigma_{B,eff}$, Z and K_D may differ for each class of sites. In general, a plot of the normalized TRNOE *vs.* L_t^{-1} will in this case yield a sum of rectangular hyperbolae. However, it will be shown in Chapter 4 below that constraining relations among the classes of sites j, such as those provided by the alternating conformer model of GLUT1 glucose transport, reduce equation (2.46) to a tractable form which can be used both to assay ligand affinities and to test the model.

REFERENCES

1. Balaram, P., Bothner-By, A. A., and Dadok, J., J. Am. Chem. Soc., 94 (1972) 4015-4017.

2. a) Clore, G. M., and Gronenborn, A. M., J. Magn. Reson., **48** (1982) 402-417.
    b) Clore, G. M., and Gronenborn, A. M., J. Magn. Reson., **53** (1983) 423-442.

3. Behling, R. W., Yamane, T., Navon, G., and Jelinski, L. W., Proc. Natl. Acad Sci. (USA), **85** (1988) 6721-6726.

4. Ni, F., Konishi, Y., and Scheraga, H. A., Biochemistry, **29** (1990)

5. Glasel, J. A., J. Mol. Biol., **209** (1989) 747-759.

6. Bevilacqua, V. L., Thomson, D. S., and Prestegard, J. H., Biochemistry, **29** (1990) 5529-5537.

7. Vold, R. L., and Vold, R. R., Prog. NMR Spectrosc., **12** (1978) 79-133.

8. Abragam, A., The Principles of Nuclear Magnetism, pp. 264-300, Oxford University Press, London, 1961.

9. Solomon, I., Phys. Rev., **99** (1955) 559-565.

10. McConnell, H. M., J. Chem. Phys., **28** (1958) 430-433.

11. Goldman, M., Quantum Description of High-Resolution NMR in Liquids, pp. 216-219, Clarendon Press, Oxford, 1988.

12. Neuhaus, D., and Williamson, M., The NOE in Structural and Conformational Analysis, pp. 63-101, VCH Publishers, New York, 1989.

13. Kalk, A., and Berendsen, H. J. C., J. Magn. Reson., **24** (1976) 343-366.

14. Sykes, B. D., Hull, W. E., and Snyder, G. H., Biophysical J., **21** (1978) 137-146.

15. Ishima, R., Shibata, S., and Akasaka, K., J. Magn. Reson., **91** (1991) 455-465.

CHAPTER 3

THE D-GLUCOSE ^{1}H TRNOE IN HUMAN ERYTHROCYTE GHOST MEMBRANE
SUSPENSIONS: OBSERVATION OF SUGAR BINDING TO *GLUT1*

INTRODUCTION

Earlier work in this laboratory demonstrated a negative NOE between two hydrogens of D-glucose in the presence of human erythrocyte membranes.[1] This TRNOE was shown to be stereospecific, occurring in D- but not L-glucose, and was essentially abolished by the glucose transport inhibitor cytochalasin B, indicating that it arose from binding of D-glucose to a site or sites on erythrocyte GLUT1. In the present study, these results were replicated and elaborated: in this chapter, after characterizing the signals and enhancements observed and demonstrating that the simplified expression derived in the preceding chapter applies, we marshall the evidence, old and new, that binding to GLUT1 is solely responsible for the stereospecific component of the observed TRNOE.

EXPERIMENTAL SECTION

Materials. D- and L-glucose and dithiothreitol (DTT) were obtained from Calbiochem. Cytochalasins A, B and D, 21,22-dihydro-cytochalasin B, D-mannitol, phloretin and phenylmethylsulfonyl fluoride (PMSF) were obtained from Sigma. Phenyl-β-D-glucoside and 4,6-O-ethylidene-D-glucose were obtained from Aldrich. n-Propyl-β-D-glucoside was prepared according to the literature procedure.[2] Deuterated solvents ^2H_2O and DMSO-d_6 were obtained from Cambridge Isotope Labs; $Na^2H_2PO_4$ was obtained from MSD Isotopes. All other chemicals used were reagent grade or better. Outdated packed human erythrocytes were a gift of the Los Angeles chapter of the American Red Cross.

Preparation of Ghost Membranes. All procedures were carried out at 0-4°C unless otherwise noted. Leaky white ghosts were prepared by osmotic shock hemolysis.[3] One unit of outdated erythrocytes of any type, not more than ten days out of date, was diluted to 1500 ml in phosphate-buffered saline (PBS) (150 mM NaCl, 5 mM NaH_2PO_4, pH adjusted to 8.0 with NaOH). The cell suspension was aliquotted into six 250 ml

centrifuge tubes (pre-wetted with PBS to minimize hemolysis). Cells were then pelleted by centrifugation at 8000 rpm in a Sorvall GSA rotor (10,400 x g_{max}) for 20 min; the supernatant and buffy coat were subsequently removed by aspiration. The cells were washed twice more by resuspension in PBS, pelleting (10 min at 3000 rpm or 1500 x g_{max}) and aspiration of the supernatant and remaining buffy coat. Following the wash steps, the cells were lysed. The pellets were resuspended in 5p8(+) buffer (5 mM NaH_2PO_4, pH 8, 130 μM DTT and 10 μM PMSF), mixed thoroughly by shaking and pelleted by centrifugation at 11,000 rpm (19,700 x g_{max}) for 20 min. The supernatant and any dense pellet (unhemolyzed cells or resealed membranes) underlying the ghost membranes were removed by aspiration. Four or five cycles of resuspension in 5p8(+) (PMSF was omitted from the final wash), centrifugation and aspiration of the supernatant were typically sufficient to leave a clear supernatant and milky-white pellets. The pellets were pooled and stored at 4°C for NMR experiments the next day. The leaky white ghosts obtained by this protocol had the expected distribution of morphologies when examined by phase contrast microscopy: largely spherical or toroidal, roughly 10% flattened disks ("crushed" ghosts, see below), a very small proportion (1-2%) of crenated morphologies, and no evident spiculation.

Immediately prior to NMR experiments, leaky ghosts were crushed and solvent-exchanged by the following protocol. Aliquots of leaky ghost pellet were mixed with one volume of 5pD7.4 buffer (5 mM $Na^2H_2PO_4$ in ^2H_2O, p^2H adjusted to 7.4 with NaO^2H (meter reading corrected for isotope effect)) by vortexing, left standing at room temperature for 15 min to allow hydrogen exchange, then pelleted by ultracentrifugation at 38,000 rpm in a 60Ti rotor (145,000 x g_{max}) for 30 min. Supernatant was pipetted off and the cycle of resuspension in fresh 5pD7.4 (2 volumes), equilibration and ultracentrifugation was repeated 3 times. The final pellet was opalescent in appearance and contained 25-30 mg/ml total ghost protein. Phase contrast microscopy revealed the ghosts thus obtained to be morphologically heterogeneous. Most of the crushed ghost

morphologies examined appeared to retain the native "right-side-out" orientation of the membrane. The predominant morphology (~90%) was cup-shaped with a much smaller internal volume than that of intact erythrocytes (by eye, $V_{CG} < 0.1V_{RBC}$). The remainder comprised a variety of distorted cup-shaped and toroidal morphologies and small proportions (~5%) of crenated and multilamellar morphologies.

NMR Sample Preparation. The final crushed ghost pellet obtained after ultracentrifugation was immediately resuspended in 5pD7.4, yielding a crushed ghost stock suspension for NMR experiments. For experiments in which the total protein concentration was varied, the pellet was resuspended in the minimum amount of buffer required to make quantitative transfers of the viscous suspension feasible (roughly one volume) and divided into aliquots which were further diluted with buffer as desired. For experiments at constant protein concentration, 1.25-1.3 volumes of buffer were added to the pellet.

For experiments in which sugar concentration was varied, 0.40 ml aliquots of ghost stock suspension were transferred into ultra-thin-walled 5 mm O.D. NMR tubes *via* syringe with an 18 ga. needle. Appropriate amounts of sugar stock solutions in 5pD7.4 were added and the final volume made up to 0.45 ml with 5pD7.4. For cytochalasin B (CB) controls of these experiments, 1 μl of CB stock in DMSO-d_6 was also added. The samples were then capped and mixed by repeated inversion and "shaking down" of the NMR tubes. For experiments in which inhibitor concentration was varied, ghost and sugar stocks were mixed prior to transfer to NMR tubes. 0.445 ml of this ghost/sugar mixture was aliquotted into each NMR tube, and the final volume was made to 0.45 ml with inhibitor stock in DMSO-d_6 and/or DMSO-d_6 as appropriate. Control experiments (not shown) showed that this amount of DMSO-d_6 had no effect on the appearance of the NMR spectrum or on sugar proton relaxation rates or TRNOEs. NMR samples were stored at room temperature in the dark until they could be analyzed spectroscopically;

generally, 12-16 hours passed between sample preparation and the completion of NMR experiments.

Sugar stock solutions were made well in advance of NMR sample preparation to allow equilibration of anomers and were usually made fresh for each experiment. Inhibitor stocks in DMSO-d_6 were used for many successive experiments and, once prepared, were kept frozen when not in use.

^{1}H NMR Spectroscopy. Spectra were acquired at 500.13 MHz on a Bruker AM 500 spectrometer. Sample temperature was $(20.0 \pm 0.5)°C$. Samples were placed in the magnet and spun at ~20 Hz for 10-15 min to allow thermal and mechanical equilibration prior to shimming. Extensive shimming (on the shapes of the swept lock signal and the FID) of each sample was generally required. The standard acquisition parameters for membrane-containing samples were as follows. The Redfield 214 pulse sequence was used to suppress the residual solvent signal[4]; the spectral width was 4000 Hz, with the carrier frequency positioned and pulse lengths adjusted to optimize solvent suppression. 16K time domain points were acquired, yielding a 2.0 s acquisition time. Steady-state NOEs were generated by 3.4 s pre-irradiation of the appropriate resonance(s) at a nominal decoupler power of 0.06 mW. No additional relaxation delay was used. An off-resonance irradiated spectrum of each sample was also acquired, as were on- and off-resonance irradiated spectra of a blank sample which contained only ghosts and buffer. Dummy scans (2 or 4) were employed prior to acquisition. A total of 64 transients were accumulated for each spectrum.

Processing of NMR Data. The unapodized FIDs were zero-filled to 32K points and Fourier-transformed. Broad spectral features (membrane proton signals, baseline distortions from the solvent suppression pulse sequence) were removed by subtraction of the appropriate blank spectrum from each experimental spectrum. On-resonance irradiated spectra were then subtracted from their off-resonance counterparts to yield TRNOE difference spectra. Linear baseline correction and integration of the peaks of

interest in both the blank-corrected off-resonance irradiated spectrum and the difference spectrum gave the experimental TRNOE values. The processing procedure was repeated three times on the data for each sample and the results averaged, to minimize phasing and baseline correction error.

Except where indicated, the NMR samples contained 9-11 mg total ghost protein per ml, determined by the Lowry protein assay[5] as modified[6] for membrane proteins. Unless otherwise indicated, samples compared to one another, such as those in the same plot, were made from the same ghost stock suspension.

RESULTS AND DISCUSSION

The ^{1}H NMR Spectrum of D-Glucose. Mutarotation of glucose is slow on the timescale of ^{1}H chemical shifts, hence the α and β anomers of the pyranose each contribute a set of resonances to the ^{1}H NMR spectrum (a portion of which is shown in Figure 3.1). At 20°C in 5pD7.4 the equilibrium anomeric distribution was determined to be 38.0% α and 62.0% β by integration of the anomeric proton peaks. The assignments indicated were determined by COSY spectroscopy and corroborate literature assignments.[7] The spectrum of L-glucose is identical. Examination of the spectrum and the structure of D-glucose shows that H-2 and H-4 of both anomers are appropriate pairs of nuclei for facile observation of an NOE: (1) they are well-resolved spectrally, both from each other and from other resonances, and (2) they are close enough to one another for significant dipolar interaction (2.65 Å in the crystal structure of β-D-glucose). Indeed, irradiation of the overlapping H-4α and H-4β multiplets produces ~4.5% enhancements in both H-2α and H-2β signal intensities in undegassed 5pD7.4 (Figure 3.2).

The Effect of Erythrocyte Membranes on the NOE. The presence of crushed ghosts has no effect on chemical shifts in the ^{1}H NMR spectra of either D- or L-glucose. However, the NOEs in H-2α and H-2β of D-glucose, but not L-glucose, are inverted

Figure 3.1

The Chemical Structure and Partial ^{1}H NMR Spectrum of D-Glucopyranose. The dispositions of substituents at C-1 for the two anomers are indicated in the structure. Only the spectral region containing the resonances of interest in the present work is displayed. The spectrum was obtained in 5pD7.4 buffer at 20 °C. Chemical shifts are referenced relative to external TSPSA.
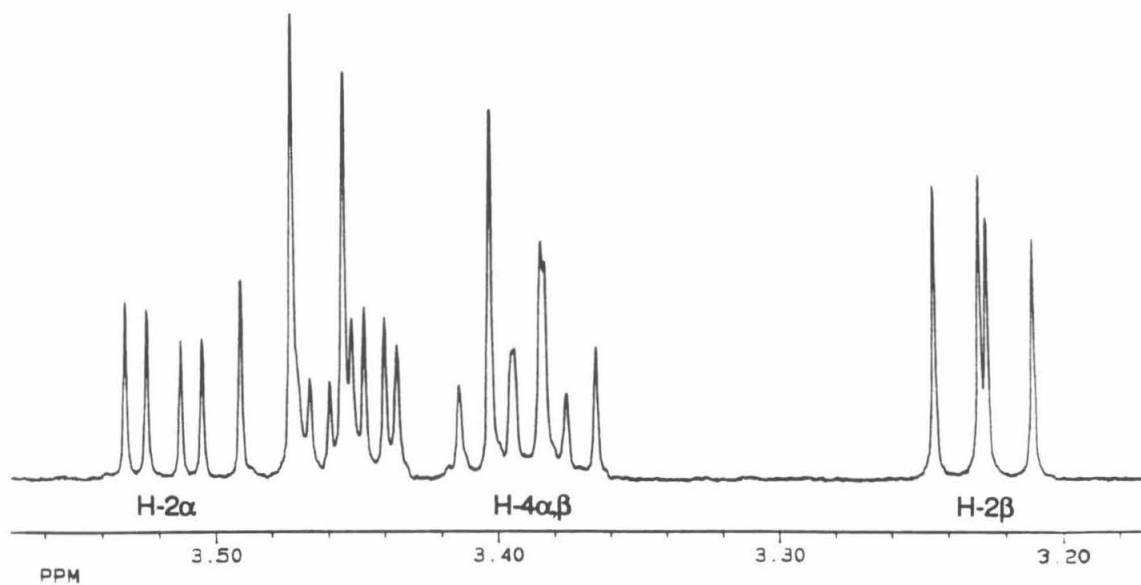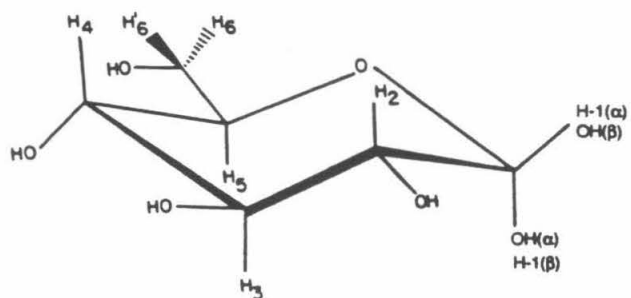
Figure 3.2

The D-Glucose NOE in Buffer. Upper trace: the NOE difference spectrum obtained as described in the Experimental Section (however, no solvent suppression was used). Lower trace: the off-resonance irradiated spectrum. The sample was 20 mM D-glucose in undegassed 5pD7.4 buffer at 20 °C. The enhancements observed in the H-2α and H-2β resonances are 4.0% and 4.5%, respectively, for the experiment shown.
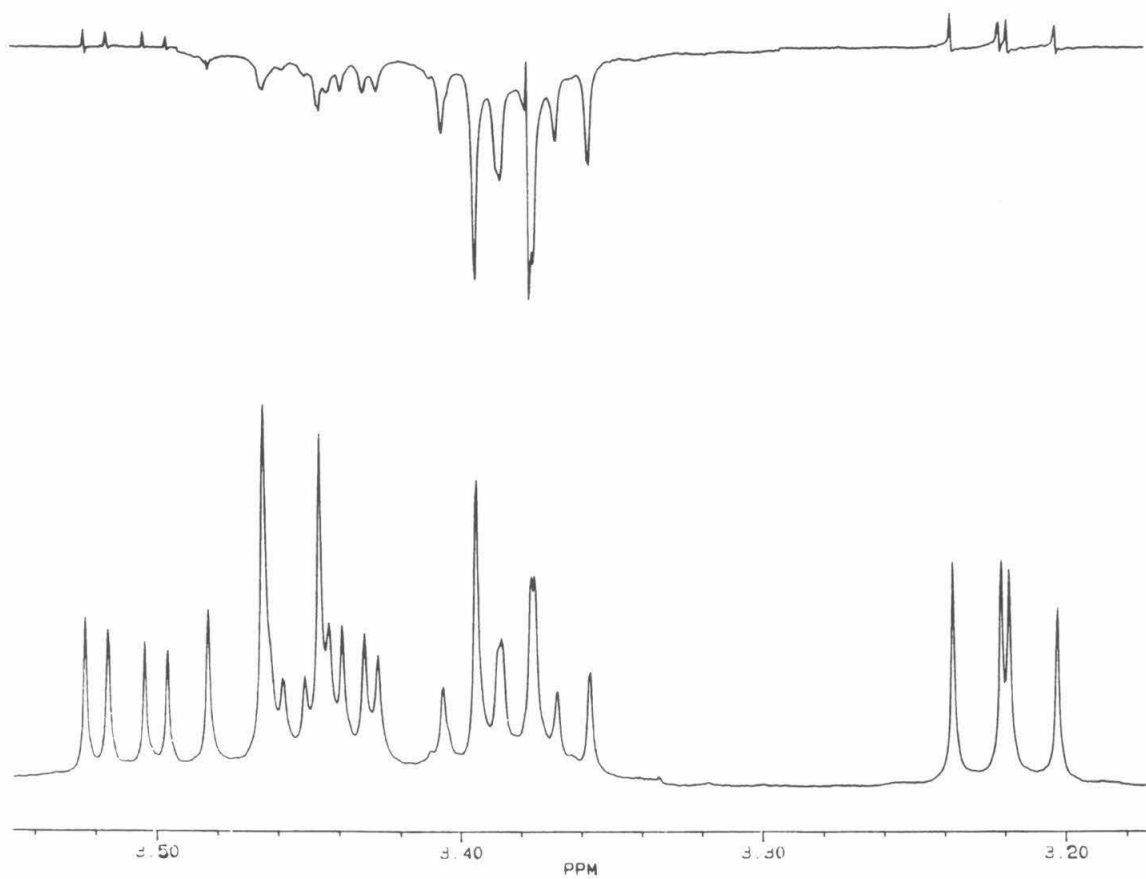
Figure 3.3

The Glucose NOE in Erythrocyte Ghosts. NOE difference spectra of 20 mM L-glucose (upper trace) and 20 mM D-glucose (middle trace) in crushed ghost suspension. The lower trace is the off-resonance irradiated reference spectrum (D-glucose). The concentration of GLUT1 was ~10 μM. The NOEs in the two samples shown, expressed as percentages of the peak areas in the appropriate reference spectra, are 0.6% for H-2α and 1.5% for H-2β of L-glucose, and -9.1% for H-2α and -16.4% for H-2β of D-glucose. Assay conditions and parameters are described in the Experimental Section.

H-2α   H-4α,β   H-2β

3.9   3.8   3.7   3.6   3.5   3.4   3.3   3.2
                        PPM

(Figure 3.3), indicating the presence of stereospecific binding sites. In Chapter 2, the relationship

$$f_I\{S\} \approx f_I^F\{S\} + \frac{\sigma_{B,eff}}{R_I^F} \frac{E_t}{K_D} \frac{L_t^{-1}}{L_t^{-1} + K_D^{-1}} \tag{3.1}$$

was derived for the TRNOE in ligand spins exchanging between bulk solution and a small homogeneous population of macromolecular binding sites (cf. equation (2.40)). This expression is valid if (1) exchange is fast on the timescale of free ligand spin-lattice relaxation, and (2) the dependence of the exchange-averaged spin-lattice relaxation rate on binding site concentration is sufficiently weak that it may be treated as constant. The first criterion is met whenever a negative NOE is observed for a gross excess of ligand over binding sites. It is established below that the binding arises from GLUT1 sites; thus in Figure 3.3 the ligand to binding site ratio is approximately 3×10^3 (if only one site is present per GLUT1 monomer). That the second criterion is met was established in the previous report[1] in two ways. First, it was shown that the presence of ghost membranes ([D-glucose] = 15 mM, [GLUT1] $\approx$ 10 μM) increased the spin-lattice relaxation rate of H-2β by only 14%. A similar result was obtained in the present work (not shown). Second, and more to the point, the TRNOE was found to be directly proportional to binding site concentration at constant [D-glucose]. In the present study, when crushed ghosts were used, the H-2β TRNOE decreased linearly over the useful concentration range of ghost suspensions (Figure 3.4).

Characterization of the TRNOE: Cytochalasin B-Sensitivity. Equation (3.1) describes the TRNOE arising from a homogeneous binding site population. It was shown in the preceeding chapter that, when present, different populations of sites contribute additively to the TRNOE (cf. equation (2.46)). In order to identify the contribution of binding sites associated with GLUT1, the effect of the glucose transport inhibitor cytochalasin B (CB) on the observed TRNOE was examined. This molecule (Figure 3.5) is a potent reversible competitive inhibitor of glucose efflux which is believed to bind to

Figure 3.4

<u>Dependence of the Glucose H-2β TRNOE on Ghost Protein Concentration.</u>   [D-glucose]
= 15.0 mM. Filled circle: D-glucose in buffer; open circles: plus crushed ghosts; open
triangles: plus crushed ghosts and 100 μM cytochalasin B. Relative NOE is the peak area
in the difference spectrum as a fraction of the peak area in the off-resonance irradiated
spectrum. The solid lines are linear least-squares fits, yielding a slope of -0.017 per
mg/ml total ghost protein for glucose plus ghosts. The slope for glucose plus ghosts plus
cytochalasin B does not differ significantly from zero. One mg/ml total ghost protein
corresponds to approximately 0.9 μM GLUT1. Assay conditions and parameters are
described in the Experimental Section.
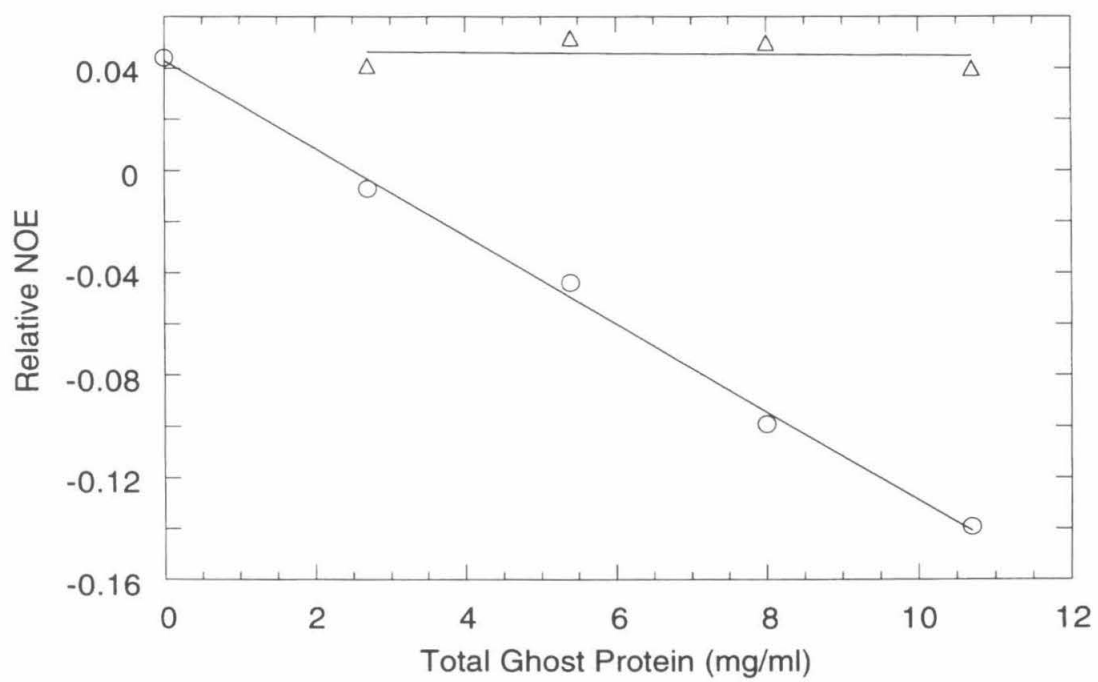
Figure 3.5

Structures of the Cytochalasins Tested for Inhibition of the D-Glucose TRNOE.
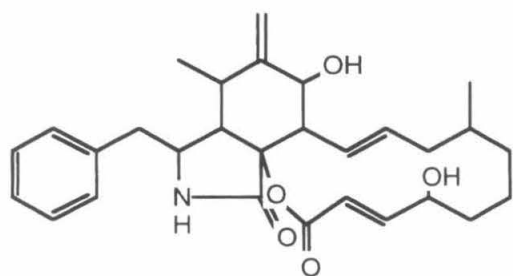
Cytochalasin B
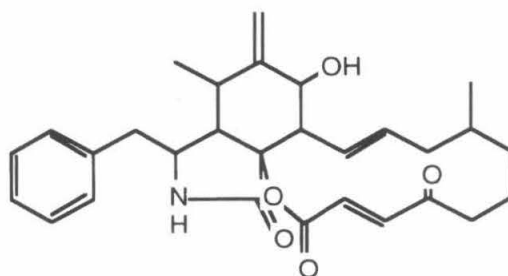
Cytochalasin A
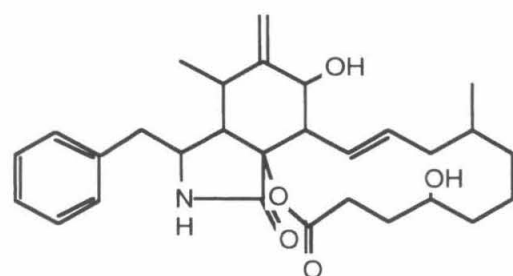
21,22-Dihydro-Cytochalasin B
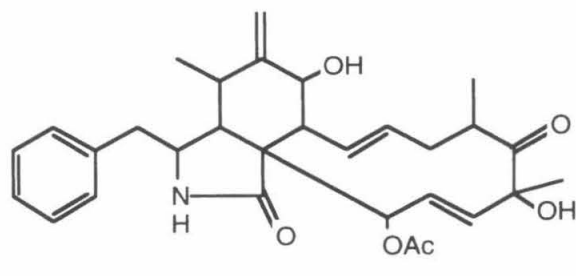
Cytochalasin D

an inward-facing conformation of GLUT1. A saturating concentration of CB essentially

eliminates the D-glucose TRNOE in crushed ghosts (Figure 3.4), indicating that sugar

binding to CB-sensitive sites constitutes *all* of the observed binding.

In many experiments, the NOE in CB-saturated samples (range: -0.005 to 0.052

for H-2β, .007 to .042 for H-2α) was slightly less than the value for D-glucose in buffer

(range: 0.006 to 0.073 for H-2β, 0.01 to 0.045 for H-2α). To determine whether this

effect was due to instrumental or sample variability or to CB-insensitive binding sites, the

dependence of this component on [glucose]$^{-1}$ was examined. Equation (3.1) predicts a

decreasing rectangular hyperbolic dependence of the TRNOE on inverse ligand

concentration. Within the scatter of the data, the CB-insensitive NOEs in H-2β (Figure

3.6) and H-2α (not shown) of D-glucose are independent of [glucose]$^{-1}$ and do not differ

significantly from those of L-glucose. Thus, CB-insensitive binding, if present, is not

detectable; in all subsequent data analyses, the CB-insensitive NOE in a sample

containing membranes is assumed to be the free ligand value in that sample ($f_l^F\{S\}$ of

equation (3.1)). The slight increase of NOE with increasing [glucose]$^{-1}$ in Figure 3.6 may

represent a radiation damping or viscosity effect.

The CB-Sensitive TRNOE Arises from Sugar Binding Sites Associated with

GLUT1. The reversal of the D-glucose TRNOE by CB appears consistent with a single

homogeneous class of CB binding sites, since CB binding is well described by a single

apparent dissociation constant (Figure 3.7). Erythrocyte membranes possess several

classes of CB binding sites, only one of which is sensitive to D-glucose.[8] The D-glucose-

sensitive CB binding sites are on GLUT1: D-glucose-sensitive CB binding has been used

as an assay for purification of GLUT1.[9] Since D-glucose displaces CB from these sites,

there must be one or more classes of D-glucose binding sites associated with them (one of

which may be the CB sites themselves). Microscopic reversibility requires that such

classes of D-glucose sites must be CB-sensitive. By extension, since the CB sites on

Figure 3.6

Cytochalasin B-insensitive H-2β NOE in Crushed Ghosts: Dependence on [Glucose]$^{-1}$.
Open circles: D-glucose (mean ± σ of results from three experiments with different
batches of crushed ghosts); Open triangles: L-glucose (one experiment). [CB] = 100 μM
for all samples. The lines are linear least-squares best-fits to the data, yielding slopes of
0.0139 ± 0.0079 (D-glucose, solid line) and 0.010 ± 0.026 (L-glucose, dashed line).
Assay conditions and parameters are described in the Experimental Section.
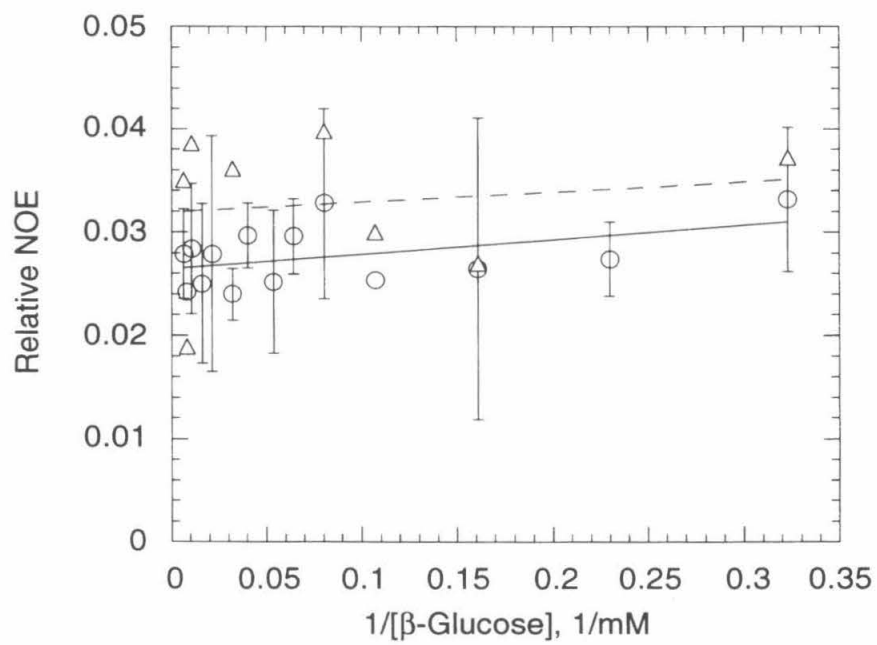
Figure 3.7

The Effect of Cytochalasin B on the D-Glucose TRNOE in Crushed Ghosts. The

TRNOE observed in H-2 of (A) α-D-glucose and (B) β-D-glucose in the equilibrium

mixture at a bulk D-glucose concentration of 10.0 mM ([α-D-glucose] = 3.80 mM, [β-D-

glucose] = 6.20 mM). The solid curves are nonlinear least-squares best fits to the

equation

$$y = a + \frac{b}{2E_t}\left(x + E_t + K_D - \sqrt{(x + E_t + K_D)^2 - 4E_t x}\right)$$

for a homogeneous population of binding sites. E_t is the concentration of GLUT1 (≈ 7

μM for the data shown). The fits yield apparent dissociation constants for CB binding of

(A) 4.6 ± 2.0 μM and (B) 6.0 ± 1.8 μM. Sample preparation and assay parameters are

described in the Experimental Section.
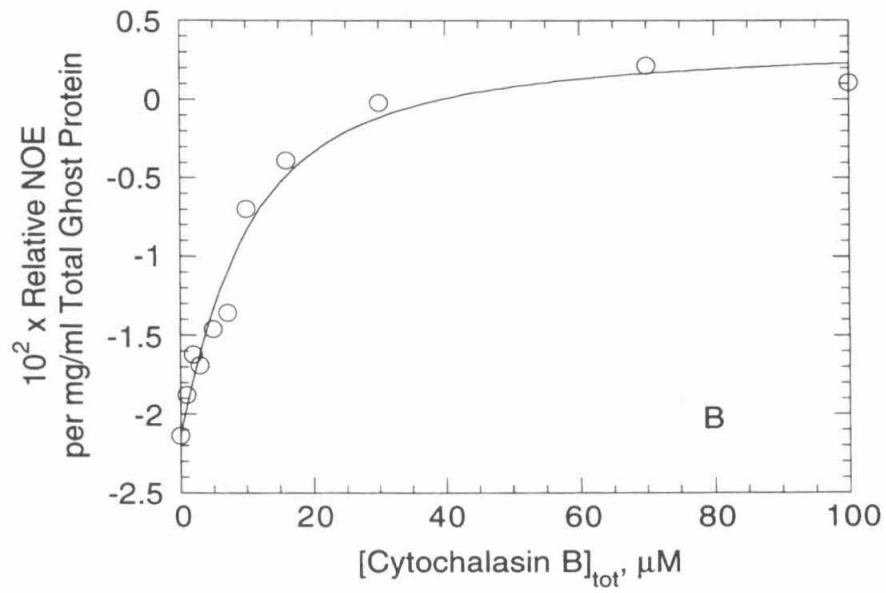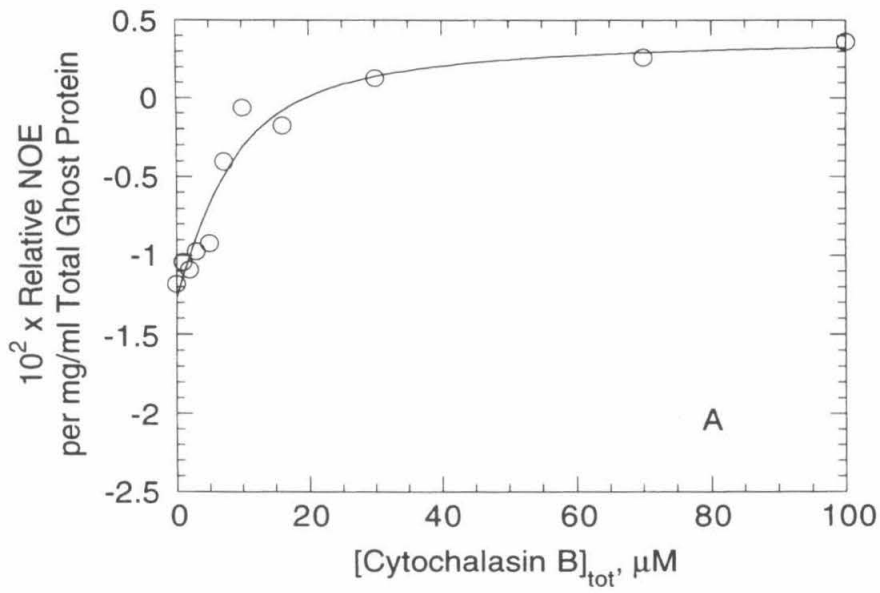
GLUT1 are the only D-glucose-sensitive CB sites present, *all* CB-sensitive D-glucose binding must be to sites associated with this protein.

The above considerations indicate that the observed TRNOE arises entirely from binding of D-glucose to sites associated with sugar transport. The effect on the TRNOE of cytochalasins other than CB supports this conclusion.

Inhibition of the TRNOE by Other Cytochalasins. The effects of three additional cytochalasins on the D-glucose TRNOE were examined: cytochalasin A (CA), 21,22-dihydrocytochalasin B (dihydro-CB) and cytochalasin D (CD) (Figure 3.5). CA inhibits glucose transport (and displaces CB from its D-glucose-sensitive sites) with an apparent affinity 10-fold smaller than that of CB. Neither dihydro-CB nor CD have been found to inhibit glucose transport, nor do they displace CB from sugar-sensitive sites.[10] In contrast, all three bind to D-glucose-insensitive CB sites with high affinities.

In the present work, all three cytochalasins were found to diminish the TRNOEs observed in α- and β-D-glucose in crushed ghosts (Figure 3.8), albeit with widely differing potencies. In particular, CA completely reverses the TRNOE, with a 10-fold smaller apparent affinity than CB, while dihydro-CB is yet another order of magnitude less affine than CA, and CD has only a slight effect over the concentration range examined. The apparent dissociation constants for CA and CB in these experiments are larger than those reported in transport and CB binding studies (Table 3.1), in part because the glucose present in the TRNOE assay samples competes with inhibitor for binding sites. (The origin of the large apparent K_D for CB inhibition of the TRNOE is considered in Chapter 5 below.) But the *relative* effectiveness of the four cytochalasins as inhibitors of the TRNOE parallels their effectiveness as inhibitors of glucose transport and sugar-sensitive CB binding, again pointing to the origin of the D-glucose TRNOE in binding of sugar to sites associated with GLUT1.

Cytochalasin B is known to bind to GLUT1 with a stoichiometry of one molecule CB per molecule of the protein in purified monomeric and dimeric GLUT1, one molecule

Figure 3.8

The Effect of Selected Cytochalasins on the D-Glucose TRNOE in Crushed Ghosts. The TRNOEs observed in H-2α (open triangles) and H-2β (open circles) of D-glucose (bulk [D-glucose] = 10 mM) in the presence of (A) cytochalasin A, (B) 21,22-dihydro-cytochalasin B, and (C) cytochalasin D. The solid curves in (A) and (B) are nonlinear least-squares best fits for a homogeneous population of sites (y = a + bx/(x + K_D)), yielding apparent dissociation constants of (A) 36 ± 12 μM (H-2α data) and 72 ± 25 μM (H-2β data) for CA binding, and (B) 280 ± 130 μM (H-2α data) and 290 ± 90 μM (H-2β data) for dihydro-CB binding. The solid lines in (C) are linear least-squares best fits (y = a + x/K_D) for a homogeneous population of low-affinity sites, yielding apparent dissociation constants for CD binding of 1.3 ± 0.3 mM (H-2α data) and 0.87 ± 0.08 mM (H-2β data). The relationship between apparent dissociation constants derived from H-2α and H-2β TRNOEs in competition experiments is discussed in Chapter 5.
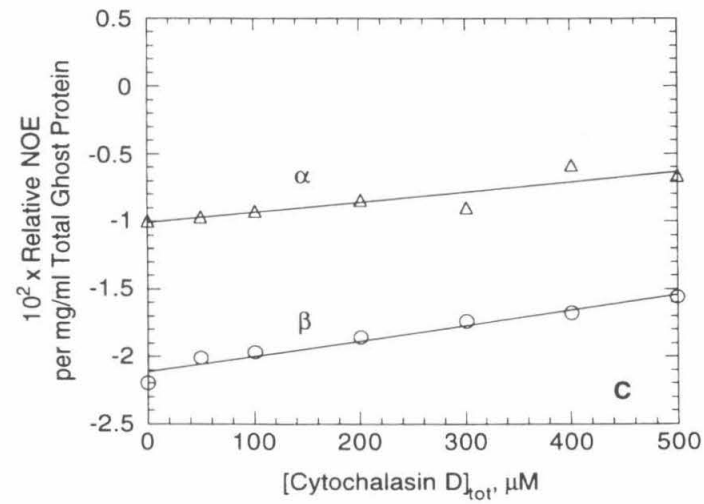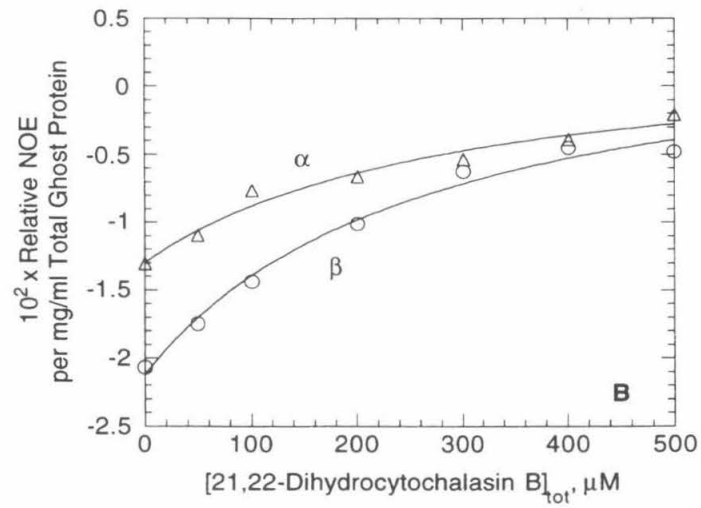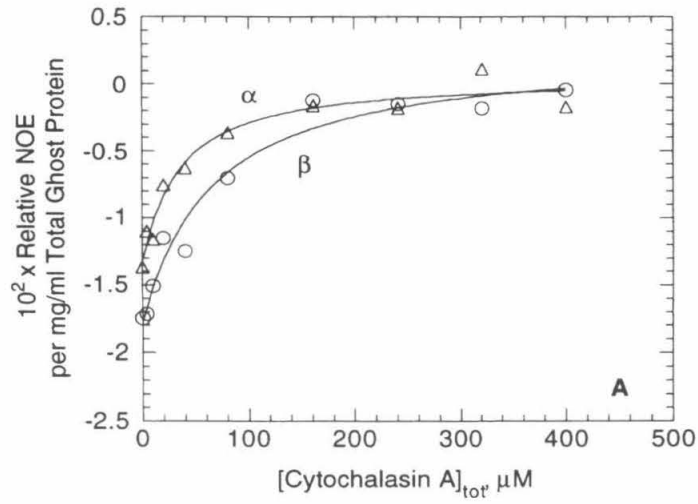
Table 3.1.

Apparent Dissociation Constants for D-Glucose and Inhibitor Binding to Sites on
Erythrocyte Membranes

	TRNOE Reversal		CB Displacement	Transport Inhibition
	Apparent K_D		Apparent K_D	Apparent K_D
	α-D-Glucose[a]	β-D-Glucose[a]		
D-Glucose	30.7 ± 6.2 mM	30.0 ± 7.3 mM	16 mM[b] 40 - 60 mM[c]	5 - 40 mM[d]
CA	36 ± 12 μM	72 ± 25 μM	1.0 - 4.0 μM[e]	1.0 - 4.0 μM[f]
CB	4.6 ± 2.0 μM	6.0 ± 1.8 μM	0.2 - 0.8 μM[e]	0.4 - 0.6 μM[f]
Dihydro-CB	280 ± 130 μM	290 ± 90 μM	> 100 μM[e]	> 100 μM[f]
CD	$1.3 \pm .3$ mM	0.87 ± 0.08 mM	> 100 μM[e]	> 100 μM[f]

a. This study. Reversal of D-glucose H-2α and H-2β TRNOEs in the equilibrium
    mixture of anomers by the indicated ligands in the presence of crushed ghosts at
    20 °C. Bulk [D-glucose] in cytochalasin experiments = 10.0 mM.

b. At 24 °C, intact erythrocytes with intracellular sugar only, from Ref. 14.

c. At 37 °C, ghosts in presence of intra- and extracellular sugar, from Ref. 8.

d. At 20 °C, range of half-saturation concentrations from equilibrium exchange
    measurements of D-glucose flux in a variety of membrane preparations, from Ref. 12.

e. At 22 °C, lyophilized ghosts, no sugar present, from Ref. 10.

f. At 22 °C, inhibition of equilibrium exchange of 1 mM D-glucose measured in resealed
    ghosts, from Ref. 10.

CB per two molecules protein in purified tetrameric GLUT1 (and probably in intact erythrocyte membranes)[11], but the number of sugar binding sites on GLUT1 is not known. While inhibition of the D-glucose TRNOE by CB and other cytochalasins demonstrates that there exist one or more classes of CB-sensitive sites associated with GLUT1 at which D-glucose is in fast exchange, the data provide no information on the number of distinct classes of such sites, nor on their relationship to GLUT1 and sugar transport. Sites affected by CB binding could include: transport sites on GLUT1, other sugar binding sites on GLUT1, or sugar binding sites on a protein or proteins other than GLUT1 which are allosterically coupled to the CB binding site. These sites may be further characterized based on their apparent affinity for glucose.

The Effect of Glucose Concentration on the TRNOE. NMR-observable D-glucose binding to crushed ghosts is consistent with a single homogeneous class of binding sites: the inverse D-glucose concentration dependence of the TRNOE measured in H-2α is well-fit by a single apparent K_D of 30.7 ± 6.2 mM, while that of the H-2β TRNOE yields an apparent K_D of 30.0 ± 7.3 mM (means ± σ of values fitted to three independent data sets, see Figure 3.9). These values fall within the range of apparent K_Ds reported for displacement of CB from GLUT1-associated sites[8] and half-saturation concentrations ("apparent K_ms") reported for equilibrium exchange D-glucose transport[12] (Table 3.1). Moreover, the apparent K_Ds obtained in the present study closely match that found by D-glucose titration of Trp fluorescence in purified GLUT1 (26.9 mM)[13], suggesting that a contribution to the TRNOE from binding to proteins other than GLUT1 is unlikely.

In Chapter 2 it was shown that, if the TRNOEs observed in both anomers result from binding to the same class of sites, the apparent dissociation constants for the two ligands (when expressed as functions of the concentrations of the individual anomers) will differ from each other only by a factor equal to the anomeric ratio (cf. equations

Figure 3.9

The Effect of D-Glucose Concentration on the TRNOE in Crushed Ghosts. The TRNOE observed in (A) H-2α and (B) H-2β in samples containing crushed ghost membranes and the equilibrium mixture of glucose anomers. The solid curves are nonlinear least-squares best-fits to the data, calculated for a homogeneous class of binding sites ($y = a + bx/(x+K_D^{-1})$). The fits yield apparent dissociation constants of 30.7 ± 5.6 mM for the α anomer and 22.1 ± 3.9 mM for the β anomer. Assay conditions and parameters are described in the Experimental Section.

A

B
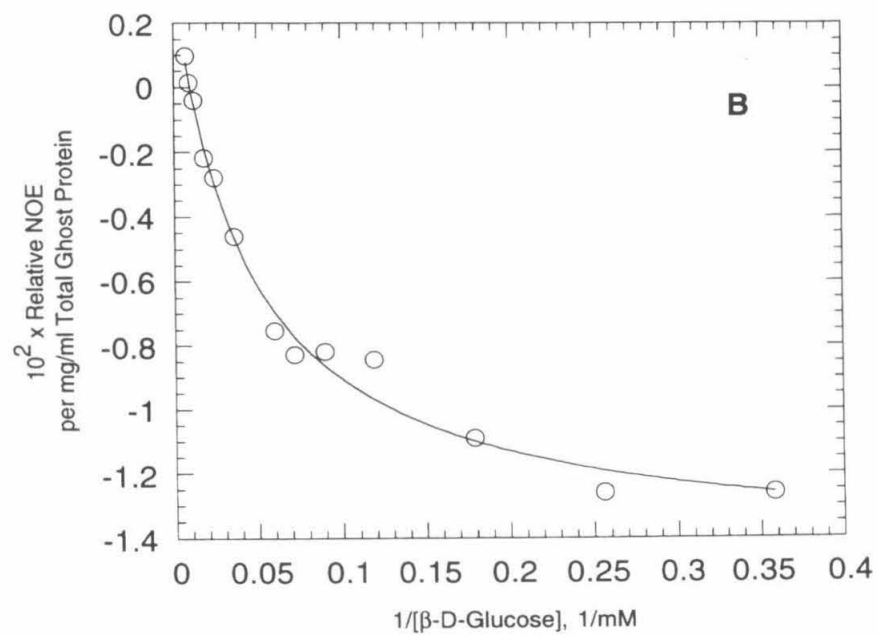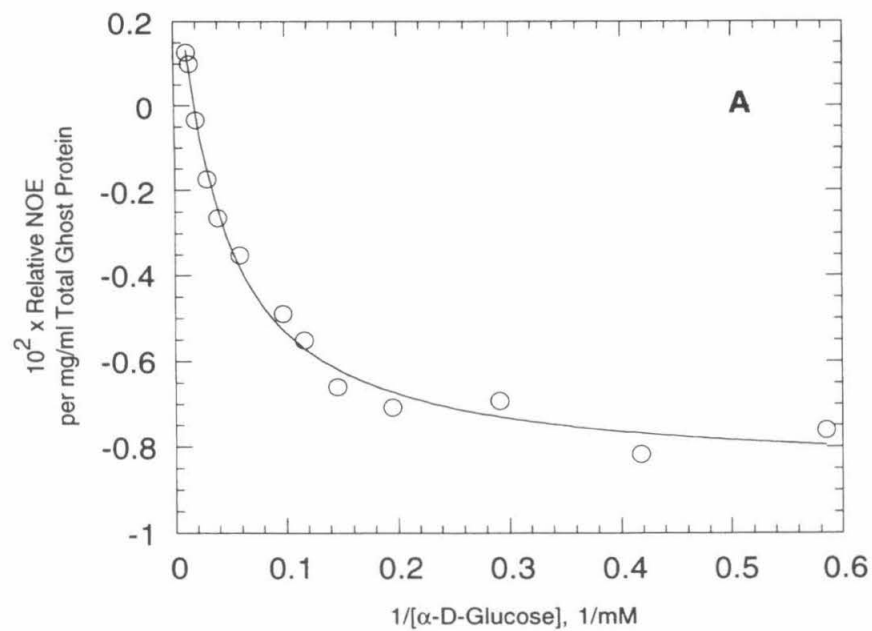
(2.44) and (2.45)). Under the conditions examined, this ratio is $\alpha/\beta = 0.380/0.620 =$ 0.613, whence if α- and β-D-glucose are binding to the same sites, $K_{D,app}(\alpha)$ should equal $0.613K_{D,app}(\beta)$. Experimentally, we find $K_{D,app}(\alpha) \approx K_{D,app}(\beta)$, within measurement error of the predicted ratio. The data presented are thus consistent with binding of both anomers to the same class of sites.

Previous studies of the erythrocyte glucose transport system have not detected carrier-mediated transport of L-glucose, nor has this enantiomer been found to inhibit transport of permeant sugars. Interestingly, the TRNOE method is sufficiently sensitive to weak interactions that CB-sensitive binding of L-glucose *is* detected. The TRNOE in H-2β of L-glucose shows the expected hyperbolic dependence on inverse sugar concentration (Figure 3.10) with an apparent K_D of 450 ± 300 mM (mean $\pm \sigma$ of results of three experiments); although H-2α also has a small CB-sensitive TRNOE, greater scatter in the H-2α data precludes evaluation of the affinity of GLUT1 for this anomer. The detection of L-glucose binding is additionally useful because it demonstrates that the method is sufficiently sensitive to detect such weak binding. If any similarly low-affinity component of D-glucose binding is present, we may be confident that it contributes to the observed CB-sensitive TRNOE.

Results from several laboratories[11,14,15] indicate that, in addition to the component of D-glucose binding of apparent K_D 10 - 40 mM, there exists a class of *high-affinity* sites (apparent K_D 1.7 - 2.0 mM). The sites are located on GLUT1 itself: displacement of CB from the purified tetrameric protein by D-glucose was found to be biphasic with apparent K_Ds of 1.7 and 25.3 mM. TRNOE measurements of D-glucose binding do not reveal such a class of sites. However, this must be considered a null result. Such sites, if present, could be in slow exchange and undetectable by the NMR method. Alternatively, if the high-affinity sites are present but are related to other, lower-affinity sites by conformational change(s) of the protein, the apparent K_D obtained from TRNOE measurements is an average of the two (or more) microscopic dissociation constants,

Figure 3.10

The TRNOE in β-L-Glucose. The solid curve is a nonlinear least-squares best-fit for a homogeneous population of sites, as in the preceeding Figure. Apparent $K_D = 360 \pm 150$ mM. Assay conditions and parameters described in the Experimental Section.
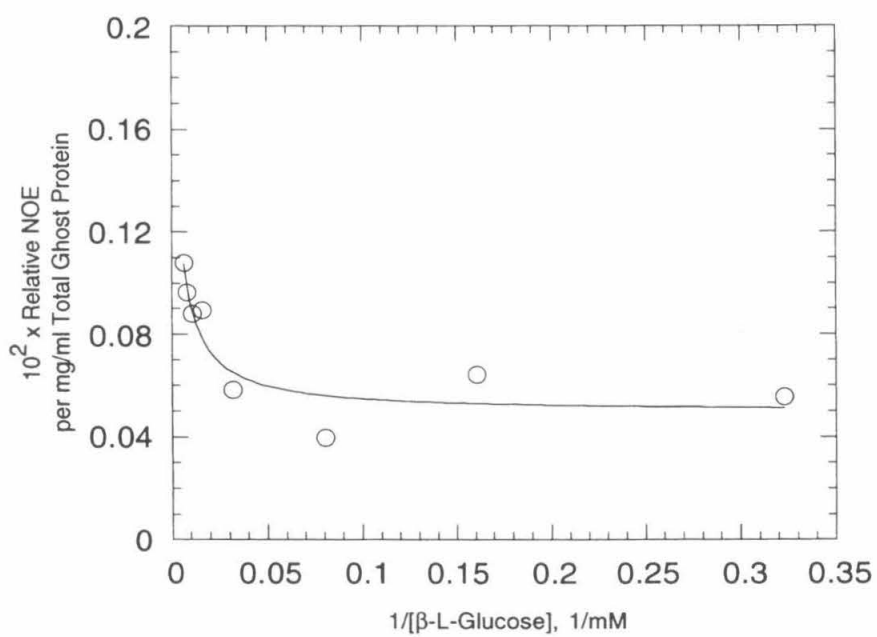
weighted by the populations of the conformational states (see Chapter 4 below); if the conformation of the protein in which the high-affinity site is exposed is negligably populated under experimental conditions, the low microscopic K_D for that site will influence the observed apparent K_D minimally.

Additional Evidence that the TRNOE Arises from Binding to GLUT1. Results of several additional experiments, while inconclusive in themselves, add to the weight of evidence that the TRNOE method monitors binding of sugars to GLUT1 in erythrocyte membranes. Preliminary experiments were carried out (1) to assess the effects of two additional inhibitors of glucose transport, and (2) to seek CB-sensitive TRNOEs in other sugars and sugar derivatives.

Phloretin (3-(4-hydroxyphenyl)-1-(2,4,6-trihydroxyphenyl)-1-propanone) is a potent competitive inhibitor of D-glucose influx in erythrocytes and displaces CB from its D-glucose-sensitive sites with an apparent K_D of 2 μM.[14] In one experiment, at a bulk D-glucose concentration of 10.0 mM, phloretin was found to completely inhibit the D-glucose TRNOE with an apparent K_D of 80 ± 30 μM. This line of inquiry was not pursued: studies of phloretin inhibition of glucose transport and CB binding are complicated by high-capacity saturable binding of the inhibitor to membrane lipid and by recently recognized keto-enol tautomerism of the molecule. In another set of experiments, partial labeling of crushed ghost membranes with maltosyl isothiocyanate (MITC), an affinity label for GLUT1[16], resulted in 30 - 55% reversal of the D-glucose TRNOE.[17] Again, this is not conclusive (MITC also labels the Band 3 protein), but it is *consistent* with inhibition of D-glucose binding to GLUT1.

NOEs were measured for several sugars and sugar derivatives in the presence of crushed ghosts. Galactose, a permeant monosaccharide, and 4,6-O-ethylidene-D-glucose, n-propyl-β-D-glucopyranoside, phenyl-β-D-glucopyranoside and maltose, impermeant inhibitors of D-glucose transport, all showed CB-sensitive TRNOEs. In contrast, no TRNOE was observed in mannitol, which is not transported by GLUT1 and doesn't

inhibit transport of permeant sugars. These observations all suggest that the observed binding is indeed binding to GLUT1.

CONCLUSIONS

Stereospecific TRNOEs have been observed in α- and β-D-glucose in the presence of erythrocyte membranes. This is the first time that binding of the two anomers has been resolved. The simplified linear TRNOE expression has been shown to apply. Essentially all of the observed TRNOE is sensitive to CB; an argument was presented which shows that the D-glucose binding monitored by the TRNOE displaces CB from GLUT1. The dependence of the TRNOE on inverse sugar concentration is consistent with a single class of binding sites, and the apparent affinities for α- and β-D-glucose indicate that this class of sites is responsible for the TRNOEs observed in both anomers. The observation of a CB-sensitive TRNOE in L-glucose demonstrates that this stereoisomer does indeed bind to GLUT1(with a 10-fold higher apparent K_D than that of D-glucose) and proves the sensitivity of the method to weak interactions. High-affinity sites, reported by several workers, were not detected; it cannot however be concluded that such sites are absent based on the TRNOE assay (see Chapter 5 below). The apparent dissociation constants extracted from TRNOE data suggest that the NMR technique monitors the same class of sites observed in most CB binding and fluorescence quenching studies and inferred from most transport data.

Having thus identified the origin of the D-glucose TRNOE in binding to GLUT1, we are in a position to further characterize the nature of the binding sites and answer questions which bear on the transport mechanism. In particular, do binding sites present at only one membrane face or at both faces contribute to the TRNOE? If sites on both surfaces are observed, how does the apparent dissociation constant obtained from TRNOE binding curves relate to the microscopic dissociation constants of the different classes of sites? Also, does the fast exchange of D-glucose at these sites implied by

detection of a TRNOE generate any useful constraints or simplifications for kinetic models of transport? These questions are addressed in the following chapter.

REFERENCES

1. Wang, J.-F., Falke, J. J., and Chan, S. I., <u>Proc. Natl. Acad. Sci.</u> (USA), 83 (1986) 3277-3281.

2. Barnett, J. E. G., Holman, G. D., Chalkley, R. A., and Munday, K. A., <u>Biochem. J.</u>, **145** (1975) 417-423.

3. Steck, T. L., <u>Methods Membrane Biol.</u>, **2** (1974) 245-381.

4. Redfield, A. G., <u>Methods Enzymol.</u>, **49** (1978) 253-270.

5. Lowry, O. H., Rosebrough, N. J., Farr, A. L., and Randall, R. J., <u>J. Biol. Chem.</u>, **193** (1951) 265-275.

6. Markwell, M. A., Haas, S. M., Bieber, L. L., and Tolbert, N. E., <u>Anal. Biochem.</u>, **87** (1978) 206-210.

7. Curatolo, W., Neuringer, L. J., Ruben, D., and Haberkorn, R., <u>Carbohydrate Res.</u>, **112** (1983) 297-300.

8. Jung, C. Y., and Rampal, A. R., <u>J. Biol. Chem.</u>, **252** (1977) 5456-5463.

9. Zoccoli, M. A., Baldwin, S. A., and Lienhard, G. E., <u>J. Biol. Chem.</u>, **253** (1978) 6923-6930.

10. Rampal, A. L., Pinkofsky, H. B., and Jung, C. Y., <u>Biochemistry</u>, **19** (1980) 678-683.

11. Hebert, D. N., and Carruthers, A., <u>J. Biol. Chem.</u>, **267** (1992) 23829-23838.

12. Stein, W. D., <u>Transport and Diffusion Across Cell Membranes</u>, pp. 231-337, Academic Press, Orlando, 1986.

13. Carruthers, A., <u>J. Biol. Chem.</u>, **261** (1986) 11028-11037.

14. Helgerson, A. L., and Carruthers, A., <u>J. Biol. Chem.</u>, **262** (1987) 5464-5475.

15. Holman, G. D., Busza, A. L., Pierce, E. J., and Rees, W. D., <u>Biochim. Biophys. Acta</u>, **649** (1981) 503-514.

16. Mullins, R. E., and Langdon, R. G., <u>Biochemistry</u>, **19** (1980) 1199-1205.

17. Blaylock, R. L., unpublished results.

CHAPTER 4

THE D-GLUCOSE ^{1}H TRNOE IN GHOST SUSPENSIONS: TESTING THE
ALTERNATING CONFORMER MODEL OF *GLUT1* GLUCOSE TRANSPORT

INTRODUCTION

GLUT1 catalyzes the unidirectional flux of glucose and other hexoses across the erythrocyte membrane, driven by the chemical potential gradient of the permeant sugar. In the absence of such a potential gradient (*i.e.*, when intracellular and extracellular sugar activities are equal), the protein mediates one-for-one transmembrane exchange of sugar molecules. Several kinetic models of the transport cycle have been put forth.[1,2,3] A common feature of these models is the presence of at least one sugar transport binding site which is alternately exposed to one membrane face or the other. In the simplest of these models, herein referred to as the alternating conformer model, this transport site is the *only* sugar binding site present. Results from the vast majority of transport studies are consistent with this model.

TRNOE measurement of glucose binding provides a test of GLUT1 mechanism complementary to kinetics studies. In this Chapter, the variation of the D-glucose TRNOE observed in preparations of ghost membranes which differ in exposure of the erstwhile intra- and extracellular membrane surfaces to solution glucose is described. These results are compared with predictions for an alternating conformer mechanism. This approach reveals that (i) binding appears to be to a single homogeneous class of sites and (ii) binding sites exist on both sides of the membrane, in accord with the alternating conformer model, but (iii) the sites sampled by the NMR method must include at least one class of sites which is confined to one membrane face or the other, *i.e.*, which sites are not transport sites. Thus while the alternating conformer model is a kinetically adequate description of transport, the molecular mechanism of GLUT1 function must perforce be more complex.

EXPERIMENTAL SECTION

Materials. D-glucose was obtained from Calbiochem. ^2H_2O was obtained from Cambridge Isotope Labs; $Na^2H_2PO_4$ was obtained from MSD Isotopes. Reagents

required for enzyme assays were obtained from Sigma. All other chemicals used were reagent grade or better. Outdated packed human erythrocytes were a kind gift of the Los Angeles chapter of the American Red Cross.

Ghost Membrane Suspensions. Crushed ghosts were prepared from leaky white ghosts exactly as described in Chapter 3. To prepare sheared ghosts from crushed ghosts, the final crushed ghost pellet obtained after ultracentrifugation was diluted with 1.25-1.3 volumes of 5pD7.4 buffer (5 mM $Na^2H_2PO_4$ in ^2H_2O, p^2H adjusted to 7.4 with NaO^2H (meter reading corrected for isotope effect)). This stock ghost suspension was then rapidly passed through a half-inch 27 ga. needle five times to yield sheared ghost stock.

NMR Sample Preparation and Spectroscopy. NMR samples were prepared exactly as described in Chapter 3, using crushed or sheared ghost stock as appropriate. Acquisition and processing of NMR spectra were also as previously described.

Enzyme Assays. Assays of acetylcholinesterase and glyceraldehyde-3-phosphate dehydrogenase activities were performed essentially as described in the literature[7], with the following adaptations. Blank NMR samples (containing no sugar) were diluted 1:200 with ice-cold 5p7.4 (no difference was found when 5pD7.4 was used instead) as soon as possible after spectroscopy for enzyme assay. Assay samples were prepared in the cold room using only chilled reagents, containers and transfer vessels; this was necessary because after dilution, ghost samples were found to evert and seal if allowed to stand at room temperature. Samples were allowed to warm to room temperature only immediately prior to the actual spectrophotometric assay.

THE TRNOE IN A MULTICOMPARTMENT SYSTEM

As detailed in Chapter 2, the TRNOE is useful as a binding assay when ligand is exchanging rapidly (relative to free ligand spin-lattice relaxation) between solution and a macromolecular binding site. In membrane systems such as the ghost suspensions of the present work, the membranes separate the bulk solution into two or more compartments.

The rate at which ligand diffuses among compartments (Figure 4.1) then affects the NMR signal. We consider the impact of two limiting cases of intercompartmental exchange on the TRNOE: (a) slow, and (b) fast exchange relative to free ligand spin-lattice relaxation, assuming the rate of this relaxation to be the same in all compartments. We also assume the stoichiometric ligand concentration L_t is the same in all compartments, and for simplicity in the present context, that only one class of binding sites exists in each compartment.

Case (a): When the diffusional barriers among compartments are sufficiently great that exchange is slow on the timescale of free ligand spin-lattice (and spin-spin) relaxation (Figure 4.1A), ligand in each compartment samples only binding sites in that same compartment. The resonance from each compartment c will in consequence exhibit a TRNOE

$$f_I\{S\}_c \approx f_I^F\{S\} + \frac{\sigma_{B,c}}{\rho_{IF}} \frac{EL_c}{L_t} \quad , \tag{4.1}$$

where $\sigma_{B,c}$ and EL_c are the I,S cross relaxation rate constant in the compartment c bound complex and the concentration of that complex within the compartment, respectively. Assuming further that all compartmental resonances are isochronous and that free ligand spin-spin relaxation in the various compartments is sufficiently slow that *all* free ligand is observed, the TRNOE in the observed composite signal is a sum of the compartmental TRNOEs, weighted by the fraction V_c/V of the total sample volume V occupied by each compartment c:

$$f_I\{S\} \approx f_I^F\{S\} + \frac{1}{V} \sum_c V_c \frac{\sigma_{B,c}}{\rho_{IF}} \frac{EL_c}{L_t} \quad . \tag{4.2}$$

Case (b): In the rapid intercompartmental exchange limit (Figure 4.1B), a typical ligand molecule visits many compartments, and binding sites within those compartments, during the NMR timescale. In this case, the free ligand NMR signal behaves as if barriers

Figure 4.1

<u>Intercompartmental Exchange of Ligand.</u> A. Slow exchange limit: membrane acts as barrier to diffusion of ligand between internal and external compartments. B. Rapid exchange limit: leaky membrane between the two compartments is not an effective barrier to diffusion.

A
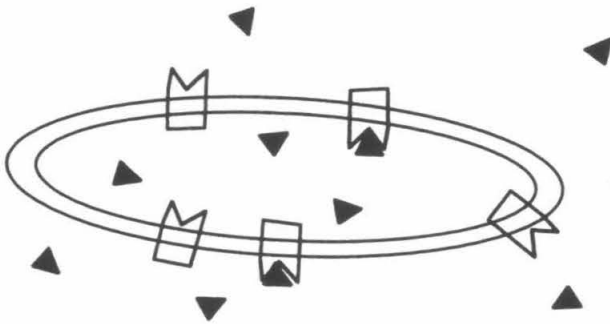
B
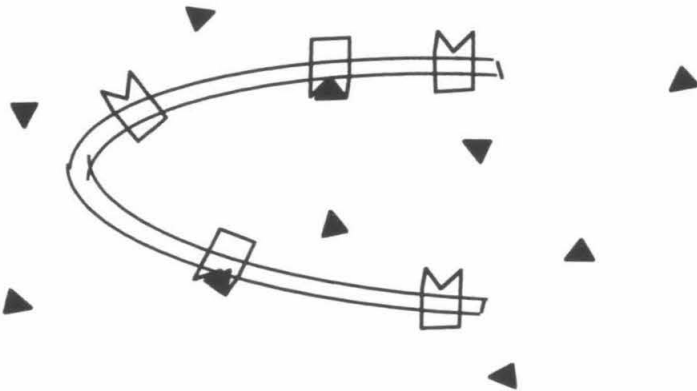
between *compartments* do not exist: all classes of binding sites are accessible to all ligand molecules. The TRNOE for this case is

$$f_I\{S\} \approx f_I^F\{S\} + \sum_c \frac{\sigma_{B,c}}{\rho_{IF}} \frac{EL_c}{L_t} \quad . \tag{4.3}$$

In the membrane preparations described below, solution extrinsic to the ghosts defines one compartment, while the volumes bounded by individual ghost membranes constitute other, much smaller compartments. The original experimental strategy was to resolve binding of ligand to intra- and extracellular sites using preparations of membranes in which the intercompartmental exchange rate is either very slow or very fast. Such preparations were never obtained. The exchange rate between compartments in the experimentally realized preparations is ill-defined; given the morphological heterogeneity of the ghost preparations, a broad distribution of exchange rates is likely. Nonetheless, we may still draw useful information from preparations which differ demonstrably in exposure of membrane faces. In particular, equations (4.2) and (4.3) show that the TRNOE will increase in magnitude as the diffusional barriers between compartments are reduced, allowing detection, if not quantitation, of any binding sites present in the compartments which are thereby rendered accessible to ligand in the bulk solution. Furthermore, it will be shown below that even partial resolution of the compartments allows for a test of transport models.

THE ALTERNATING CONFORMER MODEL OF GLUCOSE TRANSPORT

Transport of hexoses across erythrocyte membranes is observed to be a passive, saturable, stereospecific process. An interesting feature of this process is that flux of labeled substrate in one direction across the membrane is *accelerated* by the presence of unlabeled substrate at the opposite face. It can be shown that this "trans acceleration" rules out channel or pore models of GLUT1 function.[1] To account for this phenomenon kinetically and mechanistically, one must postulate that there exist (at least) two states of

the protein, one to which substrate in the extracellular compartment may bind, the other

to which substrate in the cytoplasmic compartment may bind. The alternating conformer

model, portrayed in Figure 4.2, is the simplest such model consistent with the majority of

experimental data.

For the present discussion, let the extracellular face of the membrane be "side 1,"

the cytoplasmic face, "side 2." In the presence of substrate, the model comprises four

possible states of the system: outward- and inward-facing forms of the free transporter

(E_1, E_2) and of the transporter-substrate complex (EL_1, EL_2). In an ensemble of

alternating conformer transporters at equilibrium, binding sites are present at both

membrane faces; the ratio of bound complexes at sides 1 and 2 is

$$\frac{EL_1}{EL_2} = \frac{g_2}{g_1} \quad . \tag{4.4}$$

Note that reorientations of the unloaded form of the transporter are also possible $(k_1, k_2 \neq$

$0)$; this distinguishes an alternating conformer mechanism from a "ping-pong" or

exchange-only mechanism and allows for unidirectional flux of substrate. Assuming

dissociation of ligand from binding sites is rapid relative to transporter reorientation steps

(this assumption is discussed below), an alternating conformer transporter will display

trans acceleration whenever the following relationships among rate constants obtain:

$$k_1 < g_1 \ ; \ k_2 < g_2 \tag{4.5}$$

i.e., the rate constants for conformational change of the unloaded transporter must be

smaller than the corresponding constants for conformational change of the bound

complex.

It can be shown[1] that a transporter which functions by this mechanism displays

simple Michaelis-Menten kinetics in steady-state experiments. Such experiments yield

two experimental parameters, a half-saturation concentration and a maximal velocity.

Figure 4.2

The Alternating Conformer Model. The protein E may exist in one of four states in the presence of ligand L: outward- and inward-facing conformations of the unloaded (E_1, E_2) and loaded (EL_1, EL_2) transporter. In general, ligand concentrations in the two compartments may differ (L_1, L_2); for an uncharged substrate at equilibrium, $L_1 = L_2$. This equilibrium condition leads to the detailed balance constraint $b_1 f_2 g_2 k_1 = b_2 f_1 g_1 k_2$ among the model rate constants.

$$E_1 \xrightleftharpoons[k_2]{k_1} E_2$$

$$f_1L_1 \Big\updownarrow b_1 \qquad\qquad b_2 \Big\updownarrow f_2L_2$$

$$EL_1 \xrightleftharpoons[g_2]{g_1} EL_2$$
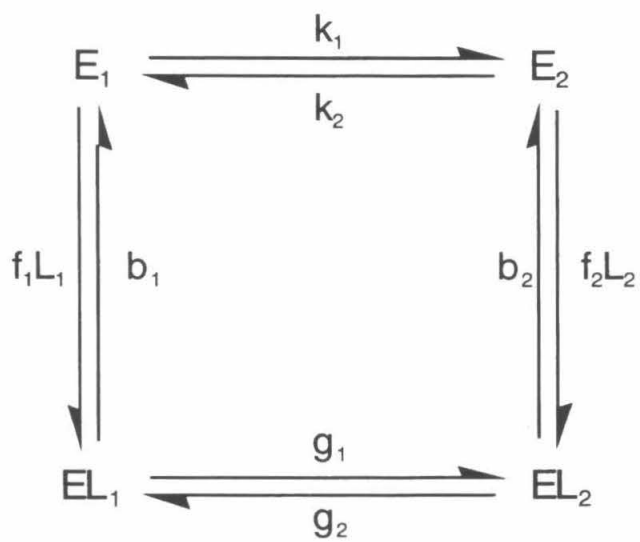
The relationship between these transport parameters and model rate constants depends on the initial conditions of the experiment. Comparison of steady-state transport parameters obtained under different initial conditions provides a test for consistency of transport data with an alternating conformer mechanism.[1] The most recent studies of GLUT1 glucose transport are all consistent with this model.[4]

Although the model is adequate to explain observed steady-state (and transient) kinetics of glucose transport, it cannot account for certain other experimental findings (particularly complexities in inhibition of transport by cytochalasin B, addressed in Chapter 5 below). With the well-known limitations of kinetic models in mind, we set out to compare the glucose binding we have observed with that predicted for an alternating conformer transporter. To that end, in the next section, we derive the TRNOE expected for this model.

THE TRNOE DUE TO AN ALTERNATING CONFORMER TRANSPORTER

The following discussion outlines results of an algebraic treatment of the alternating conformer model. The TRNOE due to binding of a single ligand species to the transport sites of an alternating conformer transporter is derived and examined as a function of a) ligand concentration, and b) exposure of membrane faces. The expression obtained is then modified for the equilibrium mixture of ligands used in the present experiments.

Definitions and Assumptions. The subscripts 1 and 2 are used to represent the forms of the protein in which a binding site is accessible to the extracellular or the cytoplasmic compartment of the membrane, respectively. The microscopic dissociation constants K_{D1} and K_{D2} in these compartments are given by the usual definitions

$$K_{D1} = \frac{b_1}{f_1} \; ; \; K_{D2} = \frac{b_2}{f_2} \; . \tag{4.6}$$

Throughout this treatment, brackets to indicate molar concentrations of species are implicit. For simplicity, it is assumed initially that all membranes are right-side-out; the system is treated as a two compartment system, with the extracellular solution constituting compartment 1 and the sum of the erstwhile cytoplasmic spaces constituting compartment 2. The concentration of ligand is much greater than the concentration of binding sites, so the stoichiometric ligand concentration L_t will be used instead of the exact ligand concentrations. The experiments are performed under equilibrium conditions, thus the concentration of ligand is identical in all compartments, $i.e.$, $L_1 = L_2 = L_t$; the equilibrium condition also implies that the inward- and outward-facing sites reach an equilibrium distribution before NMR measurements are made. We also assume that all free ligand in both compartments is detected (see Results below).

An assumption which merits some discussion concerns the relative magnitudes of binding and dissociation rate constants and reorientation rate constants. It was shown in Chapter 2 that a TRNOE will only be observed when exchange is fast relative to free ligand spin-lattice relaxation. Symbolically, this condition is $f' = fE \gg \rho_{IF}$. Since the observed relaxation rate constants in the present experimental samples are of the order of $1\ s^{-1}$, and the *total* binding site concentration is roughly $10\ \mu M$ or less, we obtain a conservative lower bound on the association rate constant(s) of the site(s) of $f \gg 10^5\ M^{-1}s^{-1}$. Thence, from the apparent dissociation constant for NMR-observable binding of ~30 mM (reported in the previous chapter), we obtain a conservative lower bound on the dissociation rate constant(s) of the detected site(s) of $b \gg 3 \times 10^3\ s^{-1}$. Comparison with literature values (reviewed in Ref. 4) of the turnover numbers (for outdated blood at 20 °C) for glucose uptake (~100 s^{-1}), efflux (~400 s^{-1}) and equilibrium exchange (~$10^3\ s^{-1}$) indicates that observed binding and dissociation are indeed much faster than GLUT1 reorientations, either loaded or unloaded. To test whether the observed binding arises from an alternating conformer transporter, then, it will be assumed below that $f_1, f_2, b_1, b_2 \gg g_1, g_2, k_1, k_2$.

The Concentrations of Bound Complexes EL_1 and EL_2. In order to calculate the TRNOE expected for this model, we must have expressions for the concentrations of the bound complexes EL_1 and EL_2 in terms of the model rate constants. This is easily done using King-Altmann diagrams (see Appendix).[5] At equilibrium, we obtain

$$\frac{EL_1}{E_t} = \frac{(f_1 f_2 g_2 L_t + f_2 g_2 k_1 + b_2 f_1 k_2 + f_1 g_2 k_2) L_t}{f_1 f_2 (g_1 + g_2) L_t^2 + [b_1 f_2 (g_2 + k_1) + b_2 f_1 (g_1 + k_2) + (f_1 k_2 + f_2 k_1)(g_1 + g_2)] L_t + (b_1 g_2 + b_2 g_1 + b_1 b_2)(k_1 + k_2)} \quad (4.7)$$

$$\frac{EL_2}{E_t} = \frac{(f_1 f_2 g_1 L_t + f_1 g_1 k_2 + b_1 f_2 k_1 + f_2 g_1 k_1) L_t}{f_1 f_2 (g_1 + g_2) L_t^2 + [b_1 f_2 (g_2 + k_1) + b_2 f_1 (g_1 + k_2) + (f_1 k_2 + f_2 k_1)(g_1 + g_2)] L_t + (b_1 g_2 + b_2 g_1 + b_1 b_2)(k_1 + k_2)} \quad (4.8)$$

These expressions are general but cumbersome. Assuming rapid association and dissociation of ligand relative to translocation of the loaded or unloaded carrier and using the definitions of the microscopic dissociation constants K_{D1} and K_{D2} and the detailed balance constraint $b_1 f_2 g_2 k_1 = b_2 f_1 g_1 k_2$, equations (4.7) and (4.8) reduce to far simpler forms:

$$\frac{EL_1}{E_t} = \frac{K_{D1}^{-1} L_t}{1 + \dfrac{k_1}{k_2} + \left(K_{D1}^{-1} + \dfrac{k_1}{k_2} K_{D2}^{-1} \right) L_t} \quad , \quad (4.9)$$

$$\frac{EL_2}{E_t} = \frac{\dfrac{k_1}{k_2} K_{D2}^{-1} L_t}{1 + \dfrac{k_1}{k_2} + \left(K_{D1}^{-1} + \dfrac{k_1}{k_2} K_{D2}^{-1} \right) L_t} \quad . \quad (4.10)$$

The TRNOE. For a two compartment system with one class of binding sites in each compartment, the TRNOE may be written as

$$f_1\{S\} - f_1^F\{S\} \approx c_1 \frac{EL_1}{L_t} + c_2 \frac{EL_2}{L_t} \quad , \quad (4.11)$$

where c_1 and c_2 are parameters which reflect both the fraction of total free ligand molecules which sample binding sites in compartments 1 and 2, respectively, and the

rates of I,S cross relaxation in the two bound complexes. Thus in the slow intercompartmental exchange limit (cf. equation (4.2)),

$$c_1 = \frac{V_1}{V} \frac{\sigma_{B,1}}{R_I^F} \quad ; \quad c_2 = \frac{V_2}{V} \frac{\sigma_{B,2}}{R_I^F} \tag{4.12}$$

while in the limit of rapid intercompartmental exchange, effectively $V_1 = V_2 = V$, and

$$c_1 = \frac{\sigma_{B,1}}{R_I^F} \quad ; \quad c_2 = \frac{\sigma_{B,2}}{R_I^F} \quad . \tag{4.13}$$

Substitution of equations (4.9) and (4.10) for EL_1 and EL_2 into equation (4.11) followed by rearrangement and normalization to the total ghost protein concentration $P = ZE_t$ leads to a simple expression comparable to equation (2.41) for the TRNOE expected from ligand binding to the transport sites of an alternating conformer transporter:

$$\frac{f_I\{S\} - f_I^F\{S\}}{P} \approx \frac{c_1 k_2 K_{D1}^{-1} + c_2 k_1 K_{D2}^{-1}}{k_1 + k_2} Z \frac{L_t^{-1}}{L_t^{-1} + \overline{K}_D^{-1}} \quad , \tag{4.14}$$

where the macroscopically averaged apparent dissociation constant $\overline{K}_D$ is

$$\overline{K}_D = \frac{k_1 + k_2}{k_2 K_{D1}^{-1} + k_1 K_{D2}^{-1}} = \frac{g_2 K_{D1} + g_1 K_{D2}}{g_1 + g_2} \quad . \tag{4.15}$$

The first expression for $\overline{K}_D$ above, containing the rate constants k_1 and k_2, is retained because it will prove the more compact form when we consider the anomeric mixture of ligands below. The second expression, in terms of the rate constants g_1 and g_2, shows more clearly that $\overline{K}_D$ is an average of the two microscopic dissociation constants, weighted by the distribution of bound complexes between inward- and outward-facing forms.

The TRNOE expression (4.14) leads to two of the predictions which are the focus of study in this chapter. First, the alternating conformer mechanism couples inward- and outward-facing binding sites in such a way that macroscopic binding behavior appears to be to a *single class of sites*, with an apparent dissociation constant given by equation

(4.15). Second, dependence of the TRNOE on the relative contributions of sites in the two compartments appears only in the term

$$\frac{c_1 k_2 K_{D1}^{-1} + c_2 k_1 K_{D2}^{-1}}{k_1 + k_2} \tag{4.16}$$

in equation (4.14). Therefore, while the TRNOE amplitude will vary with varying exposure of membrane faces to bulk ligand, the apparent dissociation constant is *independent* of which compartments are sampled. To illuminate this point, consider two extreme cases. First, in a sample where the intercompartmental exchange rate is very slow and the intracellular compartment volume is negligable compared to that of the extracellular compartment, $c_2 \approx 0$ and the term (4.16) becomes

$$\frac{k_2 K_{D1}^{-1}}{k_1 + k_2} \frac{\sigma_{B,1}}{R_1^F} . \tag{4.17}$$

In the limit of rapid intercompartmental exchange, however, regardless of the relative volumes of the two compartments, the amplitude of the TRNOE is larger: we have for the term (4.16)

$$\frac{k_2 K_{D1}^{-1} \sigma_{B,1} + k_1 K_{D2}^{-1} \sigma_{B,2}}{(k_1 + k_2) R_1^F} . \tag{4.18}$$

In both cases, the observed apparent dissociation constant is just $\overline{K}_D$ of equation (4.15).

As in the single compartment, single class of sites case (equations (2.42) - (2.43)), the presence of an equilibrium mixture of ligands does not alter the fundamental form of equation (4.14). For the anomeric mixture used in the present work, with the anomeric ratio r defined by $\alpha = r\beta$, the TRNOEs arising in α and β signals from alternating conformer transport sites are

$$\frac{f_I^\alpha \{S\} - f_I^{F,\alpha} \{S\}}{P} = \frac{c_1^\alpha k_2 (K_{D1}^\alpha)^{-1} + c_2^\alpha k_1 (K_{D2}^\alpha)^{-1}}{k_1 + k_2} Z \frac{\alpha_t^{-1}}{\alpha_t^{-1} + (\overline{K}_D^\alpha)^{-1}} , \tag{4.19}$$

$$\frac{f_I^\beta \{S\} - f_I^{F,\beta} \{S\}}{P} = \frac{c_1^\beta k_2 (K_{D1}^\beta)^{-1} + c_2^\beta k_1 (K_{D2}^\beta)^{-1}}{k_1 + k_2} Z \frac{\beta_t^{-1}}{\beta_t^{-1} + (\overline{K}_D^\beta)^{-1}} , \tag{4.20}$$

with the macroscopic apparent dissociation constants

$$\overline{K}_D^\alpha = r \frac{k_1 + k_2}{k_2\left[\left(K_{D1}^\beta\right)^{-1} + r\left(K_{D1}^\alpha\right)^{-1}\right] + k_1\left[\left(K_{D2}^\beta\right)^{-1} + r\left(K_{D2}^\alpha\right)^{-1}\right]} \quad .$$

$$\overline{K}_D^\beta = r^{-1}\overline{K}_D^\alpha \quad .$$

(See Appendix for derivation.) According to equations (4.21) and (4.22), it is not possible to deconvolute the microscopic dissociation constants for the two anomers with the present experimental design. However, as noted previously, relationship (4.22) provides a consistency test: if both anomers in the sample are binding to the same classes of sites, their apparent dissociation constants will differ only by a factor of the anomeric ratio r.

RESULTS

Erythrocyte Membrane Preparations. Previous work in this laboratory on the Band 3 system[6], as well as the prodigious literature on ghost membranes and their derivatives, led us to expect that we could readily generate preparations of erythrocyte membranes with both membrane faces equally exposed to the bulk solution or with predominantly one face or the other exposed. This proved not to be the case; apparently the sample composition and manipulations required for sensitivity and reproducibility of the TRNOE assay (to wit, essentially complete replacement of solvent and exchangeable erythrocyte protons with deuterons, relatively low ionic strength, very high membrane concentrations, and the mechanical crushing which results from the solvent exchange ultracentrifugation steps) favor different ghost morphologies than those commonly reported. It was found that manipulations expected to lead to resealing of the crushed ghosts, such as heating, failed to do so. *Any* manipulation of concentrated ghost

suspensions, including procedures reported to yield unsealed membrane fragments (sonication)[6], unsealed inside-out (IO) and sealed right side-out (RO) vesicles (incubation at very low μ, addition of divalent cations)[7] produced increased proportions of sealed IO morphologies relative to crushed ghosts. It was concluded that, in the ghost suspensions of the present work, IO morphologies are energetically favored over other membrane configurations. Addition of detergents (saponin and Triton X-100) at concentrations sufficient to permeabilize the membranes also proved unsuitable, turning the already viscous samples into gels. Two membrane preparations selected for study of the "sidedness" of the TRNOE, crushed ghosts and sheared crushed ghosts, are described below.

The only estimates available of exposure of the extracellular and cytoplasmic membrane faces to bulk solution come from the enzyme sidedness assays of Steck.[7] In these assays, the activities of enzymes known to be associated with one side of the membrane or the other are measured in the absence or presence of membrane-permeabilizing detergent. The ratio of activity in the absence of detergent to that in its presence then gives the fraction of enzyme accessible to its (membrane-impermeant) substrates in the membrane preparation tested. In particular, acetylcholinesterase and glyceraldehyde-3-phosphate dehydrogenase activities were assayed. Acetylcholinesterase is linked *via* a glycosylphosphitidylinositol anchor to the extracellular leaflet of the erythrocyte membrane. Activity of this enzyme in a ghost preparation relative to its activity in the presence of detergent thus directly yields the fraction of extracellular membrane surface accessible to the bulk solution. Subtraction of this fraction from 1 yields the fraction of membrane which is in sealed inside-out morphologies. Glyceraldehyde-3-phosphate dehydrogenase, on the other hand, is noncovalently associated with the cytoplasmic domain of the Band 3 protein. Assay of the activity of this enzyme plus or minus detergent yields the fraction of cytoplasmic membrane surface accessible to the bulk solution (and by extension the fraction of

membrane which is in sealed right side-out morphologies). It is important to note that these enzyme assays place *upper bounds* on the fractions of the two membrane surfaces which contribute to intercompartmental exchange averaging of the TRNOE. The timescale for the enzyme assays is ~1 min., while the timescale for the TRNOE is ~1 s. Comparison of these two timescales is reasonable since the substrates of the enzymes assayed are all small molecules for which intercompartmental diffusion rates should be fairly similar to that of glucose. Thus compartments which are inaccessible to the substrates of the enzyme assays are necessarily inaccessible to monosaccharides with respect to TRNOE averaging, while compartments which are accessible to the enzyme substrates do *not* necessarily contribute to the TRNOE arising from ligand in the extracellular compartment.

Crushed Ghosts. As noted in Chapter 3, examination of crushed ghosts by phase-contrast microscopy reveals them to be morphologically heterogeneous. The majority of membranes examined (~90%) retained an appearance similar to discocytes but were flattened or cup-shaped with an internal volume $\leq 10\%$ of the internal volume of an intact erythrocyte. Leaky ghosts are generally found to retain the native orientation of the membrane; eversion of entire ghosts has been observed but is less common. Thus we assume this predominant crushed ghost morphology to be right side-out. The remaining membranes observed were more distorted, including small proportions of crenated and multilamellar morphologies. We can estimate the "internal" and "external" volumes in a typical crushed ghost sample as follows: The internal volume of an intact erythrocyte at physiological ionic strength is ~80×10^{-12} cm^3, so the internal volume of a crushed ghost membrane is at most about 8×10^{-12} cm^3. A typical NMR sample contains 10 mg/ml total ghost protein, or ~1.7×10^{10} ghosts/ml; the fraction of total sample volume *inside* the ghosts is then ~0.14 ml/ml sample. The external volume fraction is thus approximately 0.86 ml/ml sample or greater, and we estimate $V_{ext} \geq 6V_{int}$. We conclude that although the bulk solution compartment predominates, the internal volume is not

negligable in crushed ghost preparations; since all compartments contribute to the observed NMR signal (see below), ligand binding to sites within the internal compartments contributes to the TRNOE (~15%) even if all intercompartmental exchange is slow.

Membrane sidedness assays of acetylcholinesterase and glyceraldehyde-3-phosphate dehydrogenase activities indicate that, on the timescale of these assays, crushed ghost preparations consist of $81 \pm 2\%$ unsealed (again, it is assumed that this reflects largely RO species), $12 \pm 3\%$ sealed IO and $7 \pm 2\%$ sealed RO morphologies (means $\pm \sigma$ of results for 5 separate batches of crushed ghosts). Thus at most 88% of exofacial binding sites are accessible to ligand in the bulk compartment, as are at most 93% of endofacial sites. The actual proportion of endofacial sites rapidly sampled (on the NMR timescale) by bulk ligand is likely less than the latter figure indicates: the erythrocyte membrane skeleton is still present in the internal compartments of crushed ghosts and probably restricts diffusion of ligand into and out of those compartments, as well as restricting diffusion of ligand to and from binding sites within the compartment. Indeed, the results below will be seen to corroborate that not all endofacial binding sites accessible on the enzyme assay timescale in crushed ghost samples are accessible on the NMR timescale.

Based on crushed ghost morphology (predominantly right side-out configuration, nonzero internal volume) and enzyme assay results (majority of both membrane surfaces accessible to bulk solution), the most complete statement we can make about crushed ghosts with respect to the TRNOE is that ligand samples the majority of exofacial sites and a significant fraction of endofacial sites. Manipulations of crushed ghosts which break up the membranes expose more of the endofacial sites. Mechanical shearing of crushed ghosts is one such manipulation.

Sheared Ghosts. Repeated rapid passage of crushed ghost suspensions through a narrow gauge needle substantially alters the distribution of morphologies observed.

Typical crushed ghost forms remain (20-30%), but the majority of membranes appear to have been sheared by the treatment, yielding highly irregular morphologies, including long strips of membrane, twisted or bent to varying degrees, and cup-shaped ghosts dangling loose flaps of membrane. Not infrequently, what appeared to be incipient vesicles budding off of a segment of membrane were observed. The proportion of crenated and multilamellar morphologies (~10%) was also greater than that observed in crushed ghosts.

Enzyme sidedness assays indicate that, as in crushed ghosts, most of the membrane surface in sheared ghosts is accessible to the bulk solution. However, partial eversion and vesiculation of the membranes has been achieved. In particular, the enzyme assays reveal $69 \pm 5\%$ unsealed (including contributions from RO and IO species and open membrane fragments), $22 \pm 4\%$ sealed IO and $9 \pm 4\%$ sealed RO morphologies (means $\pm \sigma$ of results for 4 separate batches of sheared ghosts). At most, then, 78% of exofacial sites and 91% of endofacial sites are exposed to bulk solution. Given its heterogeneity, it is impossible to estimate internal volume in this preparation; however, since the membranes are more fragmented than in crushed ghost preparations, it is probable that the total volume of compartments isolated from the bulk is smaller. By extension, it thus is likely that, compared to crushed ghosts, a larger fraction of the endofacial sites accessible on the enzyme assay timescale are also accessible on the NMR timescale.

Although both membrane preparations described are but poorly characterized with respect to compartmentalization of endo- and exofacial binding sites, it is important to note at this point that this characterization is adequate to support interpretation of the NMR results presented below.

The D-Glucose ^{1}H NMR Spectrum in Ghost Suspensions. The ^{1}H NMR spectrum of D-glucose in either crushed or sheared ghosts differs little from that in buffer (See Figures (3.1)-(3.3)): the lines are slightly broader (by ~0.3-0.4 Hz) but not

obviously non-Lorentzian (occasionally odd lineshapes were encountered, but these were always also present in spectra of sugar in buffer acquired during the same experiment, implicating field inhomogeneity rather than sample characteristics). Lineshape thus offers no evidence for separate compartments in which D-glucose protons differ significantly in T_2. Within measurement error, all of the D-glucose in both preparations contributes to the observed NMR signals: H-2β peak areas were $97 \pm 5\%$ (crushed ghosts) and $101 \pm 2\%$ (sheared ghosts) of the value for the same concentration of sugar in buffer (means $\pm \sigma$ of 5 different determinations for each preparation). This then also implies that there are no compartments of significant volume in either preparation which are isolated from the bulk compartment and in which motion of D-glucose is restricted.

The D-glucose TRNOE in Crushed and Sheared Ghosts. To test the alternating conformer model of GLUT1 glucose transport, we attend to 3 features of the glucose binding curves derived from TRNOE data from crushed and sheared ghost preparations: the shape of the curves, the TRNOE amplitude, and the apparent dissociation constants.

As reported in the preceding chapter, the TRNOEs observed in α- and β-D-glucose in crushed ghosts are consistent with binding to a single class of sites: plots of TRNOE *vs.* inverse ligand concentration are well-fit by rectangular hyperbolae (Figures 4.3A and 4.4A, see also Figure 3.9). Plots of the D-glucose TRNOEs in sheared ghosts are similarly consistent with a single class of sites (Figures 4.3B, 4.4B). Equations (4.19) and (4.20) above show that the TRNOE arising from binding to the transport sites of an alternating conformer transporter at equilibrium will behave as if ligand is binding to a single homogeneous class of sites, with an apparent dissociation constant which is a weighted average of the microscopic dissociation constants at the two transport sites. Thus the simple shape of the binding curves in both membrane preparations is consistent with the prediction for an alternating conformer transporter.

Figure 4.3

Dependence of the α-D-Glucose TRNOE on Exposure of Membrane Faces. The
TRNOEs observed in H-2 of α-D-glucose (in the equilibrium mixture of anomers) at 20
$^{\circ}$C in the presence of (A) crushed ghosts, or (B) sheared ghosts. The solid curves are
nonlinear least-squares best fits to the equation

$$y = a + \frac{bx}{x + K_D^{-1}}$$

for a homogeneous population of binding sites, yielding amplitudes (parameter b of the
fits) and apparent dissociation constants of (A) -1.52 ± 0.07 (mg/ml)$^{-1}$ and 35.6 ± 2.8 mM
for crushed ghosts, and (B) -1.76 ± 0.19 (mg/ml)$^{-1}$ and 63.7 ± 7.4 mM for sheared ghosts.
The data in (A) and (B) are from different batches of ghosts. The crushed ghost data (A)
in this Figure and in Figure 4.4A are from the same batch of ghosts, as are the sheared
ghost data (B) in this Figure and in Figure 4.4B. Crushed ghost data portrayed here and
in Figure 4.4A are from a different batch of ghosts than that portrayed in Figure 3.9.
Assay conditions and parameters are described in the Experimental Section.
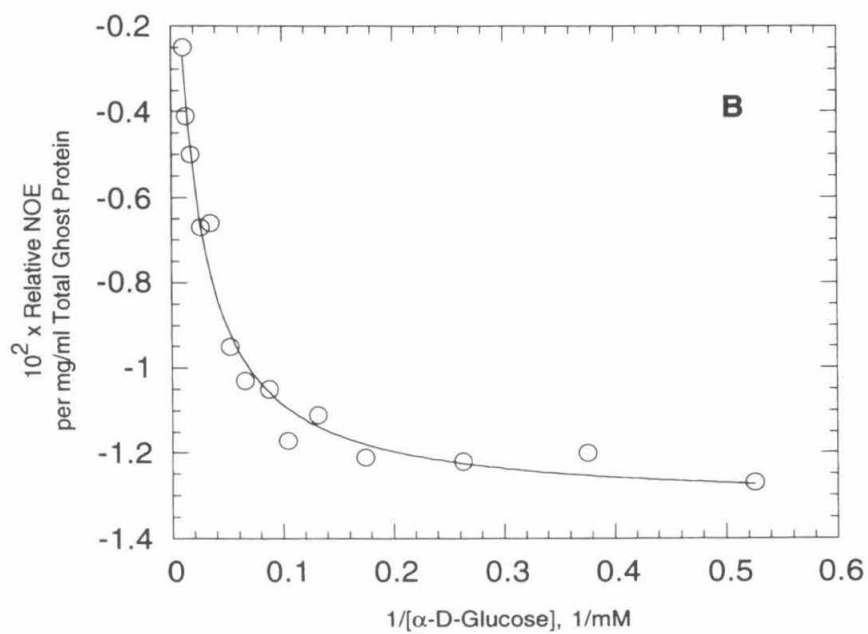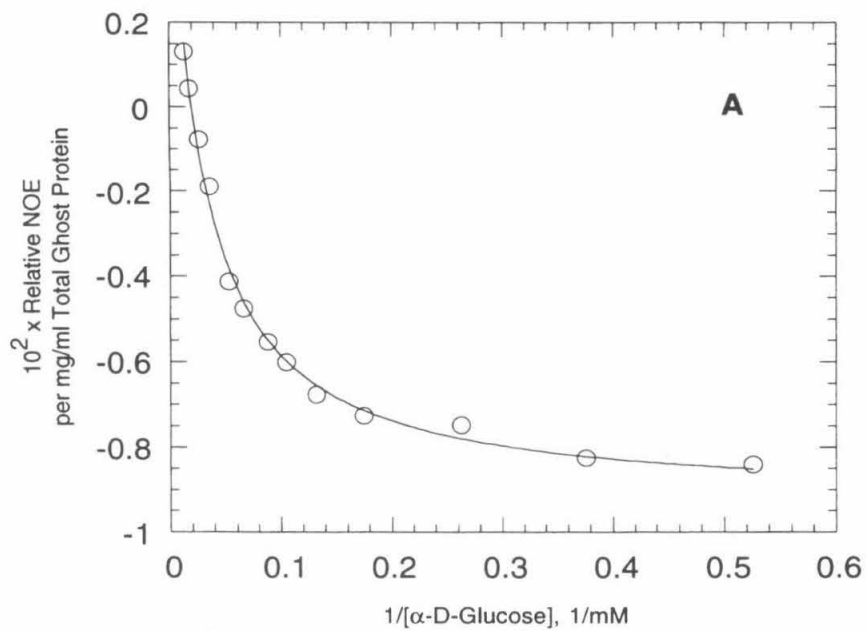
Figure 4.4

Dependence of β-D-Glucose TRNOE on Exposure of Membrane Faces. The TRNOEs observed in H-2 of β-D-glucose (in the equilibrium mixture of anomers) at 20 °C in the presence of (A) crushed ghosts, or (B) sheared ghosts. The solid curves are nonlinear least-squares best fits for a homogeneous population of binding sites, as described in the preceding Figure. The fits yield TRNOE amplitudes and apparent dissociation constants of (A) -1.80 ± 0.13 (mg/ml)$^{-1}$ and 35.3 ± 4.1 mM, (B) -1.92 ± 0.12 (mg/ml)$^{-1}$ and 76.2 ± 9.0 mM for crushed ghosts and sheared ghosts, respectively. Assay conditions and parameters are described in the Experimental Section.
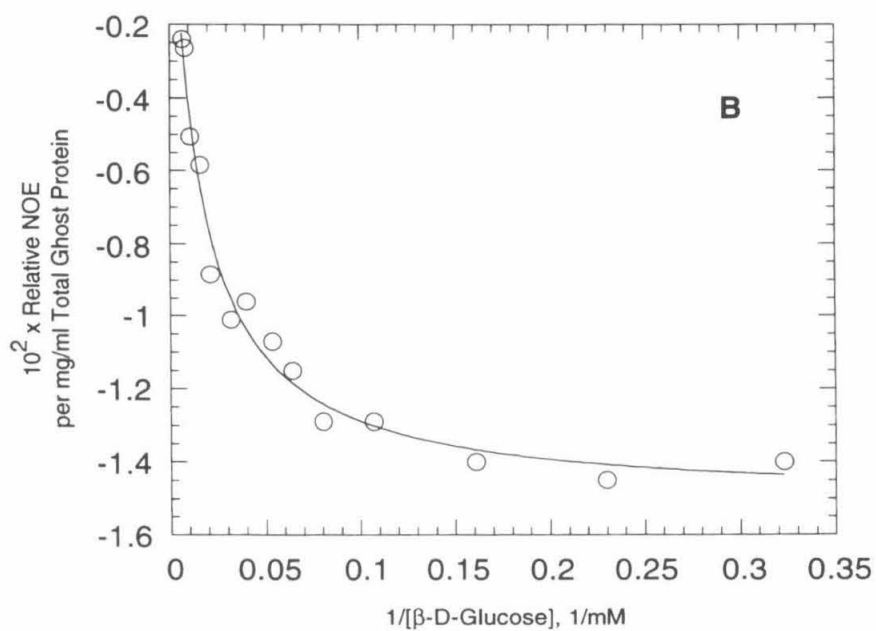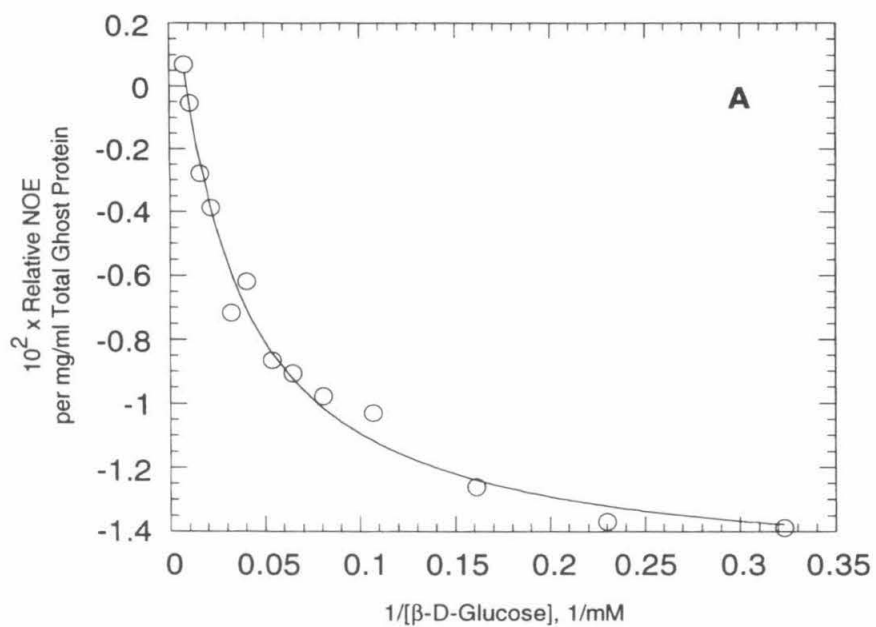
Table 4.1

D-Glucose TRNOE Amplitudes and Apparent Dissociation Constants in Crushed and Sheared Ghosts

	TRNOE Amplitude[a]		Apparent K_D[b]	
	α-D-Glucose	β-D-Glucose	α-D-Glucose	β-D-Glucose
Crushed Ghosts[c]	-1.43 ± 0.11	-1.69 ± 0.16	30.7 ± 6.2	30.0 ± 7.3
Sheared Ghosts[d]	-1.80 ± 0.17	-2.04 ± 0.21	65.8 ± 9.6	70.8 ± 12.5

a. TRNOE amplitude normalized to total ghost protein concentration. Units of (mg/ml ghost protein)$^{-1}$.

b. Units of mM.

c. Means $\pm\ \sigma$ of results for three different batches of crushed ghosts.

d. Means $\pm\ \sigma$ of results for four different batches of sheared ghosts.

Figures 4.3 and 4.4 and Table 4.1 show that the maximal TRNOE in sheared ghosts is as much as 20% larger than that in crushed ghosts. An increase in magnitude of the TRNOE implies that more binding sites are being sampled; for the two membrane preparations under study, which differ only in membrane morphology, this increase implies that sites in isolated compartments in crushed ghosts become accessible in sheared ghosts for fast exchange of bulk ligand between free and bound forms (cf. equations (4.2) and (4.3)). As detailed above, microscopy and enzyme assays of the two preparations suggest that a slightly smaller fraction of extracellular membrane surface is exposed in sheared compared to crushed ghosts, while a significant proportion of cytoplasmic membrane surface isolated from bulk solution in crushed ghosts is rendered accessible in sheared ghosts. The larger TRNOE in the latter preparation thus implies that endofacial binding sites are present.

In an alternating conformer transporter at equilibrium, binding sites are present at both membrane faces. For GLUT1 at 20 °C, estimates based on this model of the distribution of transporters between inward- and outward-facing forms range from a three-fold excess of endofacial over exofacial sites[4] to approximately equal numbers of both forms[8]. Although the present TRNOE results show that binding sites are present in the cytoplasmic compartments, the increased TRNOE magnitude in sheared ghosts relative to crushed ghosts fails to demonstrate unequivocally the presence of exofacial sites. For this, we must look to the apparent dissociation constants derived from crushed ghost and sheared ghost TRNOE data.

When additional endofacial sites are exposed by shearing of crushed ghosts, the apparent affinity of the preparation for glucose drops: the apparent dissociation constants for α- and β-D-glucose in sheared ghosts are 65.8 ± 9.6 mM and 70.8 ± 12.5 mM, respectively (means $\pm \sigma$ of results of experiments on 4 different batches of membranes), compared to about 30 mM for both anomers in crushed ghosts (Table 4.1). As in crushed ghost preparations, the apparent dissociation constants for the two anomers in sheared

ghosts are within experimental error of the ratio ($r = 0.69$) expected if both are binding to the same class of sites (cf. equation (4.22)).

This change of apparent K_D with changing exposure of membrane faces reveals much about the binding sites observed. First, it clearly indicates that a different distribution of sites is sampled as more cytoplasmic membrane surface is rendered accessible, rather than just a higher concentration of the same sites sampled in crushed ghosts. Thus exofacial sites must be present as well as the endofacial sites whose existence was established above. Second, this feature reveals that the sites which contribute to the TRNOE are *not* simply the transport sites of an alternating conformer transporter. As discussed in connection with equation (4.14) above, such transport sites behave macroscopically as a single homogeneous class of sites, for which the apparent affinity is independent of which membrane face is sampled. Finally, we may infer that, whatever the precise nature of the NMR-observable binding sites, the exofacial sites have at least a two-fold higher apparent affinity for glucose than do the endofacial sites.

DISCUSSION

With the TRNOE assay, we set out to probe D-glucose binding behavior of GLUT1 as a test of mechanism complementary to the many transport studies in the literature. This approach reveals three salient results: (i) simple rectangular hyperbolic binding curves, (ii) the presence of binding sites at both membrane faces, and (iii) variation of apparent K_D with varying exposure of membrane faces. The first two observations are consistent with the alternating conformer model, but the third is not, indicating greater mechanistic complexity than is revealed by transport kinetics. We expand on each of these three features in turn.

Binding curves consistent with a single homogeneous class of sites have been observed for two other transport proteins (Band 3[6] and *lac* permease[9]) by NMR methods in our laboratory; this feature thus appears to be a general one. Since the present data

indicate the presence of two or more classes of sites which are not macroscopically averaged, it is legitimate to question why this is not reflected in the shape of the binding curves. It was found with several representative TRNOE data sets that good fits to two classes of sites were readily obtained when both the amplitudes and affinities of each component were allowed to vary, provided the two affinities were fairly similar (differing by a factor of 10 or less). Thus the apparent simplicity of the binding curves does not necessarily reflect microscopic homogeneity.

The presence of sites at both faces of the membrane demonstrated in the present work also parallels observations in the Band 3 and *lac* permease systems. A demonstration of the presence of exofacial sites on GLUT1 more direct than the results described here was obtained by recent selective T_1 measurements of ligand binding[10] (also in our laboratory): in a preparation of resealed crushed ghosts (at physiological ionic strength) significant binding of 4,6-O-ethylidene-D-glucose, but not n-propyl-β-D-glucoside, was observed. Both of these glucose derivatives are impermeant inhibitors of glucose transport; the former a competitive inhibitor of glucose influx, the latter a competitive inhibitor of glucose efflux. The observed relaxation effects are thus consistent with exposure of only the extracellular membrane surface and binding sites thereupon to the bulk solution. Taken together with the present work, we have conclusively demonstrated that at equilibrium, an ensemble of GLUT1 proteins presents binding sites to both sides of the erythrocyte membrane.

Most interesting among the TRNOE results is the variation of apparent dissociation constants with varied exposure of membrane faces to the bulk solution. An even larger variation was found for lactose binding to *lac* permease (apparent K_Ds of approximately 20 mM and 250 mM in RO and IO vesicles, respectively).[9] In both sugar transport systems, then, sites which contribute to the TRNOE are not simply the transport sites of an alternating conformer mechanism. A further similarity between the two proteins is that, of the sites which *are* sampled, those at the extracellular face have a

higher apparent affinity for ligand than do those at the cytoplasmic face. In contrast, no significant variation with exposure of membrane faces was reported in the apparent K_D for chloride binding to Band 3.[6]

The alternating conformer model is inadequate to account for the ligand binding observed. The property of alternating conformer transport sites which makes them appear homogeneous is that they are interconverted by a conformational change of the protein; alternatively one may view this as complete anticooperativity between the endofacial and exofacial sites. More complicated models of GLUT1 mechanism which feature an additional transport site or sites, each of which may assume inward- or outward-facing forms (such as Carruthers' iso-two-site model[3]), can similarly be shown to predict an apparent dissociation constant which is independent of the particular membrane face sampled. The question becomes then, exactly what sites are detected by the TRNOE binding assay?

What is required is at least one site which is not a transport site, *i.e.*, a site which is confined to one side of the membrane or the other. Since the alternating conformer model is an adequate description of GLUT1 glucose *transport*; we retain the transport sites of this model and simply posit the presence of at least one additional site which is not directly involved in ligand translocation and which is accessible to ligand from one compartment or the other, but not from both. The tertiary structure of GLUT1 is likely to include a water-filled channel (see Chapter 1), so we refer to these sites as "channel sites" to distinguish them from transport sites. Assuming the presence of one or more channel sites allows us to interpret the TRNOE data. If only one channel site is present, then at minimum that site contributes to the TRNOE, as does the transport site at the opposite membrane face; the transport site on the same side as the channel site may (but need not necessarily) also contribute. This arrangement yields the observed variation in apparent K_D: the contribution of each site to the TRNOE depends as before on exposure to bulk ligand of the compartment in which that site is resident, but in this case both the

amplitude *and* the macroscopic K_D are averages weighted by exposures of the various compartments. A model of GLUT1 glucose transport which includes a channel site is presented in detail in Chapter 6 below.

In this view, we may not conclude that binding to both transport sites is observed. In the extreme case, if channel sites are present at both membrane faces, the TRNOE may originate in binding of glucose to these sites only and contain no information about the transport sites. The TRNOE results cannot therefore be regarded as experimental support for the assumption of rapid association and dissociation of ligand from transport sites relative to transporter reorientations, as some workers have done[11] based on the original report[12] from this laboratory.

Although disputes over the appropriate kinetic description of GLUT1 glucose transport have been resolved in favor of the alternating conformer model, the model has been shown inadequate to account for aspects of inhibition of glucose transport and ligand binding by the inhibitor cytochalasin B.[13,14] The mode of cytochalasin B inhibition of the D-glucose TRNOE is examined in the next chapter. Inhibition data provide additional support for the existence of one or more channel sites. Finally, we note that both α- and β-D-glucose bind to channel sites based on the TRNOE binding curves presented above, but these data reveal no differences in binding of the two anomers. In examination of *inhibition* of their NMR-observable binding, for the first time a differential interaction of the two anomers with GLUT1 is discerned.

REFERENCES

1. Stein, W. D., <u>Transport and Diffusion Across Cell Membranes</u>, pp. 231-337, Academic Press, Orlando, 1986.

2. Holman, G. D., <u>Biochim. Biophys. Acta</u>, **599** (1980) 202-213.

3. Carruthers, A., <u>Biochemistry</u>, **30** (1991) 3898-3906.

4. Wheeler, T. J., and Whelan, J. D., <u>Biochemistry</u>, **27** (1988) 1441-1450.

5. King, E. L., and Altman, C., <u>J. Phys. Chem.</u>, **60** (1956) 1375-1378.

6. Falke, J. J., Ph. D. thesis, California Institute of Technology, 1985.

7. Steck, T. L., in <u>Methods in Membrane Biology</u>, **2** (1974) 245-381.

8. Lowe, A. G., and Walmsley, A. R., <u>Biochim. Biophys. Acta</u>, **857** (1986) 146-154.

9. Worthen, D. L, M. S. thesis, California Institute of Technology, 1989.

10. Cavagnero, S., Candidacy report, California Institute of Technology, 1992.

11. Lowe, A. G., <u>Biochem. Soc. Trans.</u>, **17** (1989) 435-438.

12. Wang, J.-F., Falke, J. J., and Chan, S. I., <u>Proc. Natl. Acad. Sci. (USA)</u>, **83** (1986) 3277-3281.

13. Helgerson, A. L., and Carruthers, A., <u>J. Biol. Chem.</u>, **262** (1987) 5464-5475.

14. Carruthers, A., and Helgerson, A. L., <u>Biochemistry</u>, **30** (1991) 3907-3915.

APPENDIX: APPLICATION OF KING-ALTMAN METHOD TO THE
ALTERNATING CONFORMER MODEL WITH TWO PERMEANT LIGANDS

Solution of complicated reaction mechanisms for concentrations of individual chemical species under the assumption of a steady state is straightforward, but tedious. For an enzyme-catalyzed reaction (or in the present instance, for a transport mechanism) which contains n different enzyme-containing species EX_i, assumption of a steady state yields a system of n - 1 linear equations (and the mass balance relationship $E_t = \Sigma\ EX_i$, where E_t is the stoichiometric concentration of the enzyme). King and Altman[1] developed a diagrammatic method of solution of such systems based on Cramer's rule. The King-Altman method has been widely applied; useful refinements and simplifications have been reported by Huang[2] and Cha[3]. We apply the method here to solve for the concentrations of the species EL_1, EL_2, EL'_1 and EL'_2 in an alternating conformer transporter at equilibrium with two competing ligands L and L' (Figure 4.A.1).

King and Altman succinctly state the rationale for the method:

The concentration of each EX_i relative to the total concentration of enzyme, EX_i/E_t, is a quotient of two summations of terms, each term being the product of n - 1 different rate constants and the appropriate concentrations. Each term in the numerator of the expression for EX_m/E_t involves the rate constants (and appropriate concentrations) associated with reaction steps which individually or in sequence lead to EX_m, the enzyme-containing species in question. The n - 1 rate constants in each term are associated with n - 1 reaction steps in which each of the enzyme-containing species $EX_{i \neq m}$ is a reactant. All of the possible combinations of n - 1 rate constants which conform to this requirement are present as numerator terms in the expression for EX_m/E_t. The denominator of this expression is the sum of the several different numerators.[1]

To simply determine the proper terms to include in each expression we draw the set of all open diagrams of the mechanism which contain each form of the transporter. According to Huang[2], a mechanism with two closed loops, each with four lines, has 15

Figure 4.A.1

Alternating Conformer Model with Two Permeant Ligands. The transporter may exist in either of two conformations, with the transport site facing outward (denoted by subscripts "1") or inward (subscripts "2"). Two ligands L and L' are present. The concentration of a given ligand is the same in both compartments at equilibrium.

$$EL'_1 \underset{g'_2}{\overset{g'_1}{\rightleftharpoons}} EL'_2$$

$$f'_1 \quad b'_1 \qquad\qquad f'_2 \quad b'_2$$

$$\begin{array}{c} L' \\ + \end{array} \qquad\qquad \begin{array}{c} L' \\ + \end{array}$$

$$E_1 \underset{k_2}{\overset{k_1}{\rightleftharpoons}} E_2$$

$$\begin{array}{c} + \\ L \end{array} \qquad\qquad \begin{array}{c} + \\ L \end{array}$$

$$f_1 \quad b_1 \qquad\qquad f_2 \quad b_2$$

$$EL_1 \underset{g_2}{\overset{g_1}{\rightleftharpoons}} EL_2$$
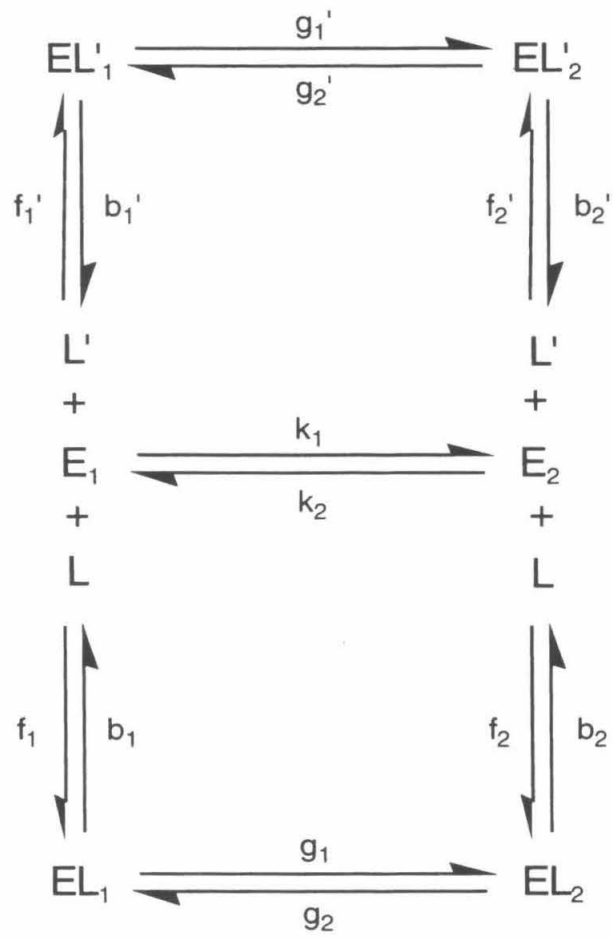
numerator terms in each concentration expression. The 15 diagrams of the mechanism are

$$\sqcup \; \sqcap \; \sqsubset \; \sqsupset \; \sqsubset \; \sqcup \; \sqsupset \; \varsigma \; \varsigma$$

$$\sqcap \; \sqcap \; \sqcup \; \sqcup \; \sqsubset \; \sqsupset \; \sqcap$$
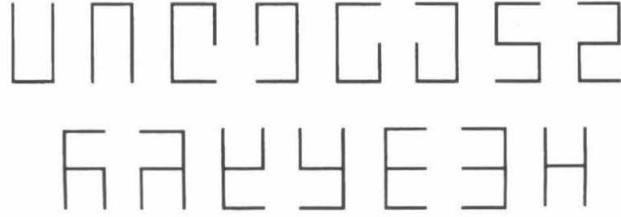
The appropriate numerator terms are obtained by multiplying the rate constants (and concentrations) for all steps leading (in a given diagram) to the species of interest. For example, for the complex EL_1 of Figure 4.A.1., the diagram $\sqcup$ yields a term $b_1'f_1f_2g_2g_2'L^2$. The steady-state concentration of EL_1 relative to E_t is then given by the sum of terms obtained in this fashion using all 15 diagrams, divided by the sum of such numerator terms for *all* EX_i. With 6 transporter-containing species in the mechanism and 15 diagrams, we have $6 \times 15 = 90$ terms in the denominator.

Carrying out the operation described above, we obtain the equilibrium concentrations

$$\frac{EL_1}{E_t} = \frac{\begin{aligned} &(b_1'b_2' + b_1'g_2' + b_2'g_1')[(b_2 + g_2)f_1k_2 + f_2g_2(k_1 + f_1L)]L \\ &+ [(b_2 + g_2)b_1'f_1f_2'g_2' + b_2'f_1'f_2g_1'g_2]LL' \end{aligned}}{\Sigma} \qquad (4.A.1)$$

$$\frac{EL_2}{E_t} = \frac{\begin{aligned} &(b_1'b_2' + b_1'g_2' + b_2'g_1')[(b_1 + g_1)f_2k_1 + f_1g_1(k_2 + f_2L)]L \\ &+ [(b_1 + g_1)b_2'f_1'f_2g_1' + b_1'f_1f_2'g_1g_2']LL' \end{aligned}}{\Sigma} \qquad (4.A.2)$$

$$\frac{EL_1'}{E_t} = \frac{\begin{aligned} &(b_1b_2 + b_1g_2 + b_2g_1)[(b_2' + g_2')f_1'k_2 + f_2'g_2'(k_1 + f_1'L')]L' \\ &+ [(b_2' + g_2')b_1f_1'f_2g_2 + b_2f_1f_2'g_1g_2']LL' \end{aligned}}{\Sigma} \qquad (4.A.3)$$

$$\frac{EL_2'}{E_t} = \frac{\begin{aligned} &(b_1b_2 + b_1g_2 + b_2g_1)[(b_1' + g_1')f_2'k_1 + f_1'g_1'(k_2 + f_2'L')]L' \\ &+ [(b_1' + g_1')b_2f_1f_2'g_1 + b_1f_1'f_2g_1'g_2]LL' \end{aligned}}{\Sigma} \qquad (4.A.4)$$

where the denominator Σ is given by

$$\Sigma = \quad (b_1'b_2' + b_1'g_2' + b_2'g_1') \left\{ \begin{array}{l} [(g_1 + g_2)k_2 + b_2(g_1 + k_2)]f_1 \\ + [(g_1 + g_2)k_1 + b_1(g_2 + k_1)]f_2 \\ \quad + f_1 f_2 (g_1 + g_2)L \end{array} \right\} L$$

$$+ (b_1 b_2 + b_1 g_2 + b_2 g_1) \left\{ \begin{array}{l} [(g_1' + g_2')k_2 + b_2'(g_1' + k_2)]f_1' \\ + [(g_1' + g_2')k_1 + b_1'(g_2' + k_1)]f_2' \\ \quad + f_1' f_2' (g_1' + g_2')L \end{array} \right\} L' \qquad (4.A.5)$$

$$+ \left\{ \begin{array}{l} [b_1'g_2'(b_2 + g_1 + g_2) + b_2 g_1(b_1' + g_1' + g_2')]f_1 f_2' \\ + [b_2'g_1'(b_1 + g_1 + g_2) + b_1 g_2(b_2' + g_1' + g_2')]f_1' f_2 \end{array} \right\} LL'$$

$$+ (k_1 + k_2)(b_1 b_2 + b_1 g_2 + b_2 g_1)(b_1'b_2' + b_1'g_2' + b_2'g_1') \ .$$

Setting L' = 0 in equations (4.A.1) and (4.A.2) above yields the concentrations of EL_1 and EL_2 in the presence of one ligand (L) only, expressions presented as equations (4.7) and (4.8) in the text.

Finally, to clarify the derivation of the apparent dissociation constants $\overline{K}_D^\alpha$ and $\overline{K}_D^\beta$ of equations (4.21) and (4.22), we note that the two ligands L, L' in the case of interest are the two glucose anomers, whose concentrations in the equilibrium mixture are related by $\alpha_t = r\beta_t$. Employing the customary definitions for the microscopic dissociation constants for each of the binding equilibria in Figure (4.A.1),

$$K_{D1}^\beta = \frac{b_1}{f_1} \ , \quad K_{D1}^\alpha = \frac{b_1'}{f_1'} \ , \quad K_{D2}^\beta = \frac{b_2}{f_2} \ , \quad K_{D2}^\alpha = \frac{b_2'}{f_2'} \ , \qquad (4.A.6)$$

the steady-state concentration expressions may be recast. For example,

$$\frac{EL_1}{E_t} = \frac{\left(1+\dfrac{g_1'}{b_1'}+\dfrac{g_2'}{b_2'}\right)\left[\left(1+\dfrac{g_2}{b_2}\right)k_2 K_{D2}^\beta + g_2\left(\dfrac{k_1}{b_1}K_{D1}^\beta+\beta_t\right)\right]K_{D1}^\alpha K_{D2}^\alpha\beta_t + \left[\left(1+\dfrac{g_2}{b_2}\right)g_2' K_{D1}^\alpha K_{D2}^\beta + \dfrac{g_2}{b_1}g_1' K_{D1}^\beta K_{D2}^\alpha\right]\alpha_t\beta_t}{\begin{aligned}&\left(1+\dfrac{g_1'}{b_1'}+\dfrac{g_2'}{b_2'}\right)\left\{\left[\dfrac{k_2}{b_2}(g_1+g_2)+(g_1+k_2)\right]K_{D2}^\beta + \left[\dfrac{k_1}{b_1}(g_1+g_2)+(g_2+k_1)\right]K_{D1}^\beta + (g_1+g_2)\beta_t\right\}K_{D1}^\alpha K_{D2}^\alpha\beta_t\\[4pt]&+\left(1+\dfrac{g_1}{b_1}+\dfrac{g_2}{b_2}\right)\left\{\left[\dfrac{k_2}{b_2'}(g_1'+g_2')+(g_1'+k_2)\right]K_{D2}^\alpha + \left[\dfrac{k_1}{b_1'}(g_1'+g_2')+(g_2'+k_1)\right]K_{D1}^\alpha + (g_1'+g_2')\alpha_t\right\}K_{D1}^\beta K_{D2}^\beta\alpha_t\\[4pt]&+\left\{\left[g_2'\left(1+\dfrac{g_1}{b_2}+\dfrac{g_2}{b_2}\right)+g_1\left(1+\dfrac{g_1'}{b_1'}+\dfrac{g_2'}{b_1'}\right)\right]K_{D1}^\alpha K_{D2}^\beta + \left[g_1'\left(1+\dfrac{g_1}{b_1}+\dfrac{g_2}{b_1}\right)+g_2\left(1+\dfrac{g_1'}{b_2'}+\dfrac{g_2'}{b_2'}\right)\right]K_{D1}^\beta K_{D2}^\alpha\right\}\alpha_t\beta_t\\[4pt]&+(k_1+k_2)\left(1+\dfrac{g_1}{b_1}+\dfrac{g_2}{b_2}\right)\left(1+\dfrac{g_1'}{b_1'}+\dfrac{g_2'}{b_2'}\right)K_{D1}^\alpha K_{D1}^\beta K_{D2}^\alpha K_{D2}^\beta\end{aligned}} \tag{4.A.7}$$

Similar expressions may be obtained for the other transporter-ligand complexes. It was shown in the text that the rate constants for conformational changes of the transporter are much smaller than those for binding and dissociation of ligand. Thus terms in g/b, k/b in equation (4.A.7) above may be dropped, leading to substantial simplification: we have

$$\frac{EL_1}{E_t} = \frac{\left(K_{D1}^\beta\right)^{-1}\beta_t}{1+\dfrac{k_1}{k_2}+\left\{\left(K_{D1}^\beta\right)^{-1}+r\left(K_{D1}^\alpha\right)^{-1}+\dfrac{k_1}{k_2}\left[\left(K_{D2}^\beta\right)^{-1}+r\left(K_{D2}^\alpha\right)^{-1}\right]\right\}\beta_t} \tag{4.A.8}$$

$$\frac{EL_2}{E_t} = \frac{\dfrac{k_1}{k_2}\left(K_{D2}^{\beta}\right)^{-1}\beta_t}{1+\dfrac{k_1}{k_2}+\left\{\left(K_{D1}^{\beta}\right)^{-1}+r\left(K_{D1}^{\alpha}\right)^{-1}+\dfrac{k_1}{k_2}\left[\left(K_{D2}^{\beta}\right)^{-1}+r\left(K_{D2}^{\alpha}\right)^{-1}\right]\right\}\beta_t} \qquad (4.A.9)$$

$$\frac{EL_1'}{E_t} = \frac{\left(K_{D1}^{\alpha}\right)^{-1}\alpha_t}{1+\dfrac{k_1}{k_2}+r^{-1}\left\{\left(K_{D1}^{\beta}\right)^{-1}+r\left(K_{D1}^{\alpha}\right)^{-1}+\dfrac{k_1}{k_2}\left[\left(K_{D2}^{\beta}\right)^{-1}+r\left(K_{D2}^{\alpha}\right)^{-1}\right]\right\}\alpha_t} \qquad (4.A.10)$$

$$\frac{EL_2'}{E_t} = \frac{\dfrac{k_1}{k_2}\left(K_{D2}^{\alpha}\right)^{-1}\alpha_t}{1+\dfrac{k_1}{k_2}+r^{-1}\left\{\left(K_{D1}^{\beta}\right)^{-1}+r\left(K_{D1}^{\alpha}\right)^{-1}+\dfrac{k_1}{k_2}\left[\left(K_{D2}^{\beta}\right)^{-1}+r\left(K_{D2}^{\alpha}\right)^{-1}\right]\right\}\alpha_t} \qquad (4.A.11)$$

Each of these expressions is readily rearranged to the form

$$\frac{EX_m}{E_t} = \text{constant} \times \frac{L}{\overline{K}_D + L}$$

where $\overline{K}_D$ is precisely $\overline{K}_D^{\alpha}$ given by equation (4.21) if $L = \alpha_t$, or $\overline{K}_D^{\beta}$ of equation (4.22) if $L = \beta_t$.

1. King, E. L, and Altman, C., J. Phys. Chem., **60** (1956) 1375-1378.

2. Huang, C., in Meths. Enzymol., v. **63**, pt. A (1978) 58-62.

3. Cha, S., J. Biol. Chem., **243** (1968) 820-826.

CHAPTER 5

THE D-GLUCOSE ^{1}H TRNOE IN CRUSHED GHOST SUSPENSIONS: INHIBITION
BY CYTOCHALASIN B

INTRODUCTION

As it has in the study of enzymes, the use of highly specific reversible inhibitors has contributed greatly to our understanding of transport protein function. The most intensively studied inhibitor of GLUT1 glucose transport is, without a doubt, cytochalasin B (CB) (Figure 5.1). As noted in previous chapters, studies of transport inhibition and equilibrium CB binding are consistent with the presence of a single class of sugar-sensitive CB sites on GLUT1, with an inhibitor: protein stoichiometry of 0.5:1 or 1:1 depending on the oligomeric state of the protein. UV irradiation of GLUT1 in the presence of CB irreversibly labels the protein at a site or sites as yet undetermined.[1]

Like many transport inhibitors, CB blocks transport with a distinct "sidedness." In earlier work, it was found that CB is a competitive inhibitor of glucose efflux, but a *noncompetitive* inhibitor of glucose influx. Devés and Krupka first interpreted these observations in terms of the alternating conformer model.[2] Such a pattern of inhibition will be observed for an alternating conformer transporter if the inhibitor binds only to the inward-facing conformer of the unloaded transporter. Furthermore, an early study showed no evidence for the existence of ternary complexes of GLUT1, CB and phloretin, which latter molecule inhibits glucose transport with "sidedness" opposite to that of CB.[3] The failure to observe this ternary complex was taken as evidence for the existence on GLUT1 of only one binding site exposed at any one time; in the alternating conformer model, a transporter with ligand bound to the inward(outward)-facing conformer would not present a binding site to the outside(inside) face of the membrane. In contrast, in more recent studies of the effects of phloretin and other outside-selective or -specific glucose transport inhibitors on equilibrium CB binding[4] and on CB inhibition of glucose transport[5], the data presented clearly indicate the existence of such ternary complexes, and by extension indicate that the alternating conformer model is insufficient to describe fully the molecular mechanism of GLUT1 function.

Figure 5.1

The Chemical Structure of Cytochalasin B.
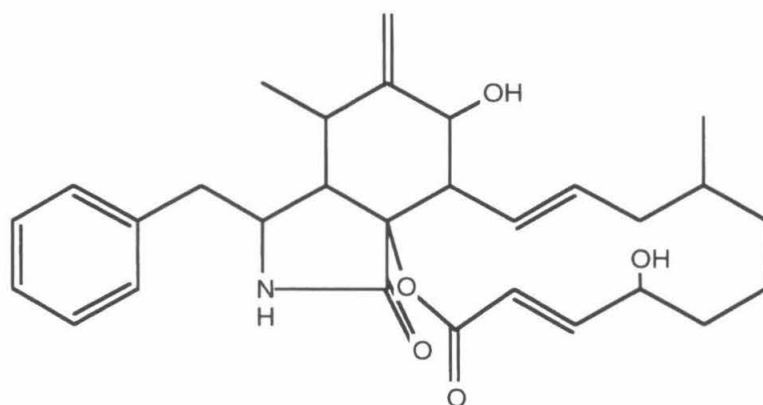
We have shown in Chapter 4 that the TRNOEs observed in α- and β-D-glucose

signals in erythrocyte ghost membrane suspensions do not arise solely from binding of

sugar to the transport sites of an alternating conformer transporter. We have also

demonstrated (Chapter 3) that CB completely reverses these TRNOEs. In an attempt to

clarify the relationship among NMR-observable sugar sites, CB sites and the transport

mechanism, we undertook a detailed study of this inhibition. Below, simple predictions

are developed for the TRNOE in the presence of a reversible inhibitor of binding, based

on a model containing one inhibitor site and one ligand site for which two ligands

compete. These predictions are compared with the results for CB reversal of the D-

glucose TRNOEs in crushed ghosts. This approach demonstrates the presence of ternary

complexes of GLUT1, CB and α-D-glucose, and indicates that the β anomer may form

such complexes as well, once again pointing to greater structural and mechanistic

complexity than predicted by the alternating conformer model. The data also show that

there are two classes of sugar-sensitive CB sites which differ in their sensitivity to the

two glucose anomers. Finally, the inhibition data provide evidence for a high affinity

sugar site specific for α-D-glucose.

EXPERIMENTAL SECTION

Materials. D-glucose was obtained from Calbiochem, cytochalasin B from

Sigma. ^2H_2O and DMSO-d_6 were obtained from Cambridge Isotope Labs; $Na^2H_2PO_4$

was obtained from MSD Isotopes. All other chemicals used were reagent grade or better.

Outdated packed human erythrocytes were a kind gift of the Los Angeles chapter of the

American Red Cross.

NMR Sample Preparation and Spectroscopy. Crushed ghosts were prepared

exactly as described in Chapter 3. For the experiments described in the present Chapter,

the crushed ghost pellets obtained from ultracentrifugation were resuspended in 1.35 -

1.45 volumes of 5pD7.4 buffer (5 mM NaPhos, p^2H adjusted to 7.4 with NaOD, meter

reading corrected for isotope effect). Immediately prior to NMR experiments, the resulting stock ghost suspension was stirred with D-glucose stock solution (also in 5pD7.4) of the appropriate concentration. 0.445 ml aliquots of this ghost/sugar stock were transferred into ultra-thin-walled 5 mm O. D. NMR tubes *via* syringe with an 18 ga. needle. The samples were then brought to the desired concentrations of CB and a final volume of 0.450 ml with CB stock in DMSO-d_6 and/or DMSO-d_6 as appropriate. Samples were mixed by repeated inversion and "shaking down" of the NMR tubes, then stored at room temperature in the dark until they could be analyzed spectroscopically; typically, 12-14 hours passed between sample preparation and the completion of NMR experiments. NMR spectroscopy was carried out at 20.0 ± 0.5 °C as described in Chapter 3. After spectroscopy, samples were stored frozen for later analysis of protein content by the modified[6] Lowry assay.[7] Total ghost protein in the samples used for the present experiments was typically 7-9 mg/ml.

THE EFFECT OF A REVERSIBLE INHIBITOR ON THE TRNOE

The TRNOE observed in a ligand resonance for a small molecule L in fast exchange between bulk solution and a single class of macromolecular binding sites E is approximately (review discussion preceding equation (2.39) for derivation and definitions of symbols):

$$f_I\{S\} - f_I^F\{S\} \approx \frac{\sigma_B}{R_I^F} \frac{EL}{L_t} \quad . \tag{5.1}$$

This expression and the assumption of fast exchange it is based on reveal three ways in which the binding of an inhibitor to the macromolecule (or to another macromolecule allosterically coupled to E) can reverse the TRNOE. First, inhibitor binding may displace L from its binding site, diminishing the concentration of the bound complex EL. Second, binding of inhibitor could block access of free L to its binding site, forcing exchange into an intermediate or slow regime. Lastly, inhibitor binding could alter ligand binding site

structure and bound ligand mobility such that the cross relaxation rate constant σ_B is substantively diminished. This final possibility seems extremely unlikely given the very large cross relaxation rates found in large bound complexes and will not be considered further. We develop now an expression for the dependence of the TRNOE on inhibitor concentration and show how the first two possibilities may be distinguished in the general case; subsequently we will consider the specific case of inhibition of the D-glucose TRNOE by CB in the context of the alternating conformer model and the known pattern of CB inhibition of glucose transport.

Definitions and Assumptions. Consider (Figure 5.2) a macromolecule E which possesses a single binding site for ligand and a single binding site for inhibitor X. In all experimental preparations in the present study, the equilibrium mixture of glucose anomers has been present; we thus include two ligands L and L' (present in the ratio $r =$ L/L') which compete for the ligand site in the scheme of Figure 5.2. We treat the general case of mixed inhibition: inhibitor can bind to any of the three species E, EL, or EL'. Seven dissociation constants then define the system, four for binding of ligands L and L' to E and EX,

$$K_D = \frac{E \cdot L}{EL}, \quad K_D^X = \frac{EX \cdot L}{ELX}, \tag{5.2}$$

$$K_D' = \frac{E \cdot L'}{EL'}, \quad K_D'^X = \frac{EX \cdot L'}{EL'X}, \tag{5.3}$$

and three for binding of inhibitor X to free (E) or liganded (EL or EL') macromolecule,

$$K_X = \frac{E \cdot X}{EX}, \quad K_X^L = \frac{EL \cdot X}{ELX}, \quad K_X^{L'} = \frac{EL' \cdot X}{EL'X} \ . \tag{5.4}$$

We assume that when an inhibitor molecule binds to a particular macromolecule, it completely eliminates the TRNOE arising from ligand binding to that macromolecule but has no effect on other macromolecules in the ensemble. In this case the TRNOE observed is given by

Figure 5.2

Ligand-Binding Equilibrium Scheme. The macromolecule E has one inhibitor site and one ligand site. One inhibitor, X, is present, as are two ligands L and L' which compete for the ligand site. The equilibrium constants indicated are dissociation constants for each of the microscopic equilibria. The principle of detailed balance yields the following relationships among the dissociation constants: $K_D K_I^L = K_D^l K_I$ and $K_D' K_I^{L'} = K_D'^l K_I$.

$$EL' + X \xrightarrow{\quad K_X^{L'} \quad} EL'X$$

$$K_D' \downarrow \qquad\qquad\qquad \downarrow K_{D'}^{X}$$

$$\begin{array}{c} L' \\ + \\ E + X \xrightarrow{\quad K_X \quad} EX \\ + \\ L \end{array} \qquad \begin{array}{c} L' \\ + \\ \\ + \\ L \end{array}$$

$$K_D \downarrow \qquad\qquad\qquad \downarrow K_D^{X}$$

$$EL + X \xleftarrow{\quad K_X^{L} \quad} ELX$$

$$f_I\{S\} - f_I^F\{S\} = \left[f_I\{S\} - f_I^F\{S\}\right]_0 (1 - P_X) \tag{5.5}$$
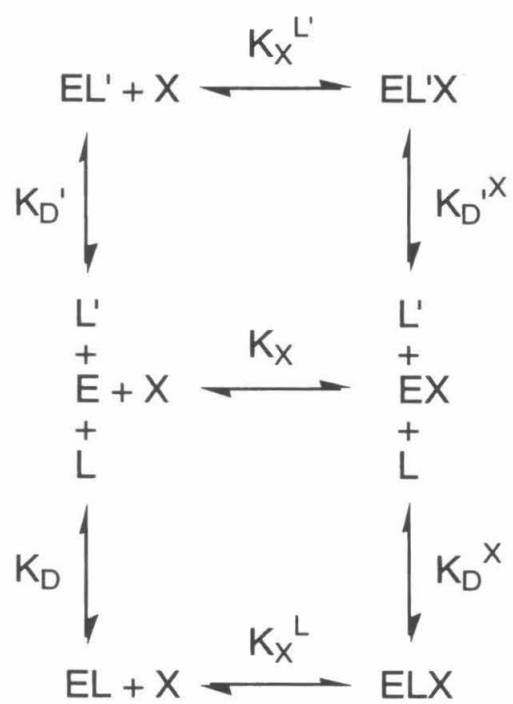
where $[f_I\{S\}-f_I^F\{S\}]_0$ is the TRNOE in the absence of X, and P_X is the fraction of total macromolecule to which X is bound.

Dependence of the TRNOE Inhibition on Inhibitor Concentration. The fractional occupancy of macromolecule by inhibitor is simply given by the concentration of X-bearing species (EX, ELX, EL'X) divided by the total macromolecule concentration:

$$P_X = \frac{EX + ELX + EL'X}{E + EL + EL' + EX + ELX + EL'X} . \tag{5.6}$$

Using the detailed balance constraints $K_D K_I^L = K_D^l K_I$ and $K_D' K_I^{L'} = K_D'^l K_I$ for the equilibrium scheme of Figure 5.2 and the dissociation constants defined in equations (5.2) - (5.4), P_X may be expressed as

$$P_X = \frac{\left(K_D^X K_D'^X + K_D'^X L + K_D^X L'\right)X}{K_X K_D^X K_D'^X + K_X^L K_D'^X L + K_X^{L'} K_D^X L' + \left(K_D^X K_D'^X + K_D'^X L + K_D^X L'\right)X} \tag{5.7}$$

$$= \frac{X}{X + \overline{K}_X} , \tag{5.8}$$

where the apparent (macroscopic) inhibitor dissociation constant $\overline{K}_X$ is given by

$$\overline{K}_X = K_X \frac{1 + (K_D)^{-1} L + (K_D')^{-1} L'}{1 + (K_D^X)^{-1} L + (K_D'^X)^{-1} L'} . \tag{5.9}$$

Equations (5.5) and (5.8) show that inhibition of the TRNOE will be rectangular hyperbolic in inhibitor concentration X, regardless of whether the inhibition is competitive, uncompetitive, or mixed. The mode of inhibition is revealed by the ligand concentration-dependence of the apparent inhibitor constant $\overline{K}_X$; to this end we next examine equation (5.9) in detail.

Dependence of $\overline{K}_X$ on Ligand Concentration. Plots of $\overline{K}_X$ vs. ligand concentration assume characteristic shapes in the limits of a) pure competitive and b) pure uncompetitive inhibition; here we discuss these limiting cases, as well as a third case c) of X as a "channel blocker." We also describe how the inhibitions observed in the two

ligands L and L' are related to one another; as in Chapter 4, comparison of L and L'

TRNOE data here provides a test of our model (in this instance the scheme of Figure 5.2).

Case a). Pure competitive inhibitors act by binding to the ligand site or to an

inhibitor site allosterically coupled to the ligand site such that when the inhibitor site is

occupied, changes in ligand site structure render it unsuitable for binding of ligand. The

microscopic dissociation constants for the ternary complexes ELI and EL'I are then very

large, and the terms linear in ligand concentration in the denominator of equation (5.9)

may be neglected. $\overline{K}_X$ becomes

$$\overline{K}_X = K_X \left[1 + (K_D)^{-1} L + (K_D')^{-1} L' \right] \ . \tag{5.10}$$

Recall that L and L' are proportional to one another, with the proportionality constant r

defined by L' = rL. Thus equation (5.10) may be cast in terms of L or L' alone. It is clear

that $\overline{K}_X$ here depends linearly on ligand concentration (cast as either L or L') with an y-

intercept equal to K_X and a slope equal to the weighted sum of the microscopic

association constants for L and L', weighted by the relative concentrations of the two

ligands (*i.e.*, by the factor r). Linearity of a plot of $\overline{K}_X$ *vs.* ligand concentration is

diagnostic of competitive inhibition. Comparison of plots of $\overline{K}_X$ *vs.* L and $\overline{K}_X$ *vs.* L'

yields several pieces of information. First, if only one inhibitor site is present on E, both

plots must have the same y-intercept. Second, if L and L' are competing for a single

ligand site on E, the plots for both ligands must be linear, with the slope of the $\overline{K}_X$ *vs.* L'

plot equal to r times the slope of the $\overline{K}_X$ *vs.* L plot.

Case b). Uncompetitive inhibition, where X may bind only if L or L' are bound,

may also eliminate the TRNOE if the X and L(L') sites interact in such a way that binding

of X slows exchange of L(L') between free and bound states. Although this limit of

cooperativity between inhibitor and ligand sites is not implicated in CB inhibition of

GLUT1 glucose transport, we consider it here because the characteristic form of $\overline{K}_X$

curve it gives rise to is instructive in understanding (more realistic) situations of mixed

inhibition. For this limit, $K_X \gg K_X{}^L, K_X{}^{L'}$. By detailed balance, this implies also K_D, $K_D' \gg K_D{}^X, K_D'{}^X$. In words, the fact that inhibitor can only bind effectively when ligand is bound means conversely that ligand can only bind effectively when inhibitor is bound. Thus the terms linear in ligand concentration in the *numerator* of equation (5.9) may be neglected, and $\overline{K}_X$ is given by

$$\overline{K}_X = \frac{K_X}{1+(K_D^X)^{-1}L+(K_D'^X)^{-1}L'} \quad . \tag{5.11}$$

For genuine uncompetitive inhibition, K_X is infinite, so $\overline{K}_X$ diverges at low ligand concentration. As L(L') is increased, $\overline{K}_X$ decreases as a rectangular hyperbola, approaching zero asymptotically at high ligand concentration.

Case c). If binding of X to E blocks exchange of L and L' between bulk solution and their binding site, but doesn't alter the structure of that site, then $K_D = K_D{}^X$ and $K_D' = K_D'{}^X$, and equation (5.9) collapses to

$$\overline{K}_X = K_X \quad , \tag{5.12}$$

independent of ligand concentration. Such a situation could occur when binding of the inhibitor obstructs a water-filled channel which connects a ligand binding site with the bulk aqueous medium. Such channels have been posited to exist in GLUT1 (see Chapters 1 and 4) and in Band 3, where the chloride transport inhibitor 1,2-cyclohexanedione exhibits a Cl⁻-independent inhibition constant.[8]

The "channel blocker" type of inhibitor is a good point of departure for consideration of mixed inhibition and the utility of equation (5.9) in the general case. First, we note that for any mode of inhibition and regardless of which ligand is observed to sample the inhibition, $\overline{K}_X = K_X$ in the limit of zero ligand concentration. Furthermore, it can be seen that, if ternary complexes such as ELI and EL'I form, $\overline{K}_X$ approaches the asymptotic value

$$\lim_{L_t \to \infty} \overline{K}_X = K_X \frac{K_D^X K_D'^X}{K_D K_D'} \frac{K_D' + rK_D}{K_D'^X + rK_D^X} \tag{5.13}$$

at high ligand concentration. This limit is also independent of which ligand is sampled. For the channel blocker, this value is K_X, and the result is a straight line of zero slope. For negative cooperativity between X and L(L') sites, dissociation constants for the binary complexes EL and EL' are smaller than those for the ternary complexes, and $\overline{K}_X$ will be an increasing function of L(L'). If the cooperativity is positive, on the other hand, L(L') will bind more tightly in the ternary complexes than in the binary, and $\overline{K}_X$ will be a decreasing function of L(L').

In the discussion above it was assumed for expository simplicity that the relationships between K_D and $K_D{}^X$ and between K_D' and $K_D'^X$ are similar, *i.e.*, that the modes of inhibition of L and L' binding by X are the same. This is not necessarily the case. For example, binding of L may be cooperative with binding of X, while binding of L' may be anticooperative with binding of X. Such a scenario is not at all unreasonable in the system under consideration: the ligand site is chiral and the two ligands (the two D-glucose anomers) are diastereomers. If we were able to monitor inhibition of binding of one ligand in the absence of the other, we would then see a decrease of $\overline{K}_X$ with increasing L, but an increase of $\overline{K}_X$ with increasing L'. Since the ligands are present in the equilibrium mixture, however, the macroscopically observed inhibition depends on linear combinations of the microscopic dissociation constants for the two ligands. Thus although the microscopic modes of inhibition of L and L' binding may differ, the inhibition observed in either ligand is a composite of both interactions.

We summarize now the information contained in the ligand concentration-dependence of $\overline{K}_X$. For pure competitive inhibition, $\overline{K}_X$ increases linearly with L(L'). Any nonlinearity implies the existence of the ternary complexes ELI and/or EL'I. If ternary complexes can form but are less stable than the binary complexes EL and EL', $\overline{K}_X$ still increases, but curves to plateau at high L(L'). For a pure channel blocker, $\overline{K}_X$ is

independent of ligand concentration. If binding of X and L(L') show positive cooperativity, $\overline{K}_X$ is a decreasing function of L(L'), again eventually approaching an asymptotic value. In the limit of uncompetitive inhibition, the asymptote is the x axis. In the present study, equation (5.9) is also very important for the simple qualitative tests it provides of the hypothesized scheme of one inhibitor site and one ligand site for which L and L' compete. First, whatever the mode of inhibition, if inhibition of L and L' binding is due to binding of X to a single class of inhibitor sites, plots of $\overline{K}_X$ *vs.* L and $\overline{K}_X$ *vs.* L' must have the same y-intercept. Second, if L and L' are binding to the same site (or set of transport sites, *vide infra*), the relationship between these two plots is straightforward: they both assume the same form (linear, nonlinear increasing, nonlinear decreasing, hyperbolic) and differ only by the factor r in slope (in the linear, competitive inhibition case) or tend to the same asymptotic value at high ligand concentrations (in the nonlinear cases).

THE ALTERNATING CONFORMER MODEL OF GLUT1 GLUCOSE TRANSPORT AND REVERSAL OF THE D-GLUCOSE TRNOE BY CB

The expressions developed above assume a single class of inhibitor sites and a single class of ligand sites. These expressions are appropriate to testing whether inhibition of the D-glucose TRNOE by CB is consistent with an alternating conformer model of GLUT1 mechanism for the following reasons. First, most previous studies have indicated the presence of only one class of sugar-sensitive CB sites. Second, the present experiments were conducted under equilibrium conditions, with the same ligand concentration in all compartments. It was shown in Chapter 4 that under these conditions, the two transport sites of an alternating conformer transporter behave macroscopically as a single homogeneous class of sites. Thus equations (5.5), (5.8) and (5.9) above would retain their forms and the features here of interest if we treated the conformational equilibrium of the transport sites explicitly, with conformationally-

averaged values replacing each microscopic dissociation constant of Figure 5.2. For comparison of our data with predictions (described below) of the alternating conformer model, we note only that the averaging of the dissociation constants K_D and K_D' for the binary complexes EL and EL' is identical to that derived in Chapter 4 (equations (4.21) and (4.22)).[9] Since we cannot deconvolute these microscopic parameters, the scheme of Figure 5.2 was adopted as the simplest model with which to evaluate CB inhibition of glucose binding to GLUT1.

Devés and Krupka[2] showed that competitive inhibition of glucose efflux and noncompetitive inhibition of glucose influx by CB is consistent with binding of the inhibitor to the inward-facing form of an alternating conformer transporter, either at the endofacial transport site or at a distinct inhibitor site, which when occupied locks the transporter in the inward-facing conformer and excludes sugar from the endofacial transport site (Figure 5.3A). Carruthers[5] generalized this model to account for the observation of simultaneous binding of maltose (an impermeant outside-selective inhibitor of glucose transport) and CB while retaining a one-site alternating conformer model. In this variant (Figure 5.3B), CB binds to an inhibitor site which is present in both conformers of the unloaded transporter. As before, binding of CB to this site excludes sugar from the endofacial transport site (and *vice versa*). However, it doesn't block isomerization of the unloaded transporter; sugar may thus bind to the exofacial site even when CB is bound. This model is consistent with the experimentally observed competitive inhibition of glucose efflux, noncompetitive inhibition of glucose influx and competitive inhibition by glucose of CB binding if a) binding of CB blocks translocation of sugar bound to the exofacial transport site and b) the CB site and the exofacial transport site show no cooperativity.

These two models of the effect of CB on GLUT1 lead to simple predictions for reversal of the D-glucose TRNOE in the presence of the inhibitor. The scheme of Figure 5.3A predicts strict competition between CB and sugar. According to equation (5.10), if

Figure 5.3

Models of CB Interaction with an Alternating Conformer Transporter. Model A. CB
interacts only with the inward-facing conformer of the transporter E, displacing ligand L
(permeant sugar) from the endofacial transport site. Binding of CB locks the protein into
the inward-facing conformer. Model B. CB binds to either conformer of the transporter,
again displacing L from the endofacial transport site. In this model CB binding does not
prevent isomerizations of the unloaded transporter. Ligand may bind to the exofacial
transport site even when inhibitor is bound (forming the ternary complex EL_1CB), but
occupancy of the inhibitor site prohibits translocation of bound sugar. Subscripts 1 and 2
in both models indicate outward- and inward-facing conformers of the transporter,
respectively. Transporter isomerization steps are represented by double arrows; binding
equilibria are indicated by double-headed single arrows.
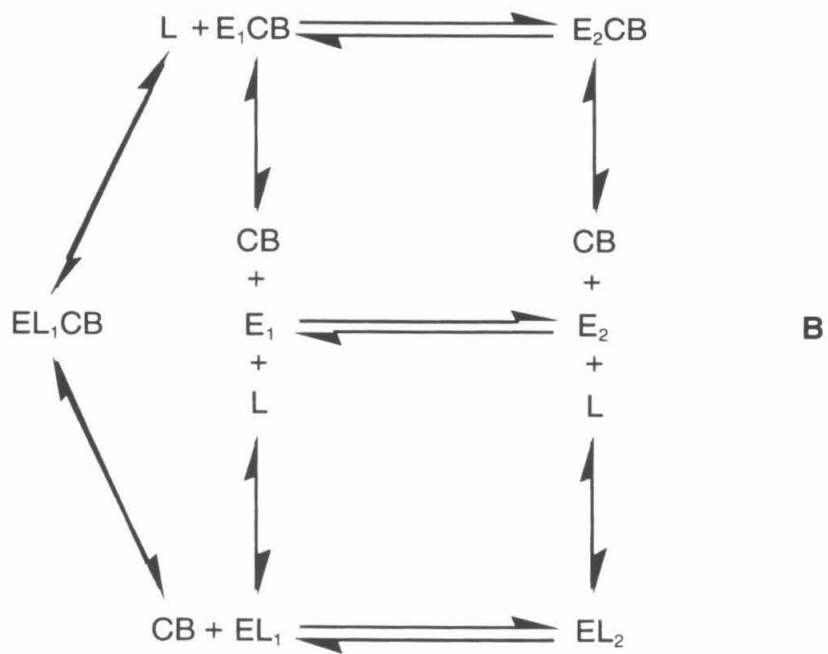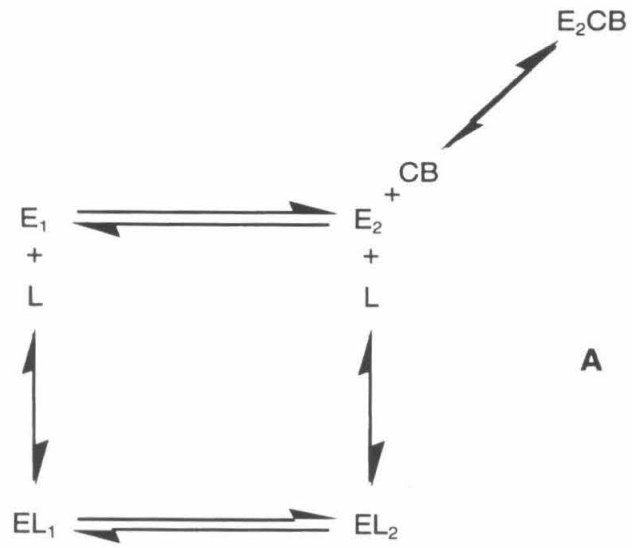
this model is correct, the apparent inhibitor constant $\overline{K}_X$ will be linear in ligand concentration.

The form of $\overline{K}_X$ is slightly more opaque if the scheme of Figure 5.3B is correct. In this case, in addition to the competitive component due to sugar binding to the endofacial transport site, the effect of the exofacial site must be considered. Recall that a saturating concentration of CB was shown in Chapter 3 to eliminate the D-glucose TRNOE; thus if sugar binds to the exofacial site when CB is bound, it must be in slow exchange at this site. The requirement that the inhibitor and exofacial transport sites must show no cooperativity implies then that CB acts as a channel blocker with respect to the exofacial transport site, slowing exchange without altering the affinity of the site for sugar. Since channel blocking leads to a ligand concentration-independent $\overline{K}_X$, the net observed dependence of $\overline{K}_X$ on ligand concentration will be linear, with a slope greater than zero but less than that predicted by equation (5.10). The relative contributions of endo- and exofacial sites to the TRNOE (and thence to $\overline{K}_X$) depend on the equilibrium distribution of transporters between inward- and outward-facing conformers.

Testing the consistency of TRNOE inhibition data with these models is straightforward. Both models of CB inhibition of an alternating conformer transporter predict a linear dependence of $\overline{K}_X$ on ligand concentration. As discussed above, the y-intercept of plots of $\overline{K}_X$ vs. ligand concentration is predicted to be independent of which ligand signal is sampled. (Note that this intercept is no longer simply a microscopic inhibitor dissociation constant; rather it is an average of the microscopic constants for the two transporter conformers, weighted by the distribution of transporters between the two.) Also, in the two schemes of Figure 5.3 as in the single ligand site competitive case of equation (5.10), the slope of the $\overline{K}_X$ vs. L' plot is predicted to be r times the slope of the $\overline{K}_X$ vs. L plot.

RESULTS

Dependence of D-glucose TRNOEs on CB Concentration. Over the range of sugar concentrations examined (total D-glucose 2-100 mM), plots of the TRNOEs observed in α- and β-D-glucose resonances in crushed ghost suspensions *vs.* CB concentration are well-fit by a single rectangular hyperbola in accord with equation (5.8) (except in two cases, in the β anomer signals at 75 mM total sugar and in the α anomer signals at 100 mM total sugar, where scatter in the data prevented the fitting routine from converging). Representative data are shown in Figures 5.4 and 5.5 (see also Figure 3.7). The floated values of the maximal TRNOE amplitude over this range of sugar concentrations provide an interesting test of consistency with sugar binding in the absence of inhibitor: fitting these values as a function of inverse ligand concentration (Figure 5.6) yields macroscopic dissociation constants of 22.2 ± 6.1 mM and 25.9 ± 4.7 mM for the α and β anomer in the crushed ghost system, respectively, quantitatively similar to the values extracted directly from the inverse sugar concentration-dependence of the TRNOE (30.7 ± 6.2 and 30.0 ± 7.3 mM, respectively; see Table 3.1).

Dependence of $\overline{K}_X$ on D-Glucose Concentration. Values of the apparent CB dissociation constant $\overline{K}_X$ obtained from fits to α- and β-D-glucose inhibition curves including those of Figures 5.4 and 5.5 are plotted as functions of ligand concentration in Figure 5.7. It is immediately apparent that the large uncertainties in the fitted $\overline{K}_X$ values propagate into very large uncertainties in the parameters of the fits of these data to equation (5.9). Weighted nonlinear least-squares fits to the data yield for the α-D-glucose TRNOE (Figure 5.7A) values of 1.5 ± 1.1 μM for the apparent CB dissociation constant at zero sugar concentration, 0.47 ± 0.64 mM for the apparent dissociation constant for the binary complex of sugar and GLUT1, and an apparent constant of 2.1 ± 1.5 mM for dissociation of the α anomer from a ternary complex of GLUT1, CB and sugar. The same parameters from the fit to the β-D-glucose data (Figure 5.7B) are 6.0 ± 1.3 μM, 86 ± 270 mM and 11 ± 11 mM, respectively.

Figure 5.4

The Effect of CB on the α-D-Glucose TRNOE in Crushed Ghosts. The TRNOEs observed in H-2α in the equilibrium anomeric mixture at bulk D-glucose concentrations of 2.0 mM (filled triangles), 20 mM (open squares) and 75 mM (filled circles). The solid curves are nonlinear least-squares best fits to the equation

$$y = a + \frac{b}{2E_t}\left(x + E_t + \overline{K}_X - \sqrt{(x + E_t + \overline{K}_X)^2 - 4E_t x}\right)$$

for a homogeneous population of inhibitor binding sites. E_t is the concentration of GLUT1 (between 7 and 8 μM for the data sets shown). The fits yield apparent dissociation constants of 2.9 ± 1.5 μM, 5.2 ± 1.9 μM and 6.0 ± 2.4 μM at 2 mM, 20 mM and 75 mM bulk D-glucose, respectively. Each bulk D-glucose concentration represents a different experiment from a different batch of ghost membranes. Experimental conditions and assay parameters are described in the Experimental Section.
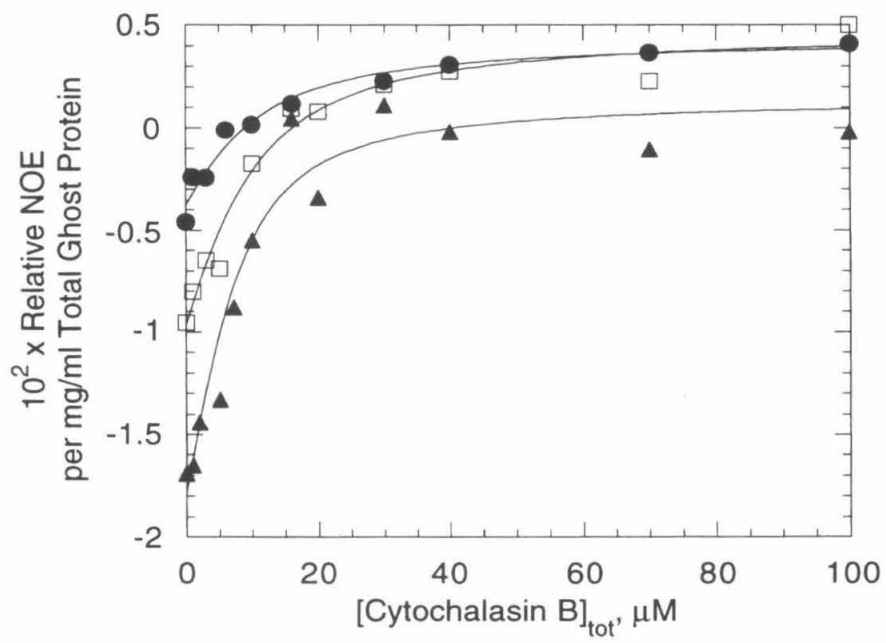
Figure 5.5

The Effect of CB on the β-D-Glucose TRNOE in Crushed Ghosts. The TRNOEs observed in H-2β in the equilibrium mixture at bulk D-glucose concentrations of 2.0 mM (filled triangles), 20 mM (open squares) and 50 mM (filled circles). The solid curves are nonlinear least-squares best fits to the equation

$$y = a + \frac{b}{2E_t}\left(x + E_t + \overline{K}_X - \sqrt{(x + E_t + \overline{K}_X)^2 - 4E_t x}\right)$$

for a homogeneous population of inhibitor binding sites. E_t is the concentration of GLUT1 (between 7 and 8 μM for the data sets shown). The fits yield apparent dissociation constants of 5.3 ± 2.3 μM, 3.3 ± 1.0 μM and 2.5 ± 1.4 μM at 2 mM, 20 mM and 50 mM bulk D-glucose, respectively. Data for 2 and 20 mM D-glucose are from the same experiments as the corresponding α-D-glucose data in Figure 5.4. Experimental conditions and assay parameters are described in the Experimental Section.
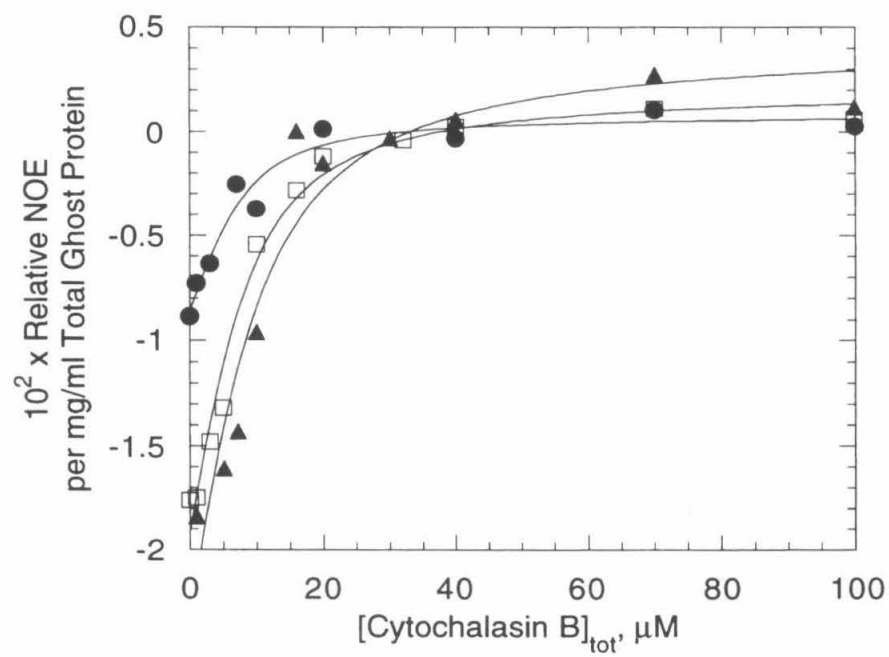
Figure 5.6

Maximal TRNOE Amplitudes from Inhibition Experiments: Dependence on Inverse

Sugar Concentration. (A) α- and (B) β-D-glucose data were obtained from fits to

inhibition curves such as those in Figure 5.4 and represent parameter "a" from that fit

(which is equivalent to $[f_I\{S\}-f_I^F\{S\}]_0$ of equation (5.5)). The error bars represent $\pm \sigma$ in

the fitted parameter, as calculated by the fitting routine. The solid curves are weighted

nonlinear least-squares fits for a single class of binding sites ($y = b/(x + K_D^{-1})$). The fits

yield apparent dissociation constants of (A) 22.2 ± 6.1 mM and (B) 25.9 ± 4.7 mM.

Experimental conditions and assay parameters are described in the Experimental Section.
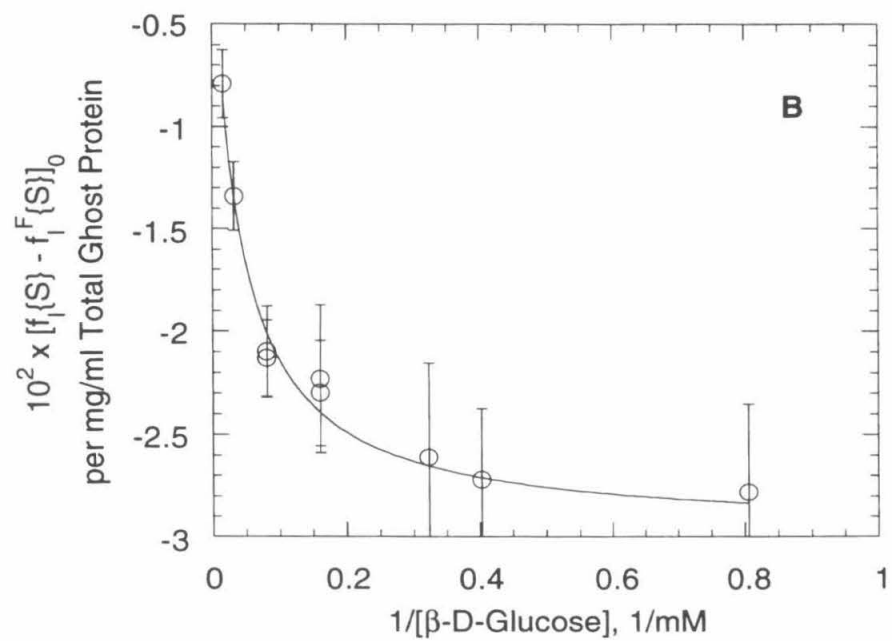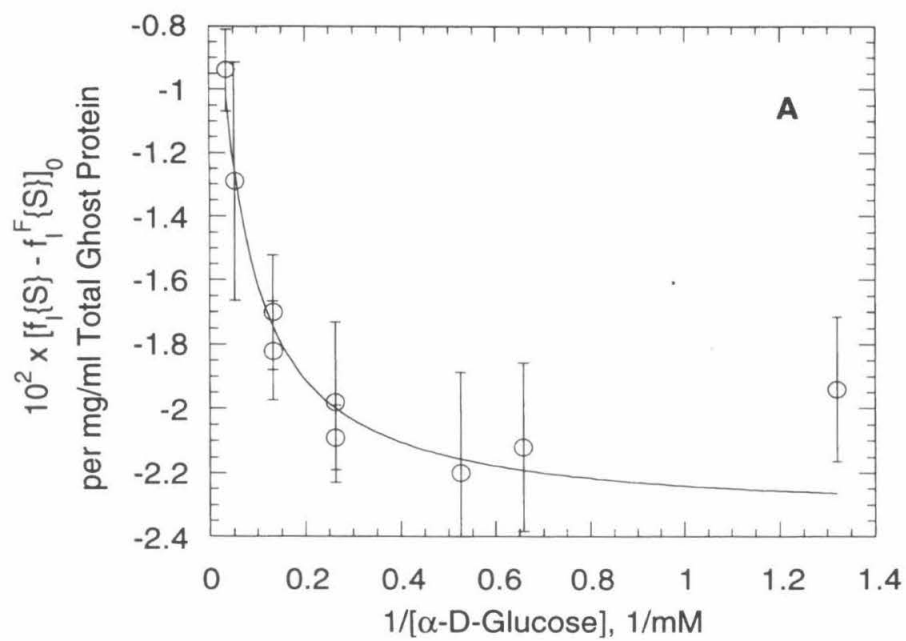
Figure 5.7

$\overline{K}_X$ for CB Reversal of the D-Glucose TRNOE: Dependence on Sugar Concentration.

The individual data points are values of the apparent dissociation constant $\overline{K}_X$ obtained from least-squares fits of CB inhibition of the TRNOE in (A) H-2α and (B) H-2β of D-glucose in the equilibrium mixture of the anomers. Error bars represent $\pm\,\sigma$ in the fitted values, as calculated by the fitting routine. The solid curves are weighted nonlinear least-squares fits to the equation

$$y = a\left(\frac{1+bx}{1+cx}\right)$$

(cf. equation (5.9)), where a is the intrinsic dissociation constant K_X, b is the (macroscopic) inverse dissociation constant $\overline{K}_D^{-1}$ for binary complexes of ligand and transporter, and c is the (macroscopic) inverse ligand dissociation constant $(\overline{K}_D^X)^{-1}$ for ternary complexes of ligand, inhibitor and transporter. The fits yield the values (A) $K_X = 1.5 \pm 1.1\ \mu M$, $\overline{K}_D = 0.47 \pm 0.64$ mM and $\overline{K}_D^X = 2.1 \pm 1.5$ mM for the α-D-glucose data, and (B) $K_X = 6.0 \pm 1.3\ \mu M$, $\overline{K}_D = 86 \pm 270$ mM and $\overline{K}_D^X = 11 \pm 11$ mM for the β-D-glucose data. The broken lines represent literature predictions for the interaction of CB with an alternating conformer transporter (specifically the model of figure 5.3A), using reasonable values of $K_X = 0.4\ \mu M$, $\overline{K}_D = 30$ mM (see Table 3.1) and $\overline{K}_D^X = \infty$ in the above equation. Experimental conditions and assay parameters are described in the Experimental Section.
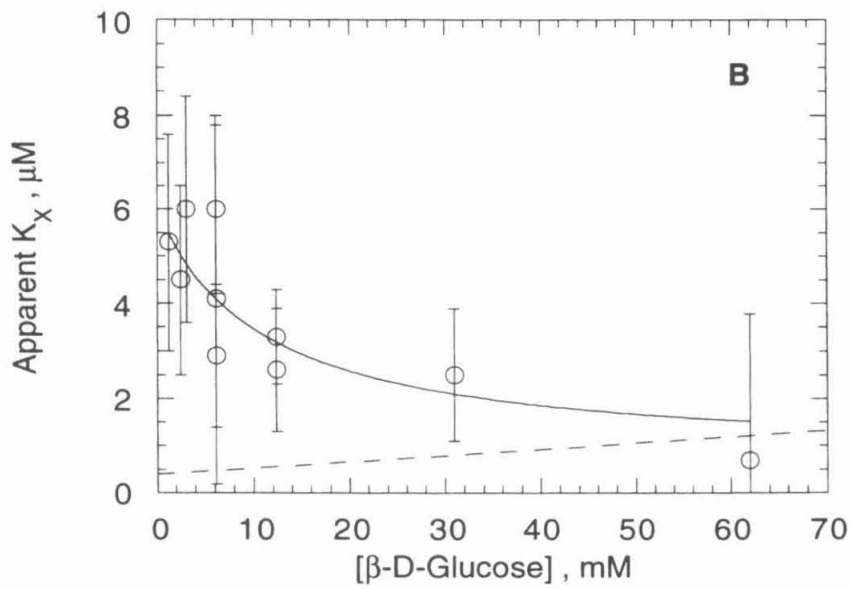
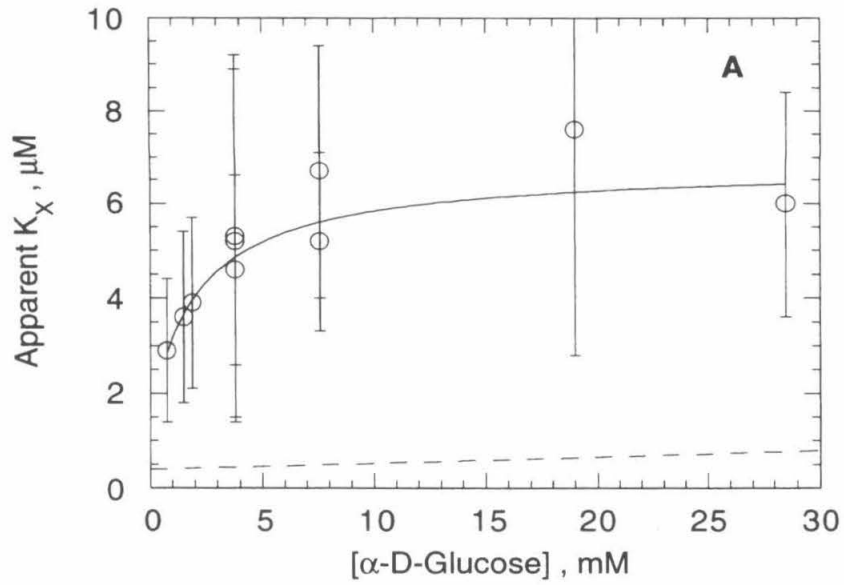Despite the considerable uncertainties in several of the fitted parameters, the data support two important quantitative conclusions. First, the α anomer data is significantly different from a straight line with a nonnegative slope ($p < 0.05$). Although to the eye the β anomer data appears to differ from such a line as well, scatter in the data renders the difference in this case far less significant ($p < 0.2$) Second, the y-intercepts of the fits to the two data sets are significantly different from each other ($p < 0.05$).

DISCUSSION

CB inhibits the TRNOEs observed in both D-glucose anomers in a hyperbolic fashion over the range of sugar concentrations sampled, consistent with the presence of a single class of CB sites (Figures 5.4 and 5.5). This result is consonant with literature reports of the pattern of D-glucose inhibition of equilibrium CB binding[3,4] and CB inhibition of glucose transport[2,5] and with the models of CB interaction with an alternating conformer transporter portrayed in Figure 5.3.

It was shown above that the models of Figure 5.3 predict a linear dependence of the apparent inhibitor dissociation constant $\overline{K}_X$ on ligand concentration; nonlinearity indicates the simultaneous binding of ligand and inhibitor to the protein (cf. equation (5.9)). Carruthers[4] observed such nonlinearity in the interactions of maltose, 4,6-O-ethylidene-D-glucose and phloretin with CB and GLUT1, with anticooperativity between the exofacial inhibitor site (presumed in the cases of maltose and ethylidene glucose to be identical with or to include the exofacial transport site) and the CB site, but failed to detect simultaneous binding of D-glucose and CB. A unique feature of the method described in the present work is the resolution of the two glucose anomers. The data of Figure 5.7 demonstrate clearly that α-D-glucose and CB bind simultaneously, with anticooperativity between the two sites. The data are more equivocal with respect to the β anomer, however here too it appears that sugar and inhibitor bind simultaneously. In this case, binding of the glucose anomer and CB appear *cooperative*. We speculate that

the earlier failure to detect formation of these ternary complexes was due to a lack of resolution of the effects of the two anomers and reflects the observation of an average of the anticooperative and cooperative interactions.

Another novel result of the present work is the difference in y-intercepts of Figures 5.7A and 5.7B. This difference implies that there exist (at least) two distinct classes of sugar-sensitive sites to which CB binds: One class ($K_X = 1.5 \pm 1.1 \ \mu M$) detected by the α-D-glucose TRNOE, and another ($K_X = 6.0 \pm 1.3 \ \mu M$) detected by the β-D-glucose TRNOE. There is no precedent for this observation in the literature; again this may at least in part be due to the fact that interactions of the two anomers with CB and the transporter have not previously been resolved. Also, the nonphysiological buffer composition required for the ^{1}H NMR experiments may alter protein structure sufficiently to resolve classes of inhibitor sites indistinguishable under the conditions of previous studies (*vide infra*).

Although the data reveal two classes of inhibitor sites, the number and anomeric specificity of sugar sites involved remains ill-defined. There is no evidence that only one sugar site is coupled to each of these CB sites; the minimum requirement for consistency with the observed difference of y-intercepts is that there exists one class of anomer-specific sugar sites which is coupled to one, but not the other, CB site. The sites which give rise to the observed TRNOEs must be affected. The apparent affinity of these sites for D-glucose (apparent $K_D \approx 30 - 70$ mM, see Table 4.1) is similar to the apparent affinity of the sites detected by CB inhibition of the β-D-glucose TRNOE (Figure 5.7B; apparent $K_D = 86 \pm 270$ mM for the binary complex, 11 ± 11 mM for the ternary complex). The apparent dissociation constants for sugar from binary and ternary complexes (0.47 ± 0.64 mM and 2.1 ± 1.5 mM, respectively) detected by inhibition of the α-D-glucose TRNOE, however, appear to include contributions from relatively high-affinity sites. This may represent observation of the GLUT1 high-affinity sugar sites ($K_D \approx 2$ mM) reported by several workers.[4,10,11] Ligand may be in intermediate or slow

exchange on the NMR timescale at such sites, thus not directly detectable in TRNOE binding curves such as those of Figures 4.3, 4.4 and 5.6.

Literature values for the apparent dissociation constant for CB from sugar-sensitive sites and the apparent inhibition constant for CB inhibition of glucose transport fall in the range 0.15 - 0.8 μM (see Table 3.1), showing no strong dependence on temperature (over the range 4 °C - 37 °C) or the assay employed. Although the value of K_X obtained from the fit to the α-D-glucose TRNOE data is within experimental error of these values, that from the β anomer data is not. (Dashed lines in Figure 5.7 represent literature predictions for interaction of CB with GLUT1, using reasonable values of 0.4 μM for K_X and 30 mM for $\overline{K}_D$.) This discrepancy does not arise from failure to account for sugar-insensitive CB sites or nonspecific interaction of CB with erythrocyte membranes.[3] In the workup of several representative data sets, this additional CB binding was treated explicitly; it was found that the $\overline{K}_X$ values obtained differed by only ~10% from those obtained neglecting the additional interactions. A possible source of the difference is in the composition of the NMR samples. Particularly, about 90% of solvent protons and exchangeable protons in GLUT1 were replaced by deuterons in the NMR samples, potentially altering binding site structure in the protein. Also, the NMR experiments were carried out in 5 mM phosphate buffer, whereas all previous studies were at physiological ionic strength. CB is a relatively hydrophobic molecule. In a higher ionic strength medium, partitioning of inhibitor into the lipid phase of the membrane should be favored. If the inhibitor site on GLUT1 is accessible to the lipid phase, or even merely if the site consists in part of a hydrophobic domain of the protein, such a salting-out effect would result in a lower apparent dissociation constant.

It was shown in Chapter 4 that the alternating conformer model is inadequate to account for the binding of D-glucose to GLUT1 detected by the TRNOE method and that at least one sugar site must be present in addition to the transport sites of this model. Based on diffraction studies of a large number of cytochalasins, Jung and coworkers have

shown that portions of the cytochalasin B molecule are isosteric with the $^4C_1$ conformer of D-glucopyanose with respect to the positions of hydrogen bond donors and acceptors and that the presence or absence of these moieties at least in part determines whether or not a particular cytochalasin is an effective inhibitor of glucose transport.[12,13] These results suggest that CB site(s) on GLUT1 may overlap or include sugar sites. The present observation of two classes of CB sites is provacative in this connection; it may be that CB can bind to a site contiguous with a channel site or to one contiguous with the endofacial transport site.

In summary, we have shown that α-D-glucose and probably β-D-glucose form ternary complexes with CB and GLUT1, a finding inconsistent with the alternating conformer model of glucose transport. Evidence has been presented for the existence of two classes of CB sites which differ in their sensitivity to the two glucose anomers. In the case of the α anomer but not the β, the inhibition data indicate the presence of one or more high-affinity sugar sites which are not directly detectable by the TRNOE. Such differences in interaction of GLUT1 with the anomers are not unprecedented. The rate constant for association of β-D-glucose with exofacial GLUT1 sites in intact erythrocytes has been reported to be about 30% faster than that for the α anomer.[14] Although a study of infinite-cis uptake in intact human erythrocytes revealed no significant difference in transport parameters for the two anomers[15], preferential uptake of the β anomer has been demonstrated in rat erythrocytes[16], and a pair of NMR studies showed faster efflux (from human erythrocytes) of the β anomers of D-glucose and 3-fluoro-3-deoxy-D-glucose under equilibrium exchange conditions.[17,18] Sugar transporters from other organisms also demonstrate anomeric discrimination: The transporter of *Saccharomyces cerevisiae* has a 1.5-fold higher affinity for the α anomer, while the bacteria *Lactococcus cremoris* and *Escherichia coli* appear to have independent phosphotransferase systems specific for each anomer.[19]

The inhibition data reported herein are inconsistent with the alternating conformer model of glucose transport, but they are not particularly suggestive of an appropriate alternative model. In the following (and final) chapter of this thesis, a model of GLUT1 mechanism is presented which is consistent with previous transport and ligand binding results but also accommodates the TRNOE results presented in Chapter 4 and the CB inhibition results presented above.

REFERENCES

1. Carter-Su, C., Pessin, J. E., Mora, R., Gitomer, W., and Czech, M. P., <u>J. Biol. Chem.</u>, **257** (1982) 5419-5425.

2. Devés, R., and Krupka, R. M., <u>Biochim. Biophys. Acta</u>, **510** (1978) 339-348.

3. Jung, C. Y., and Rampal, A. L., <u>J. Biol. Chem.</u>, **252** (1977) 5456-5463.

4. Helgerson, A. L., and Carruthers, A., <u>J. Biol. Chem.</u>, **262** (1987) 5464-5475.

5. Carruthers, A., and Helgerson, A. L., <u>Biochemistry</u>, **30** (1991) 3907-3915.

6. Markwell, M. A., Haas, S. M., Bieber, L. L., and Tolbert, N. E., <u>Anal. Biochem.</u>, **87** (1978) 206-210.

7. Lowry, O. H., Rosebrough, N. J., Farr, A. L., and Randall, R. J., <u>J. Biol. Chem.</u>, **193** (1951) 265-275.

8. Falke, J. J., Ph. D. thesis, California Institute of Technology, 1985.

9. Ross, S. A., Candidacy Report, California Institute of Technology, 1987.

10. Hebert, D. N., and Carruthers, A., <u>J. Biol. Chem.</u>, **267** (1992) 23829-23838.

11. Holman, G. D., Busza, A. L., Pierce, E. J., and Rees, W. D., <u>Biochim. Biophys. Acta</u>, **649** (1981) 503-514.

12. Rampal, A. L., Pinkofsky, H. B., and Jung, C. Y., <u>Biochemistry</u>, **19** (1980) 679-683.

13. Griffin, J. F., Rampal, A. L., and Jung, C. Y., <u>Proc. Natl. Acad. Sci. (USA)</u>, **79** (1982) 3759-3763.

14. Janoshazi, A., and Solomon, A. K., <u>Biophys. J.</u>, **61** (1992) A521.

15. Carruthers, A., and Melchior, D. L., <u>Biochemistry</u>, **24** (1985) 4244-4250.

16. Duan, Y.-J., Fukatsu, H., Miwa, I., and Okuda, J., <u>Mol. Cell. Biochem.</u>, **112** (1992) 23-28.

17. Kuchel, P. W., Chapman, B. E., and Potts, J. R., <u>FEBS Letts.</u>, **219** (1987) 5-10.

18. Potts, J. R., Hounslow, A. M., and Kuchel, P. W., <u>Biochem. J.</u>, **266** (1990) 925-928.

19. Benthin, S., Nielsen, J., and Villadsen, J., <u>Biotech. Bioeng.</u>, **40** (1992) 137-146.

CHAPTER 6

A CHANNEL SITE MODEL OF *GLUT1* MECHANISM

INTRODUCTION

Only recently has it been possible to apply spectroscopic and molecular biological techniques to the study of GLUT1. Work to accurately identify intermediate forms of transporter-sugar complexes and the molecular basis of substrate translocation is thus in its infancy. Historically, study of this system has been primarily focused on kinetic descriptions of sugar transport. Although a kinetic model of transporter function is a crude level of description, it is a general one and a necessary one. As molecular details of the transport mechanism emerge, they will be interpreted in terms of, and in turn aid in refinement of a kinetic model of the transport cycle. The present work represents an initial step in such refinement. Below we describe the constraints placed on any revised model of GLUT1 mechanism by the wealth of steady-state transport kinetics data in the literature and by the TRNOE results reported in previous chapters. A model is then presented which incorporates these features. Finally, the limitations of the model are examined, as is its relevance to transporters other than GLUT1.

CONSTRAINTS ON MODELS OF GLUT1 MECHANISM

Constraints from Transport Kinetics. Steady-state glucose transport across human erythrocyte membranes displays simple saturation kinetics.[1] Trans-acceleration, the enhancement of unidirectional flux of labeled substrate by the presence of unlabeled substrate in the opposite (trans) compartment, and counterflow, transient unidirectional flux of labeled substrate in the presence of a much larger flux of unlabeled substrate in the opposite direction, were both originally observed in this system. These two phenomena are inconsistent with the behavior of a simple transmembrane channel: their observation led to the postulate that two conformational states are available to the transporter, one in which a ligand binding site is accessible only to the cytoplasmic compartment, the other in which the site is accessible only to the extracellular

compartment. The alternating conformer model frequently referred to in previous chapters (see Figure 4.2) is the simplest formulation of this postulate.

For a system displaying hyperbolic kinetics, a steady-state transport experiment yields two parameters: a half-saturation concentration K (analogous to the Michaelis constant of enzyme kinetics) and a maximal velocity V. The relationships among these transport parameters and microscopic rate constants depends on the initial conditions of the experiment. Four classes of steady-state transport experiments are distinguished based upon these initial conditions: 1) zero-trans (zt), in which unidirectional flux of substrate into a compartment initially devoid of substrate is monitored, 2) infinite-trans (it), in which unidirectional flux of labeled substrate into a saturating concentration of unlabeled substrate in the trans compartment is monitored, 3) infinite-cis (ic), in which net flux of substrate from an initial saturating concentration in the cis compartment is measured as a function of initial substrate concentration in the trans compartment, and 4) equilibrium exchange (ee), in which substrate concentration is the same in both compartments and unidirectional flux of label is monitored. Each type of experiment may be used to monitor influx or efflux. The maximal velocity of equilibrium exchange, V^{ee}, is independent of whether influx or efflux is measured, and in the particular case of interest, since glucose transport is passive, the half-saturation concentration K^{ee} is independent of direction as well. Thus steady-state transport experiments yield a set of seven related half-saturation concentrations and seven related maximal velocities.

Kinetic rejection criteria have been articulated which make good use of these parameters. First, for any passive diffusion system which has hyperbolic kinetics, the parameters from zt and ee experiments must obey[2]

$$\frac{V^{ee}}{K^{ee}} = \frac{V^{zt}_{12}}{K^{zt}_{12}} = \frac{V^{zt}_{21}}{K^{zt}_{21}} \quad . \tag{6.1}$$

(Superscripts indicate the experimental procedure; subscripts indicate the direction of unidirectional flux monitored.) Relationships among the microscopic rate constants of

the alternating conformer model and the macroscopic transport parameters provide additional tests of consistency.[2,3] Steady-state kinetic data are consistent with this model if, in addition to the relations of equation (6.1), the relations

$$\frac{V_{12}^{zt}}{K^{(1)}} = \frac{V_{21}^{zt}}{K^{(2)}} \tag{6.2}$$

and

$$\frac{V_{21}^{zt}}{K^{ee}} = \frac{\tilde{V}}{K^{(1)}} \tag{6.3}$$

obtain, where

$$K^{(1)} = K_{12}^{it} = K_{21}^{ic} \quad , \tag{6.4}$$

$$K^{(2)} = K_{21}^{it} = K_{12}^{ic} \quad , \tag{6.5}$$

$$\tilde{V} = [(V_{12}^{zt})^{-1} + (V_{21}^{zt})^{-1} - (V^{ee})^{-1}]^{-1} \quad . \tag{6.6}$$

Human erythrocyte glucose transport data are consistent with relations (6.1) - (6.3); transport parameters derived from our model of GLUT1 mechanism must also conform to them.

Constraints from D-Glucose TRNOEs. Results of the present work place four constraints on possible models of GLUT1 glucose transport. First, binding sites at which ligand is in fast exchange must be present on both sides of the membrane. A related constraint is that the macroscopic ligand dissociation constant measured at equilibrium (equal ligand concentrations in both compartments) must be dependent on which compartment is sampled (Chapter 4). The model must predict competitive inhibition of sugar efflux and noncompetitive inhibition of sugar influx by cytochalasin B while allowing for formation of ternary complexes of sugar, CB and transporter. Finally, the model must allow for the presence of at least one site (at which ligand is in slow exchange) specific for the α anomer (Chapter 5).

A CHANNEL SITE MODEL

The simplest approach to formulating a revised model for GLUT1 which displays alternating conformer kinetics is to cleave to the essential features of the alternating conformer model. We retain the single transport site which may adopt inward- or outward-facing conformations: in addition to the evidence for such a site from steady-state kinetics and inhibition studies detailed above and in Chapter 5, temperature-jump and stopped-flow kinetics results[4] are consistent with redistributions of transport sites between endofacial and exofacial forms, and fluorescence studies[5,6] indicate that such redistribution is accompanied by a conformational change of the protein.

We posit the existence of one sugar site in addition to the transport site. (We treat only one additional site for simplicity; such analysis reveals the pertinent consequences of the presence of any number of such sites.) This site is exposed to one compartment only; there are no states of the protein in which free ligand in the opposite compartment has access to it. The available evidence of GLUT1 structure suggests the presence of an aqueous channel which partially penetrates the membrane bilayer (see Chapter 1); such a site might reside in the wall of such a channel. For convenience, then, we refer to this site as a channel site, recognizing that its actual location is not a crucial detail.

Definitions and Assumptions. In its most general form (Figure 6.1), the model comprises 8 states of the transporter in the presence of ligand. The transport site may face either compartment 1 or compartment 2, and be either empty or occupied by ligand. For each of these 4 states, the channel site, denoted by E_c in Figure 6.1, may also be empty or occupied by ligand. Thus far, no experimental evidence has been presented which discriminates between a cytoplasmic or an extracellular location for the channel site. We therefore postulate that the channel site is accessible to compartment 1, without identifying this compartment with either of the physiological spaces. Symbols representing rate constants for transporter reorientations and interaction of ligand with the transport sites are the same as those used previously; the superscript "c" is added to

Figure 6.1

Channel Site Model. The transporter has two ligand binding sites, a channel site E_c and a transport site, which may face the compartment 1 (E_1) or the compartment 2 (E_2) medium. L_1 and L_2 denote free ligand concentrations in compartments 1 and 2, respectively. The rate constants for binding and dissociation of ligand from the transport site (b, f) and for transport site reorientations (g, k) in general may be sensitive to occupancy of the channel site; rate constants for steps involving forms of the transporter possessing a loaded channel site are denoted by the superscript "c." The following detailed balance constraints arise from this model (the dissociation constants employed are defined in the text):

$$k_1 k_2^c K_i = k_1^c k_2 K_{ii} \;\; ; \;\; \frac{k_{ct}}{k_{tc}} = \frac{K_i}{K_{D1}} = \frac{K_{iii}}{K_{D1}^c} \;\; ; \;\; K_{ii} K_{D2}^c = K_{iv} K_{D2} \;\; ;$$

$$g_1 g_2^c K_{iii} = g_1^c g_2 K_{iv} \;\; ; \;\; g_2 k_1 K_{D1} = g_1 k_2 K_{D2} \;\; ; \;\; g_2^c k_1^c K_{D1}^c = g_1^c k_2^c K_{D2}^c \;\; .$$
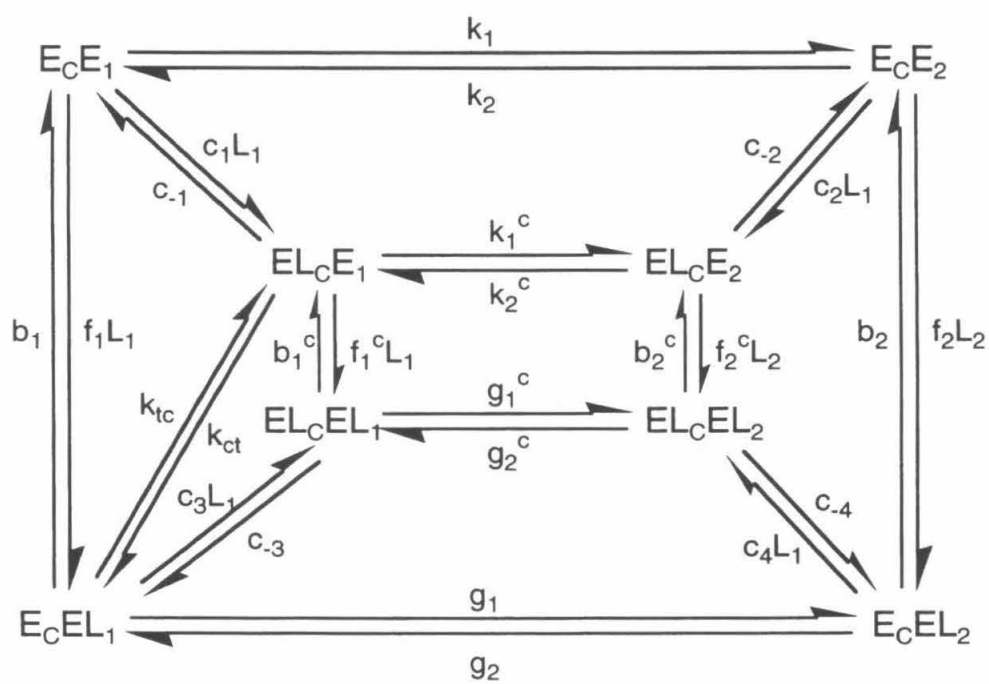
denote rate constants for steps involving forms of the transporter in which the channel site is occupied. The rate constants for association of ligand with and dissociation of ligand from the channel site are themselves denoted by the symbol "c" (appropriately subscripted, see Figure 6.1), except for those involving direct transfer of ligand from channel site to transport site or *vice versa*, which are denoted by "k_{ct}" and "k_{tc}," respectively.

To simplify analysis of the model, we assume ligand exchanges rapidly between the channel site and bulk solution in compartment 1, and between the transport site and bulk solution in compartment 2. The presence of NMR-observable sites at both membrane faces (Chapter 4) validates this assumption in part. Fast exchange in compartment 1 at the channel site rather than the transport site was selected since it has been shown that the TRNOE does not arise from binding to transport sites only. Exchange may be rapid at the compartment 1 transport site as well, but it is not necessary to assume this. The portion of our rapid equilibrium assumption which remains untested is that exchange of ligand between compartment 1 solution and the channel site is rapid for all four states of the *transport* site; the NMR data require only that fast exchange occur at at least one of these. The assumption is completely valid for compartment 2: the transport site must be the rapid equilibrium site as it is the only site accessible to compartment 2 ligand.

Microscopic dissociation constants in this model are given by

$$K_{D1} = \frac{b_1}{f_1} \quad , \quad K_{D1}^c = \frac{b_1^c}{f_1^c} \quad , \quad K_{D2} = \frac{b_2}{f_2} \quad , \quad K_{D2}^c = \frac{b_2^c}{f_2^c}$$

for ligand bound to the transport site, and

$$K_i = \frac{c_{-1}}{c_1} \quad , \quad K_{ii} = \frac{c_{-2}}{c_2} \quad , \quad K_{iii} = \frac{c_{-3}}{c_3} \quad , \quad K_{iv} = \frac{c_{-4}}{c_4}$$

for ligand bound to the channel site.

<u>Steady-State Concentrations</u>. Applying the method of King-Altman diagrams[7] (see Appendix to Chapter 4) with rapid equilibrium segments[8], we obtain for the steady-state concentrations of the various transporter species:

$$\frac{E_c E_1}{E_t} = \frac{\left[\left(k_2 K_{ii} + k_2^c L_1\right)K_{D2}^c + \left(g_2 K_{iv} + g_2^c L_1\right)L_2\right]K_{D1}^c K_i}{D} \quad , \tag{6.7}$$

$$\frac{E_c E_2}{E_t} = \frac{\left[\left(k_1 K_i + k_1^c L_1\right)K_{D1}^c + \left(g_1 K_{iii} + g_1^c L_1\right)L_1\right]K_{D2}^c K_{ii}}{D} \quad , \tag{6.8}$$

$$\frac{E_c EL_1}{E_t} = \frac{\left[\left(k_2 K_{ii} + k_2^c L_1\right)K_{D2}^c + \left(g_2 K_{iv} + g_2^c L_1\right)L_2\right]K_{iii} L_1}{D} \quad , \tag{6.9}$$

$$\frac{E_c EL_2}{E_t} = \frac{\left[\left(k_1 K_i + k_1^c L_1\right)K_{D1}^c + \left(g_1 K_{iii} + g_1^c L_1\right)L_1\right]K_{iv} L_2}{D} \quad , \tag{6.10}$$

$$\frac{EL_c E_1}{E_t} = \frac{\left[\left(k_2 K_{ii} + k_2^c L_1\right)K_{D2}^c + \left(g_2 K_{iv} + g_2^c L_1\right)L_2\right]K_{D1}^c L_1}{D} \quad , \tag{6.11}$$

$$\frac{EL_c E_2}{E_t} = \frac{\left[\left(k_1 K_i + k_1^c L_1\right)K_{D1}^c + \left(g_1 K_{iii} + g_1^c L_1\right)L_1\right]K_{D2}^c L_1}{D} \quad , \tag{6.12}$$

$$\frac{EL_c EL_1}{E_t} = \frac{\left[\left(k_2 K_{ii} + k_2^c L_1\right)K_{D2}^c + \left(g_2 K_{iv} + g_2^c L_1\right)L_2\right]L_1^2}{D} \quad , \tag{6.13}$$

$$\frac{EL_c EL_2}{E_t} = \frac{\left[\left(k_1 K_i + k_1^c L_1\right)K_{D1}^c + \left(g_1 K_{iii} + g_1^c L_1\right)L_1\right]L_1 L_2}{D} \quad , \tag{6.14}$$

where $E_t = E_c E_1 + E_c E_2 + E_c EL_1 + E_c EL_2 + EL_c E_1 + EL_c E_2 + EL_c EL_1 + EL_c EL_2$ is the stoichiometric concentration of transporter, and the denominator is

$$D = \left[\left(k_1 K_i + k_1^c L_1\right)K_{D1}^c + \left(g_1 K_{iii} + g_1^c L_1\right)L_1\right]\left[\left(K_{ii} + L_1\right)K_{D2}^c + \left(K_{iv} + L_1\right)L_2\right]$$
$$+ \left[\left(k_2 K_{ii} + k_2^c L_1\right)K_{D2}^c + \left(g_2 K_{iv} + g_2^c L_1\right)L_2\right]\left[\left(K_i + L_1\right)K_{D1}^c + \left(K_{iii} + L_1\right)L_1\right] \quad . \tag{6.15}$$

<u>Steady-State Fluxes</u>. With the rapid equilibrium assumption described above, the steady-state unidirectional substrate fluxes from compartment 1 to compartment 2 and *vice versa*, v_{12} and v_{21} respectively, are

$$v_{12} = g_1 E_c EL_1 + g_1^c EL_c EL_1$$

$$= \frac{\left(g_1 K_{iii} + g_1^c L_1\right)\left[\left(k_2 K_{ii} + k_2^c L_1\right)K_{D2}^c + \left(g_2 K_{iv} + g_2^c L_1\right)L_2\right]L_1 E_t}{D} \quad (6.16)$$

and

$$v_{21} = g_2 E_c EL_2 + g_2^c EL_c EL_2$$

$$= \frac{\left(g_2 K_{iv} + g_2^c L_1\right)\left[\left(k_1 K_i + k_1^c L_1\right)K_{D1}^c + \left(g_1 K_{iii} + g_1^c L_1\right)L_1\right]L_2 E_t}{D} \quad . \quad (6.17)$$

Equations (6.17) and (6.18) predict nonhyperbolic kinetics in the general case, contrary to experimental results for erythrocyte glucose transport. Thus we must seek the limits in which the channel site model yields hyperbolic kinetics. Two such limits may be identified: a) the channel site is only appreciably occupied when the transport site is empty and facing toward compartment 1, or b) occupancy of the channel site has no thermodynamic effect on ligand binding to or translocation of the transport site.

Case a). Assuming $EL_c E_1$ is the only state of the transporter in which the channel site is significantly occupied is equivalent to allowing the channel site dissociation constants K_{ii}, K_{iii} and K_{iv} to grow very large. The steady-state unidirectional fluxes then reduce to a hyperbolic form which can be shown to obey the relationships (6.1) - (6.3). Inspection reveals this to be a trivial case, however. The complex $E_c EL_1$ is now merely a kinetically transparent intermediate. The channel site displays total anticooperativity with the compartment 2 transport site, effectively becoming a compartment 1 transport site. Equilibrium assays of ligand binding would then yield a membrane orientation-independent macroscopic dissociation constant (a weighted average, in this case, of the microsopic affinities at the channel and compartment 2 transport sites) just as predicted by the alternating conformer model itself and contrary to experiment. We thus discard this limit.

Case b). If the channel and transport sites are independent, we may replace the dissociation constants K_i - K_{iv} with a single channel site dissociation constant K_c. Also in

this case, $K_{D1} = K_{D1}{}^c$ and $K_{D2} = K_{D2}{}^c$. Assuming furthermore that occupancy of the channel site doesn't affect the rates of transport site reorientation steps, *i.e.*, that $g_1 = g_1{}^c$, $g_2 = g_2{}^c$, $k_1 = k_1{}^c$ and $k_2 = k_2{}^c$, the fluxes (6.16) and (6.17) collapse to

$$v_{12} = \frac{\left(k_2 K_{D2} + g_2 L_2\right) g_1 L_1 E_t}{\begin{array}{l}\left((k_1 + k_2)K_{D1}K_{D2} + (g_1 + k_2)K_{D2}L_1\right.\\ \left. + (g_2 + k_1)K_{D1}L_2 + (g_1 + g_2)L_1 L_2\right.\end{array}} \quad , \tag{6.18}$$

$$v_{21} = \frac{\left(k_1 K_{D1} + g_1 L_1\right) g_2 L_2 E_t}{\begin{array}{l}\left((k_1 + k_2)K_{D1}K_{D2} + (g_1 + k_2)K_{D2}L_1\right.\\ \left. + (g_2 + k_1)K_{D1}L_2 + (g_1 + g_2)L_1 L_2\right.\end{array}} \quad , \tag{6.19}$$

identical to the expressions for an alternating conformer transporter under the assumption of ligand binding and dissociation rapid relative to transport site reorientations (equation (4.2) of Ref. 1.). Given this identity, it is clear that the required conditions (6.1) - (6.3) are fulfilled. We next show that the membrane orientation-dependence of the apparent dissociation constant for D-glucose in the presence of GLUT1 is consistent with the model of Figure 6.1 in this limit

The TRNOE Due to Equilibrium Ligand Binding to Independent Channel, Transport Sites. Only the sites at which ligand is in fast exchange contribute to NMR-observable binding. By construction, these sites are the channel site and the compartment 2 transport site. Making the substitutions indicated for case b) above and setting $L_1 = L_2 = L$ in equations (6.11) - (6.15), the equilibrium concentrations of the relevant species are

$$\frac{E_c E L_2}{E_t} = \frac{K_c L}{\left(K_c + L\right)\left[K_{D2} + L + \dfrac{g_2}{g_1}(K_{D1} + L)\right]} \quad , \tag{6.20}$$

$$\frac{EL_c E_1}{E_t} = \frac{\dfrac{g_2}{g_1}K_{D1}L}{\left(K_c + L\right)\left[K_{D2} + L + \dfrac{g_2}{g_1}(K_{D1} + L)\right]} \quad , \tag{6.21}$$

$$\frac{EL_cE_2}{E_t} = \frac{K_{D2}L}{\left(K_c + L\right)\left[K_{D2} + L + \frac{g_2}{g_1}\left(K_{D1} + L\right)\right]} \quad , \tag{6.22}$$

$$\frac{EL_cEL_1}{E_t} = \frac{\frac{g_2}{g_1}L^2}{\left(K_c + L\right)\left[K_{D2} + L + \frac{g_2}{g_1}\left(K_{D1} + L\right)\right]} \quad , \tag{6.23}$$

$$\frac{EL_cEL_2}{E_t} = \frac{L^2}{\left(K_c + L\right)\left[K_{D2} + L + \frac{g_2}{g_1}\left(K_{D1} + L\right)\right]} \quad . \tag{6.24}$$

The species EL_cE_1, EL_cE_2, EL_cEL_1 and EL_cEL_2 exchange ligand with compartment 1, while E_cEL_2 and EL_cEL_2 exchange ligand with compartment 2. The TRNOE observed in a multicompartment system consists of contributions from the binding sites in each compartment. In the present case, we have

$$f_I\{S\} - f_I^F\{S\} \approx c_1 \sum_j \frac{EL_cE_j}{L_t} + c_2 \frac{E_cEL_2 + EL_cEL_2}{L_t} \tag{6.25}$$

where the sum is over the four possible states of the transport site, and the parameters c_1 and c_2 reflect (in part) the extent to which compartment 1 and 2 sites are sampled by bulk ligand. (These parameters also contain relaxation rate terms. For convenience, it is assumed here that the I, S cross relaxation rate constant for ligand bound to one site is independent of the state of the other site; the conclusions drawn below are not dependent on this assumption. See equations (4.1) - (4.3), (4.11) - (4.13) and accompanying text for a discussion of intercompartmental exchange and the parameters c_1 and c_2.)

Summing the concentration expressions (6.21) - (6.24) and dividing by total ligand concentration L_t ($\approx L$), the first term of equation (6.25) is found to be

$$c_1 \sum_j \frac{EL_c E_j}{L_t} = c_1 \frac{\left[K_{D2} + L_t + \frac{g_2}{g_1}(K_{D1} + L_t) \right] E_t}{(K_c + L_t)\left[K_{D2} + L_t + \frac{g_2}{g_1}(K_{D1} + L_t) \right]}$$

$$= c_1 \frac{E_t}{K_c} \frac{L_t^{-1}}{L_t^{-1} + K_c^{-1}} \quad . \tag{6.26}$$

The compartment 1 TRNOE, then, is rectangular hyperbolic in L_t^{-1}, with a dissociation constant equal to that of the channel site. For the compartment 2 TRNOE, equations (6.20) and (6.24) yield for the second term of equation (6.25)

$$c_2 \frac{E_c EL_2 + EL_c EL_2}{L_t} = c_2 \frac{(K_c + L_t)E_t}{(K_c + L_t)\left[K_{D2} + L_t + \frac{g_2}{g_1}(K_{D1} + L_t) \right]}$$

$$= c_2 \frac{g_1 E_t}{g_2 K_{D1} + g_1 K_{D2}} \frac{L_t^{-1}}{L_t^{-1} + \overline{K}_D^{-1}} \quad , \tag{6.27}$$

again rectangular hyperbolic in L_t^{-1}, with an apparent dissociation constant

$$\overline{K}_D = \frac{g_2 K_{D1} + g_1 K_{D2}}{g_1 + g_2} \tag{6.28}$$

identical to that derived for the alternating conformer transport sites (equation (4.15)).

Provided that K_c is not fortuitously equal to $\overline{K}_D$, the observed TRNOE is then a sum of two different hyperbolae. It was noted in Chapter 4 that such a sum might easily not be distinguishable from a single hyperbola given the limited range of ligand concentrations assayed and the scatter in the TRNOE data. The critical feature of the TRNOE observed in the presence of channel and transport sites is that, when fit to a single hyperbola, the apparent dissociation constant depends on the exposure of each compartment to observable ligand. For example, if only compartment 1 is sampled by bulk ligand ($c_2 \approx 0$), the macroscopic dissociation constant is equal to K_c. At the opposite extreme, if only compartment 2 is sampled and $c_1 \approx 0$, the fit yields $\overline{K}_D$ of equation (6.28). In real experimental preparations, both compartments are likely to contribute to NMR-observable binding. The macroscopic dissociation constant in such

preparations will fall between K_c and $\overline{K}_D$. In the present work, crushed ghosts and sheared crushed ghosts were shown to differ slightly in exposure of membrane faces to bulk solution, the latter preparation likely having a larger fraction of erstwhile cytoplasmic sites accessible. The observation of significantly different values of the macroscopic ligand dissociation constant in the two preparations is thus consistent with the existence of a channel site.

Inhibition of Transport and Ligand-Binding by Cytochalasin B. The required kinetic pattern of inhibition of glucose transport by CB (competitive inhibition of exit, noncompetitive inhibition of entry) is retained in the channel site model by the presence of the alternating conformer transport sites, provided only that if an additional exofacial sugar site is present, binding of sugar to this site is not anticooperative with CB binding to the inhibitor site. The TRNOE inhibition results presented in Chapter 5 above are also consistent with the presence of one or more channel sites, indeed they provide evidence for the existence of such a site and provide additional constraints on a channel site model. Our analysis of inhibition of the D-glucose TRNOE by CB led to three significant conclusions: (i) α- (and probably β-) D-glucose forms ternary complexes with CB and GLUT1, (ii) there exists a high affinity sugar site specific for the α anomer, and (iii) there exist (at least) two classes of CB sites. We now explore each of these features in turn in the context of the model of Figure 6.1.

(i). The existence of ternary complexes of sugar, CB and transporter is easily accommodated by the presence of a channel site. Transport inhibition results imply that binding of inhibitor must block ligand binding to the endofacial transport site, but a scheme (Figure 5.3B) in which ternary complexes may nonetheless form with an alternating conformer transporter has already been described. The presence of an additional site and its compartmental localization is indicated by the anticooperativity detected in CB inhibition of the α-D-glucose TRNOE. If the scheme of Figure 5.3B were correct, binding of sugar to the exofacial transport site could not be anticooperative with

CB binding to its site, else competitive inhibition of glucose entry would be observed. In contrast, occupancy by sugar of a channel site accessible to the cytoplasmic compartment which displays anticooperativity with CB binding yields the experimentally observed forms of inhibition of sugar entry and exit.

(ii). At least one of the sugar sites whose occupancy by α-D-glucose produces anticooperativity between that site and a CB site is specific for this anomer and of relatively high affinity ($K_D < 2$ mM). This class of sites is unlikely to be one of the transport site conformers, since the microscopic affinities at these latter sites cannot be deconvoluted at equilibrium (Chapter 4) and the resultant macroscopic affinity is at least an order of magnitude lower, as are most estimates of transport site affinities from steady-state and transient kinetics and from fluorescence studies (see Table 3.1). Although several studies[9,10,11] have ascribed to the exofacial transport site an apparent dissociation constant of ~1.6 mM, by the argument above the high-affinity site inferred from the TRNOE results must be endofacial. Finally, and most telling, the transport site cannot be specific for one anomer: both are transported.[12]

(iii). The detection of two distinct classes of sugar-sensitive CB sites is, as previously noted, unprecedented. Again, the observed pattern of transport inhibition leads to pertinent constraints: binding of CB to either class of sites must (i) prevent binding of sugar to the endofacial transport site, and (ii) either lock the transporter in the inward-facing conformer (analogous to the scheme of Figure 5.3A for an alternating conformer transporter) or block translocation of the loaded exofacial transport site (analogous to the scheme of Figure 5.3B). Beyond these constraints, the NMR results admit of little elaboration. As discussed in Chapter 5, CB binding sites may overlap sugar sites. If this is the case in GLUT1, one of the observed classes of inhibitor sites could include the endofacial transport site, the other an endofacial channel site. (It is important to note at this point that the assumption of no thermodynamic interaction between channel and transport sites when D-glucose is bound to both in no way implies

that the two sites are independent if CB binds to one and sugar to the other.) Finally, the observed stoichiometry of at most one molecule of CB bound per transporter monomer implies either that the two inhibitor sites are mutually exclusive if present on the same monomer, or that monomers possess a single inhibitor site, which allosteric interactions resolve into two distinguishable classes upon oligomerization.

Generalization: Two or More Channel Sites. The model of Figure 6.1 is but an incremental modification of the alternating conformer model, the simplest case to develop and demonstrate the properties of a transporter which possesses substrate sites in addition to the transport site. The presence of additional channel sites subject to the constraints placed on the single channel site of Figure 6.1 does not alter the qualitative features revealed in this analysis. Independence of the channel sites from ligand binding to and reorientations of the transport site leads to hyperbolic steady-state kinetics. The restriction that each channel site is accessible to only one compartment ensures that different classes of sites will be sampled and the macroscopic apparent affinity for ligand will vary as exposure of the two compartments to bulk solution is varied (provided again that the microscopic affinities at the various sites differ).

Comparison of the TRNOE binding data of Chapter 4 with the inhibition data of Chapter 5 in fact argues for the presence of at least two classes of channel sites in addition to the transport site. D-glucose TRNOE binding curves were shown to imply the existence of at least one class of channel sites at which both anomers are in fast exchange, while the inhibition data suggest the existence of at least one class of high-affinity sites specific for α-D-glucose. We have argued for a endofacial location for the latter site, but the data are equivocal with respect to the transmembrane disposition of the lower-affinity site. Finally, it should again be noted that, aside from the similarity of the macroscopic affinity for D-glucose of the NMR-observable sites to literature estimates of transport site affinities, no evidence has been presented which establishes that the transport sites are

observed at all. It is possible that the TRNOEs arise from ligand binding to two or more rapidly-exchanging channel sites, at least one at each membrane face.

DISCUSSION

The alternating conformer model of GLUT1 mechanism has been shown to be inadequate to explain the results of the present study. Postulation of the presence, in addition to a transport site, of one or more sites which are fixed with respect to exposure to one compartment or the other produces a scheme which can account for these results. Transport by a protein possessing such sites is indistinguishable from alternating conformer transport to the extent that their occupancy by sugar has no effect on transport site dissociation constants or translocation rate constants. The NMR results specifically indicate the presence of at least two classes of such sites. One of these binds both anomers and is of uncertain compartmental localization. D-glucose is in fast exchange at this first class of sites. The second class of sites is accessible to the cytoplasmic compartment and specific for the α anomer, which exchanges slowly on the NMR timescale between this site and the cytoplasm. Figure 6.2 depicts a plausible arrangement of sugar sites in GLUT1, based on transport and NMR results.

Even as the alternating conformer model is the simplest model which can account for glucose transport kinetics, the model of Figure 6.1 is the simplest model which displays the effects of additional sites. The experimental evidence argues for at least two channel sites, likewise it is important to recognize that additional transport sites may be present, yet transparent to both transport kinetics and equilibrium binding studies. In particular, Carruthers has shown that under many experimental conditions, steady-state glucose transport by a protein containing two coupled transport sites is indistinguishable from that by one containing one transport site.[13] It can be shown that equilibrium ligand-binding measurements, such as the TRNOE assay of the present work, also cannot distinguish the presence of an additional transport site or sites.

Figure 6.2

A Schematic of the Number and Disposition of Substrate and Inhibitor Sites on GLUT1.
This cartoon portrays a possible arrangement of the minimum number of sites consistent
with transport and NMR data for (A) the outward-facing, and (B) the inward-facing
conformations of the transporter. The protein is depicted as a transmembrane channel
with a diffusional barrier somewhere in the channel. Sugar sites are represented by
triangles, CB sites by half-circles. The transport site (t) is associated with the barrier; a
conformational change involving that domain results in transport site reorientation, either
empty (as shown) or bearing substrate. Sugar is in fast exchange at at least one of the
transport site conformers, assumed here to be the endofacial form. There exists a channel
site at which sugar is also in fast exchange and which is accessible to the compartment
opposite the fast-exchange transport site; this channel site is represented by "c_f" near the
extracellular surface. A slow-exchange, high-affinity channel site (c_s) specific for α-D-
glucose is present in the channel near the cytoplasmic surface. Two CB sites, completely
anticooperative with one another, are present in the the inward-facing conformer only.
The CB sites may overlap sugar sites; they are drawn adjacent to the two intracellular
substrate sites (c_s and t) to indicate this possibility. (This depiction of the CB sites is
analogous to Figure 5.3A. Alternatively, the CB sites may exist in both conformers, but
block binding of sugar to the endofacial t site and block t site reorientation when ligand is
bound to the exofacial form, analogous to Figure 5.3B.)

OUTSIDE

INSIDE
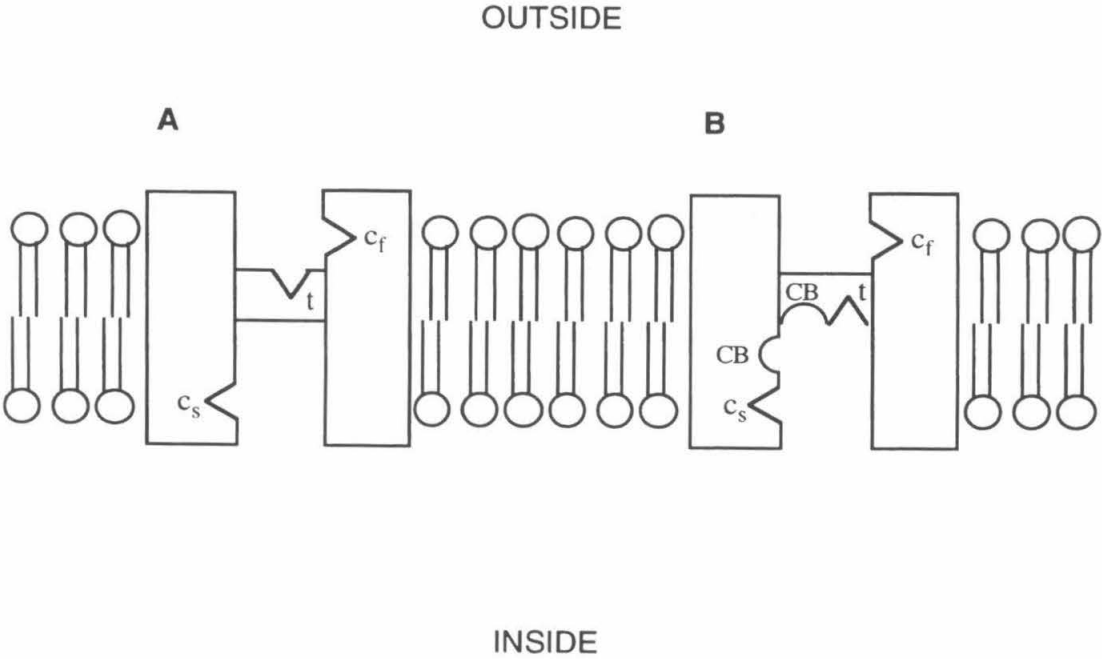
The requirement of independence of the channel and transport sites may at first blush appear to render the channel site model a trivial improvement on the alternating conformer model. We address two aspects of this issue. First, the two sites are required to be independent only to the extent that steady-state glucose transport is observed to be hyperbolic. Couplings between channel site occupancy and transport site occupancy and translocation may exist which are sufficiently small that their perturbation of the kinetic form has not been detected. Second, even if the two sites are thermodynamically independent, it is easy to envision ways in which the channel site may substantially alter transport kinetics under the non-steady-state conditions of the circulatory system. For example, fast exchange of ligand between bulk solution and a channel site and between that channel site and the cis transport site could provide a pathway for rapidly shuttling sugar to or from the transport site if direct exchange between that transport site and bulk solution is slow (as was assumed in deriving the steady-state concentrations and fluxes for the model of Figure 6.1). Or, as another possibility, a relatively high-affinity channel site could serve as a "ligand sink," diminishing the free ligand concentration in the vicinity of the transport site.

The alternating conformer model has been successful in accounting for transport in a large number of passive diffusion and countertransport systems.[1] One consequence of the success of this model (as well as of the historical lack of experimental handles other than steady-state kinetics) has been that most workers neglect the possibility of the presence of substrate sites other than the transport sites. Prior to the present work, the presence of sites confined to one membrane face or the other has been considered only for a very few transport systems. For example, a "modifier site" has been proposed to exist on the Band 3 anion transporter.[14] A careful analysis of chloride binding to this protein by ^{35}Cl NMR revealed no evidence for such a site.[15] The same method, however, did reveal a class of kinetically transparent low-affinity chloride sites on the protein halorhodopsin.[16] Also, as described in Chapter 4, a previous TRNOE study of lactose

binding to *lac* permease[17] indicates the presence of at least one class of channel sites on this protein. In three out of four cases where sites other than transport sites have been sought, then, they have been discovered. Clearly it is no longer acceptable for students of transport to imagine that a focus on transport sites is sufficient to understand transporter function.

CONCLUDING REMARKS

It is hoped that the work presented in this thesis portrays convincingly the complexity of sugar-transporter interactions in the GLUT1 system and that it stimulates new experimental and theoretical approaches to the study of glucose transport. The strategy employed, comparison of the ligand-binding behavior of GLUT1 with its transport behavior, has proven a valuable one, yielding insights that neither measurements of binding nor of transport alone could reveal. This strategy is quite generalizable to other systems. Finally, the value of NMR methods such as the TRNOE binding assay employed here is inestimable. Methods so sensitive to weak ligand-macromolecule interactions are few, while such interactions are likely to be prevalent throughout biochemistry.

REFERENCES

1. Stein, W. D., <u>Transport and Diffusion Across Cell Membranes</u>, pp. 231-337, Academic Press, Orlando, 1986.

2. Krupka, R. M., <u>Biochem. J.</u>, **260** (1989) 885-891.

3. Lieb, W. R., in <u>Red Cell Membranes: A Methodological Approach</u>, Ellory, J. C., and Young, J. D., eds., pp. 135-164, Academic Press, London, 1982.

4. Lowe, A. G., and Walmsley, A. R., <u>Biochim. Biophys. Acta</u>, **903** (1987) 547-550.

5. Appleman, J. R., and Lienhard, G. E., <u>J. Biol. Chem.</u>, **260** (1985) 4575-4578.

6. Appleman, J. R., and Lienhard, G. E., <u>Biochemistry</u>, **28** (1989) 8221-8227.

7. King, E. L., and Altman, C., <u>J. Phys. Chem.</u>, **60** (1956) 1375-1378.

8. Cha, S., <u>J. Biol. Chem.</u>, **243** (1968) 820-826.

9. Lacko, L., Wittke, B., and Kromphardt, H., <u>Eur. J. Biochem.</u>, **25** (1972) 447-454.

10. Carruthers, A., <u>J. Biol. Chem.</u>, **261** (1986) 11028-11037.

11. Hebert, D. N., and Carruthers, A., <u>Biochemistry</u>, **30** (1991) 4654-4658.

12. Carruthers, A., and Melchior, D., <u>Biochemistry</u>, **24** (1985) 4244-4250.

13. Carruthers, A., <u>Biochemistry</u>, **30** (1991) 3898-3906.

14. Knauf, P. A., <u>Curr. Topics Membr. Transp.</u>, **12** (1979) 249-363.

15. Falke, J. J., Ph. D. thesis, California Institute of Technology, 1985.

16. Falke, J. J., Chan, S. I., Steiner, M., Oesterhelt, D., Towner, P., and Lanyi, J. K., <u>J. Biol. Chem.</u>, **259** (1984) 2185-2189.

17. Worthen, D. L., M. S. thesis, California Institute of Technology, 1989.